AD 690868

UNIVERSITY OF SOUTHERN CALIFORNIA

CONSOLIDATED SEMIANNUAL PROGRESS REPORT

NO. 9

Covering Research Activity During The Period

1 October 1968 through 31 March 1969

ELECTRONIC SCIENCES LABORATORY

228

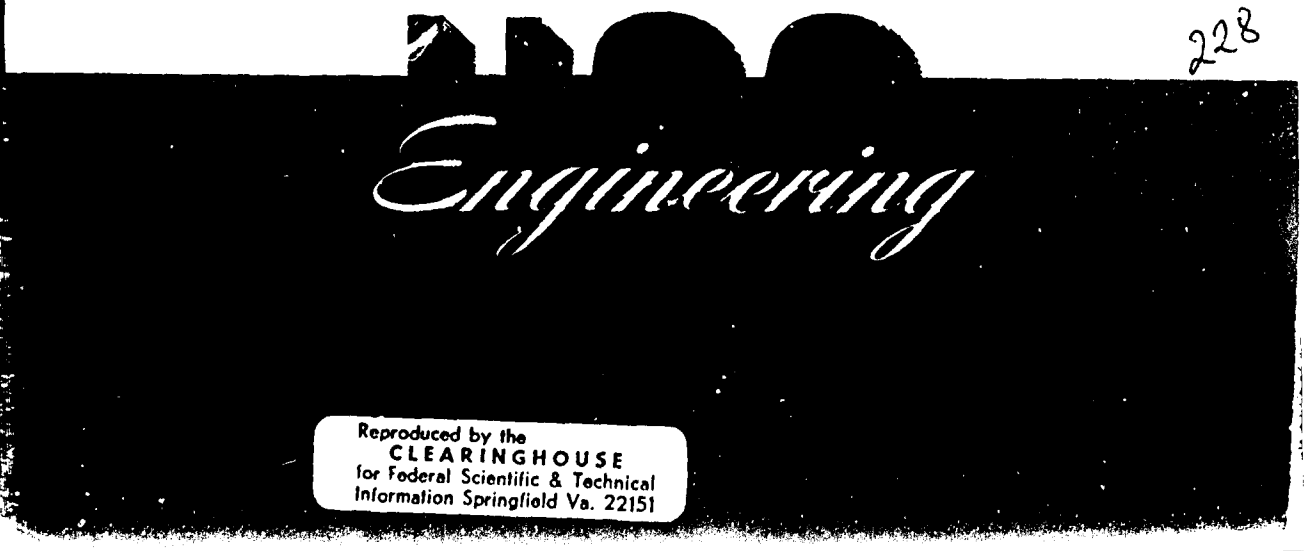

CONSOLIDATED SEMIANNUAL PROGRESS REPORT
NO. 9

Covering Research Activity During The Period
1 October 1968 through 31 March 1969

Prepared By
The
Electronic Sciences Laboratory
of the
School of Engineering
University of Southern California
Los Angeles, California 90007

TABLE OF CONTENTS

ACKNOWLEDGEMENT

This document is Semiannual Progress Report No. 9 issued by the Electronic Sciences Laboratory, University of Southern California, Los Angeles. It summarizes the research activity conducted during the period 1 October 1968 through 31 March 1969.

The Laboratory hereby acknowledges the following support:

Contract or Grant	Agency
AF-AFOSR-67-188	Air Force Office of Scientific Research
AF-AFOSR-67-1013B	Air Force Office of Scientific Research
AF-AFOSR-67-1029B	Air Force Office of Scientific Research
AF-AFOSR-68-1405, #1	Air Force Office of Scientific Research
AF-AFOSR-68-1414	Air Force Office of Scientific Research
AF-AFOSR-68-1555	Air Force Office of Scientific Research
AF-AFOSR-69-1622A	Air Force Office of Scientific Research
F19628-68-C-0169	Air Force Cambridge Research Laboratories
F19628-68-C-0342	Air Force Cambridge Research Laboratories
JPL-952210	Jet Propulsion Laboratory
JPL-952312	Jet Propulsion Laboratory
GK-1764	National Science Foundation
GK-2536	National Science Foundation
GK-2716	National Science Foundation
GK-2908	National Science Foundation
GK-3303	National Science Foundation
GK-3904	National Science Foundation
GK-4056	National Science Foundation
GK-4066	National Science Foundation
GK-4386	National Science Foundation
GK-10633	National Science Foundation
GP-7804	National Science Foundation
GP-8636	National Science Foundation

Contract or Grant	Agency
GP-8960	National Science Foundation
GP-10931	National Science Foundation
GU-1559	National Science Foundation
DAHC-04-69-C-0003	Department of the Army
DA-ARO-D 31-124-G450	U. S. Army Research Office, Durham
DA-ARO-D 31-124-G764	U. S. Army Research Office, Durham
DA-ARO-D 31-124-G929	U. S. Army Research Office, Durham
DA-ARO-D 31-124-G930	U. S. Army Research Office, Durham
DA-ARO-D 31-124-G1044	U. S. Army Research Office, Durham
DA-ARO-D 31-124-G1045	U. S. Army Research Office, Durham
DA-ARO-D 31-124-G1054	U. S. Army Research Office, Durham
N00014-67-A-0269-0006	Office of Naval Research
N00014-67-A-0269-0007	Office of Naval Research
N00014-67-A-0269-0010	Office of Naval Research
NGR-05-018-022	National Aeronautics and Space Administration
NGR-05-018-104	National Aeronautics and Space Administration
NGR-05-018-044	National Aeronautics and Space Administration
FR 07012-02	Department of Health, Education and Welfare
GM 01724-03	Department of Health, Education and Welfare
GM 16197-01	Department of Health, Education and Welfare
GM 16437-01	Department of Health, Education and Welfare
GM 35509-02	Department of Health, Education and Welfare
NB 08207-0151	Department of Health, Education and Welfare
AT(11-1)-113#19	Atomic Energy Commission
AT(11-1)-113#20	Atomic Energy Commission

PARTICIPATING PERSONNEL OF THE UNIVERSITY OF SOUTHERN CALIFORNIA ELECTRONIC SCIENCES LABORATORY

DIRECTOR

Z. A. Kaprielian

Albares, D.
Anderson, R.
Andrews, H. C.
Arguello, C. A.
Aseltine, J.
Bedrosian, E.
Bekey, G. A.
Bellman, R. E.
Beroza, P. P.
Bruer, M. A.
Brook, R. J.
Collins, D. C.
Crowell, C. R.
Daybell, M. D.
DeShazer, L. G.
Faust, W. L.
Gagliardi, R. M.
Gershenzon, M.
Ginsburg, S.
Golomb, S. W.
Grodins, F. S.
Halloran, M. H.
Hurrell, J. P.
Kane, J.
Kashef, R.
Kell, C.
Kim, Y. B.
Kleinman, D. A.
Kroger, F. A.
Kuehl, H. H.
Lempel, A.
Lindsey, W. C.
Louisell, W. G.
McGhee, R. B.
McNabb, A.
Macmillan, R. S.
Mager, G. E.
Makowski, K.
Mann, M.
Marburger, J. H.
Meisel, W. S.
Meritt, M. J.
Mitchel, F.
Moore, G. P.
Munushian, J.
Murr, L. E.
Nabeshima, I.
Nahi, N. E.
Neustadt, L. W.
O'Brien, B. B.
Ogawa, S. H.
Ohlson, J. E.
Parks, J.
Payne, R. T.
Penaloza, J.
Porter, J.
Porto, S. P. S.
Pratt, W. K.
Reed, I. S.
Reichert, J. D.
Rice, H. G.
Rousseau, D. L.
Rusch, W. V. T.
Scholtz, R. A.
Silverman, L. M.
Smit, J.
Spitzer, W. G.
Steier, W. H.
Stover, H. L.
Sugiyama, H.
Sworder, D. D.
Tooper, R. F.
Vemuri, R. V.
Wagner, W. G.
Wang, R.
Weber, C. L.
Welch, L. R.
Whelan, J. M.
Wilcox, W. R.
Wittry, D. B.
Wolf, M. B.
Yanagida, H.
Young, G. O.

LECTURERS AND GRADUATE RESEARCH ASSISTANTS

Achterberg, D.
Alfven, H.
Anderson, C. L.
Angel, E. S.
Arguello, Z.
Arnett, J. D.
Asa, M. L.
Assefi, T.
Axelband, E.
Baenziger, G.
Baker, J. E.
Basu, R.
Bayley, R.
Beguwala, M.
Bhatia, R. K.
Bloom, G. S.
Bottlik, I. P.
Borrey, R. G.
Bowman, C. K.
Bradford, W. G.
Brewer, J. H.
Bochove, E. J.
Canter, L. H.
Card, R. E.

LECTURERS AND GRADUATE RESEARCH ASSISTANTS (cont'd)

Chan, W-Y.
Chandler, W. J.
Chang, J. C-C.
Chang, S-J.
Chern, S. S.
Chiang, C-L.
Christiansen, R. G.
Coggshall, J. C.
Cooper, C. A.
Cosand, A. E.
Culbertson, G. T.
Cumming, G. D.
Davidheiser, R.
Dawson, L. R.
Diebel, J. C.
Eastment, J. G.
Elliott, D. F.
Fielding, R. M.
Flannery, M. R.
Fraas, L. M.
Fuzak, C.
Garen, E. R.
Germann, D. A.
Giuliano, J. A.
Gordon, B. J.
Goasain, G. L.
Gray, R. M.
Greene, J. E.
Gundersen, M. A.
Hammerwold, G.
Haney, G. M.
Hartman, R. C.
Hawk, W. E.
Herron, B. G.
Hershman, G. H.
Hon, D. T.
Hopgood, W. C.
Horylev, R.
Hsieh, J. J.
Huang, H.H.C.
Huang, S-C.
Huff, L.
Huth, G. K.
Kadomoto, N.
Karush, R.
Kato, H.
Klement, R.
Kumar, V.
Kung, J. K.
LaFrance, T.
LaFrieda, J. A.
Lee, L. C.
Leung, P. C.
Levy, M. E.
Lew, A. Y.
Li, C-T.
Lin, W-N.
Little, G. W.
Maloney, J. C.
Marks, R. A.
McAdam, P. L.
McAllister, G. L.
McCoy, J. H.
Meier, G. D.
Mikhalkin, B.
Miller, D. S.
Millstone, S. D.
Mittledorf, J. J.
Mohanty, N. C.
Mowery, J. W.
Murata, P. T.
Ng, W. K.
Niho, Y.
Norton, R.
Otaguro, W. S.
Parker, R. D.
Parnavelas, J. G.
Peratt, A. L.
Powell, S. R.
Proffitt, W. P.
Prussin, S. A.
Rao-Sahib, T.
Reynolds, R.
Rideout, V. L.
Roberts, G. I.
Robinson, V. G.
Rosenberg, J.
Rogers, R. O.
Rice, D. K.
Schaefer, B. M.
Schlose, H.S.E.
Shoemaker, C.
Skolnik, L. H.
Slobin, S. D.
Stein, J. J.
Stokes, R. B.
Storwick, R.
Tauseworth, R.
Thoene, R.
Thompson, G.
Trachtenberg, H.
Trujillo, D.
Tsay, J. C-Y.
Turner, G. B.
Van Der Embse, U.
Van Der Meulen, Y.J.
Widersich, H.
Wielin, S. A.
Williams, T. G.
Yakush, A.
Yamashiro, S. M.
Yee, J. F.
Yeh, L. S.
Young, J. W.
Yuang, J. W.
Yuang, L. T.
Yuan, W. W.

TECHNICIAN SUPPORT PERSONNEL

Belda, J. F.
Bruckmann, K. S.
Buell, J. M.
Csige, G.
Flink, M.
Fung, A. M.
Gardner, E. D.
Garlinger, E. D.
Hamada, S. S.
Howland, D. L.
Krebs, W. E.
Maunders, E. A.
Molnar, E.
Morris, L.
Mueller, G. H.
O'Niel, M.
Owen, H. R.
Potosky, J. C.
Ruskin, H.
Soberay, W. G.
Wong, G.
Wong, R.

ADMINISTRATIVE

Baker, W. P.
Blood, L. J.
Caldwell, C. J.
Di-Bernardo, L.
Dillon, E. P.
Done, D. M.
Harrison, A.
Hightower, C.
Iskandar, R. Z.
Lambert, J. W.
Lopez, F.
Luginbuehl, A.
Lum, G. T.
Lyness, C. J.
Marshall, J. W.
McKenzie, J.
Maron, S.
Milhalka, M. F.
Mitchell, S. R.
Nihei, J. T.
Plaster, P. S.
Rice, G. L.
Sakmar, M. C.
Sherwood, M.
Shioya, K. H.
Swett, D. R.
Tanno, D. V.
Tierney, R.
Ward, R. A.

1. SOLID STATE

1.1 SEMICONDUCTORS

1.1.1 Infrared Studies of Semiconductors

Grant GK 10633, National Science Foundation
Contract F 19628-68-C-0169, Air Force Cambridge Research Laboratories

W. G. Spitzer, A. E. Cosand, M. Levy, L. Skolnik, P. C. Leung, R. Eaglet

Several types of defects or impurity-induced infrared absorption in semiconductors are being studied. These studies are of interest both for understanding of the physics of semiconductors and for providing information of technological importance in the production and characterization of semiconductor materials. Three of the projects are discussed in subsections that follow.

Also, work is being done by M. Levy on a data acquisition system for one of the infrared spectrophotometers which will improve the signal to noise ratio of the measurements and will simplify computer processing of the data. This will greatly facilitate comparative studies of spectra when several experimental parameters are to be varied and many spectra must be compared. An example would be the study of localized vibrational modes of lithium complexes in GaAs where the observed spectra depend on the temperature at which lithium is diffisued into the GaAs and the ratio of abundance of ^{6}Li and ^{7}Li isotopes.

1.1.1.1 Local Modes and Resonant Modes in Ge_xSi_{1-x} Alloys

A. E. Cosand

Alloys of the form Ge_xSi_{1-x} form a continuous solid solution over the entire composition range. The lattice paran eter and density of the alloys vary almost linearly from that of pure Ge to pure Si[1]; the variation of electronic band gap is smooth and monotonic.

The vibrational spectrum of Ge is quite similar to that of Si with the frequencies scaled by the square root of the ratio of the atomic masses. The lattice vibrations are optically inactive to first order; only multi-phonon processes produce any IR absorption. The vibrational spectrum of a GeSi alloy is qualitatively different from that of either pure substance[2], [3].

In the case of Si-rich alloys ($0 \leq x \leq .12$) the presence of Ge gives rise to resonant modes. These have frequencies lying within the range of normal phonon frequencies (up to 518 cm^{-1} in Si) and are coupled to the lattice. In contrast to ordinary phonons, which are spatially uniform in amplitude, the resonant modes have an anomalously large amplitude of vibration of the defect atom. These modes may have a first order dipole moment and thus be observable in direct I.R. absorption. Such resonant absorption, identified as a single phonon process by its lack of temperature dependence, is clearly observable. There is a broad band centered around 480 cm^{-1}, a relatively sharp band around 400 cm^{-1}, and an extremely broad band extending from about 100 cm^{-1} to about 230 cm^{-1}.

In Ge-rich alloys ($.85 \leq x \leq 1.00$) there can be resonant modes and also local modes with frequencies outside the range of normal lattice frequencies. The local mode of isolated Si is seen. A pair of bands which may be due to Si-Si pairs is observed in samples with a large concentration of Si. It is not expected that there should be much difference in relative charge between Ge and Si in a crystal of the alloy; this is consistent with the weak absorption observed for the Si local mode, which is weaker than

other local modes that have been observed by 10^2 or 10^3.

The localized modes of boron in Si-rich alloys electrically compensated by lithium have been studied in detail. As in silicon[4], the boron is almost entirely paired with lithium at or below room temperature, and for each boron isotope there are two prominent absorption lines. The higher frequency line is the doubly degenerate vibration transverse to the B-Li axis, the lower frequency line is the axial vibration. In the alloy, the irregularity of the local environment adds structure to the observed lines. A Ge atom in a first neighbor site changes the frequency enough to split off a new line. Second neighbor Ge atoms broaden the line assymetrically. An initial attempt to calculate the line shape expected for second neighbor broadening assuming purely random distribution of the alloying atoms has yielded a surprising close fit to the observed line shape.

References

1. Dismukes, J. P., R. Ekstrom, and R. J. Paff, J. Phys. Chem. 68, 10 (1964).

2. Braunstein, R., Phys. Rev. 130, 879-887 (1963).

3. Maradudin, A. A., "Localized, Gap, and Resonance Modes", in Localized Excitations in Solids, ed. by R. Wallis, Plenum Press, New York, 1968.

4. Spitzer, W. G., and M. Waldner, J. Appl. Phys. 36, 2450-2453 (1965).

1.1.1.2 Infrared Absorption by Free Carriers in P-Type Silicon

P. C. Leung

Infrared absorption by "free carriers" in semiconductors has been studied both experimentally and theoretically for a number of years[1]. Some of the most extensive studies were concerned with germanium[2]-[6], both n-type and p-type. There has been also considerable work on silicon and compound semiconductors[7]-[10]. Up to the present time, however,

the only studies of p-type silicon have been of limited scope[11]-[13], usually measurements of a few samples or a small frequency range. The lack of a detailed experimental study is surprising in view of the present ease in obtaining good quality samples and the technological importance of the material.

The present investigation presents measurements of a number of samples over a frequency range from $\tilde{\nu} \sim 10^4 cm^{-1}$ to $3 \times 10^2 cm^{-1}$ or less and in several cases, at several temperatures. The absorption at room temperature is seen to vary smoothly approximately as $\tilde{\nu}^{-2}$ at high frequencies. As the frequency is decreased, the transition from the frequency dependent conductivity σ_{ac} to the frequency independent conductivity σ_{dc} is clearly observed. The observed absorption is not easily interpreted despite the availability of relatively sophisticated quantum theories of free carrier absorption. Some aspects of the results appear to be most readily interpretable in terms of the simple "classical Drude-Zener" theory of optical properties. It is not surprising, however, that there are some serious inconsistencies of the data with the simple theory. The absorption for a boron-doped silicon sample measured at near liquid nitrogen temperature indicates absorption bands at $\tilde{\nu} = 320\ cm^{-1}$ and $\tilde{\nu} = 278\ cm^{-1}$. Measurements at other temperatures and measurements of samples of a different dopant are necessary to identify these bands. Additional measurements of boron-doped samples at different temperatures over the entire frequency range are being carried out to further study the scattering mechanisms involved in the absorption.

References

1. H. Y. Fan, Semiconductors and Semimetals, Vol. III (Edited by R. K. Willardson and A. C. Beer, Academic Press, New York, 1967), p. 405.
2. H. J. G. Meyer, Phys. Rev. 112, 298 (1958).
3. R. Rosenberg and M. Lax, Phys. Rev. 112, 843 (1958).
4. H. Y. Fan, W. G. Spitzer, and R. J. Collins, Phys. Rev. 101, 566 (1956).

5. A. H. Kahn, Phys. Rev. 97, 1647 (1955).
6. W. Kaiser, R. J. Collins and H. Y. Fan, Phys. Rev. 91, 1380 (1953).
7. W. G. Spitzer and H. Y. Fan, Phys. Rev. 108, 268 (1957).
8. S. Visuanathan, Phys. Rev. 120, 376 (1960).
9. E. Haga and H. Kimura, J. Phys. Soc. Japan 18, 777 (1963).
10. H. G. Lipson and A. Kahan, Phys. Rev. 133, A800 (1964).
11. V. S. Vavilov, Soviet Physics - Solid State 2, 346 (1960).
12. H. Hara and Y. Nishi, J. Phys. Soc. Japan 21, 1222 (1966).
13. T. Staflin, J. Phys. Chem. Solids 27, 65 (1966).

1.1.1.3 Determination of Segregation Coefficients of Dopants by Local Mode Measurements

L. Skolnik

A preliminary investigation has been initiated to determine the feasibility of measuring segregation coefficients by optical means. The method utilizes measuring of localized vibrational modes (LVM) produced by light impurity atoms in the host crystal. Since the strength of the LVM is proportional to the concentration of impurity atoms in the crystal, it is possible to trace the impurity profile of a crystal ingot. The method consists of taking several slices from an ingot and measuring the strength of the LVM in each slice. In this manner, the impurity concentration can be directly measured at each point in the crystal, and hence the segregation coefficient can be determined.

The method also shows promise for investigating localized or inhomogeneous segregation of impurity atoms. Thus far segregation coefficients of phosphorus impurity in InSb and aluminum, silicon, and phosphorous impurities in GaAs have been measured with this local mode technique.

1.1.2 Crystal Growth

AF-AFOSR-69-1622, Joint Services Electronics Program

W. R. Wilcox and W. Allred

Solid state research and development depends on the availability of suitable materials and these are usually single crystals. The objectives of the crystal growth program at USC are two-fold: (1) To do research on crystal growth phenomena and techniques; (2) To develop a crystal growth capability so that researchers needing materials will be able to prepare them.

During the past six months we have significantly expanded our materials preparation capability by acquiring two horizontal tube furnaces, an electron-beam floating-zone refiner, an arc-melting unit, and a resistance-heated Czochralski crystal grower. We are in the process of installing these in the new crystal growth laboratory. Two horizontal-boat directional solidification aparatuses have been constructed and are being used for research on III-V compound crystal growth. The following crystals have been grown in our laboratories for research at USC since September 1968: GaAs, Ge, Si, Ge-Si alloys, InSb, $Cs_3Zn(Co)Cl_5$, KI, KCl, NaCl, KBr and $Pb(NO_3)_2$.

A new and improved technique for growth of GaAs crystals is being developed. GaAs is grown by directional solidification in a horizontal boat by pulling the boat slowly through the furnace. Thermal insulation has been removed from a portion of the top of the furnace to permit direct viewing of the melt-crystal interface. It was found that seeding with the proper orientation of the seed allowed low dislocation density GaAs to be produced. Preliminary experiments with vapor transport of GaAs in a closed tube have also shown promise. The goal of this research is to produce bulk crystals with mobilities normally observed in crystals grown by the vapor epitaxial technique.

A theoretical calculation has shown that the stagnant film model for mass transfer in crystal growth is valid for most situations[1].

The possible use of ultracentrifugation for removal of inclusions from crystals was recently proposed[2]. Preliminary experiments with a chemical engineering graduate student, Ahmed Kasem, showed that aqueous inclusions in KI and $Pb(NO_3)_2$ did move in a centrifugal field. When crystalline reagent-grade chemicals were treated this way most of the occluded moisture was removed. However, the chemicals were sintered into a compact coherent mass. Further experiments on an ultracentrifuge at the McDonnell-Douglas Advanced Research Laboratories are being performed in conjunction with their personnel. Inclusions in KI were observed to move at about 0.05 mm/hr in a field of 210,000 g at room temperature.

Alkali halide crystals with deliberately formed inclusions were grown at USC for the centrifuge experiments. In the process, several interesting growth phenomena were observed and deserve further investigation. The growth habit of KI was found to be pH sensitive, forming rounded (111) planes in neutral or acid solution and (100) surfaces in basic solution. KBr solutions produced a most unusual twin form. Pairs of (100) platelets were joined in a <211> relationship to form butterfly twins. One of the platelets usually continued beyond the other, only very much reduced in thickness.

References

1. W. R. Wilcox, Mat. Res. Bull. (in press).
2. W. R. Wilcox, Ind. Eng. Chem. 60, 13 (March 1968).

1.1.3 Electron Probe Analysis of Semiconductors

AF-AFOSR-68-1414, Air Force Office of Scientific Research

D. B. Wittry, N. Gardner, J. H. McCoy, H. C. Marciniak, J. Potosky, T. Rao-Sahib, P. A. Sullivan and R. Tamura

1.1.3.1 Cathodoluminescence of Semiconductors

H. Marciniak and D. B. Wittry

The ultrahigh vacuum chamber and beam column which was described in the last semiannual report is now completed. Testing of the entire system (including the electron gun, magnetic lens the Air Products and Systems Cryo Tip refrigerator, and an electric sample heater) is now in progress.

The first application of this system will be the study of the temperature dependence of cathodoluminescence of semiconductors.

There are plans to add a mass spectrometer to the system so as to be able to determine the nature of the residual gases in the system as well as the nature of material that may be desorbed from the semiconductor surfaces.

1.1.3.2 Electron Beam Modulated Optical Properties of Semiconductors

J. H. McCoy and D. B. Wittry

The electron beam of the electron probe microanalyzer has been periodically gated to modulate the optical properties of semiconductors, and the modulated reflectance of germanium was reported previously[1]. Recent investigation has been made of the physical mechanism of reflectance modulation, modulated absorption by excess carriers, and the modulated reflectance spectrum of gallium arsenide.

Several models have been presented for the modulation of reflectance by electron beams. The large density of excess carriers

produced by the beam could change the periodic potential of the crystal or flatten the normal surface potential[2]. The latter would produce a Franz-Keldysh effect similar to the electroreflectance[3]. The electron beam also causes a change in temperature of the surface and could result in a modulation similar to thermo-reflectance[4].

Temperature modulation by the gated electron beam has a limited frequency response as indicated on the lock-in amplifier detector. The transient heat transport equation for a disc source was computer solved. The fundamental sine component of the Fourier series was calculated as a function of the modulating frequency. This corresponds to what is measured by the lock-in amplifier. The results for gallium arsenide and germanium are shown in Figure 1. The parameter b is related to the spot size a, heat capacity c, heat conductivity k, and density ρ by

$$b = a\sqrt{\frac{c\rho}{4k}}$$

Figure 1 also shows the expected response for a $\frac{1}{3}$ power dependence on the excess carrier density which rises and decays exponentially when the beam is gated. This curve may be shifted along the frequency scale for various carrier lifetimes. The lifetime for the germanium was not known and could have fallen in the range of interest. The shape of the curve, however, closely fits the calculated one for heating response. In the case of gallium arsenide the carrier lifetime could not affect the response at the frequencies measured, and again the fit to the calculated curve is good. Thus the modulation is mostly due to temperature change.

Absorption of photons with energy less than the band gap of a semiconductor is mainly caused by free carriers. If excess carriers are produced periodically and only the transmitted light which varies in the same phase and frequency is detected, the resulting quantity will be directly proportional to the excess carrier density integrated over the path of the light. To observe this affect in germanium the same experimental system was used as in the modulated reflectance, but a

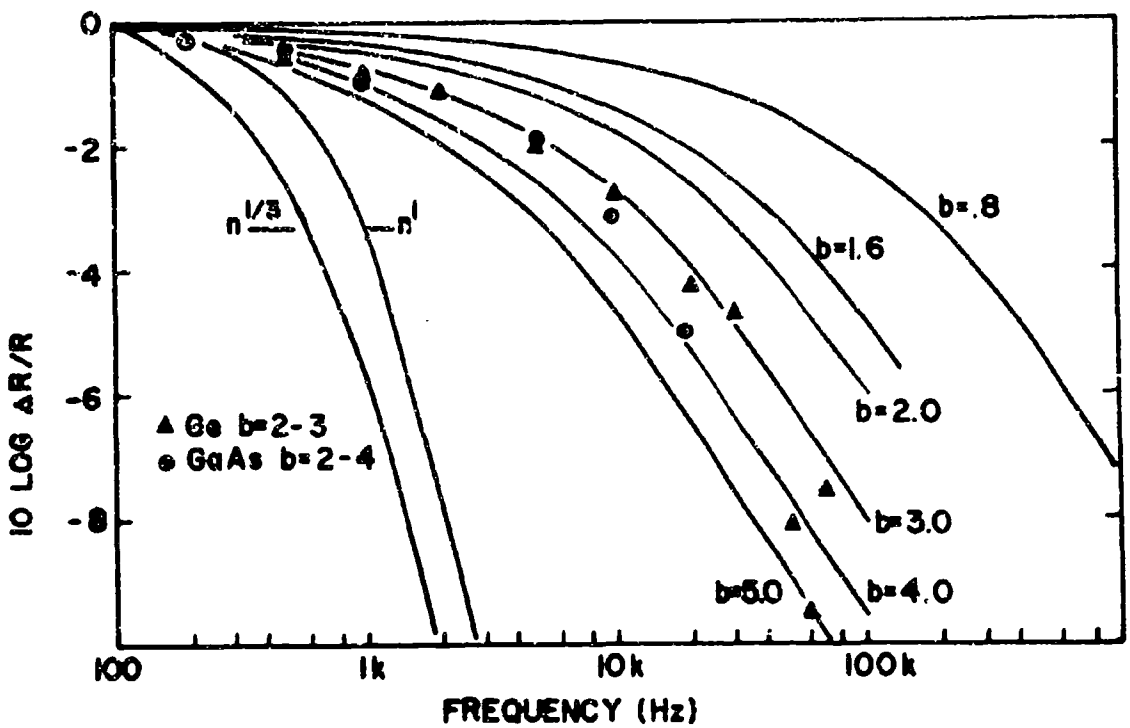

Figure 1. The response of $\Delta R/R$ at a fixed wavelength for various frequencies is shown. The solid curves are calculated for the transient heating response using six values of the parameter b which depends on thermal properties and spot size. The two solid curves marked $n^{1/3}$ and n represent the responses which are proportional to the carrier concentration n to the one third and first powers respectively. The experimental points are for high resistivity Ge at the 2.35 eV peak and for n-type GaAs at the 2.85 eV peak.

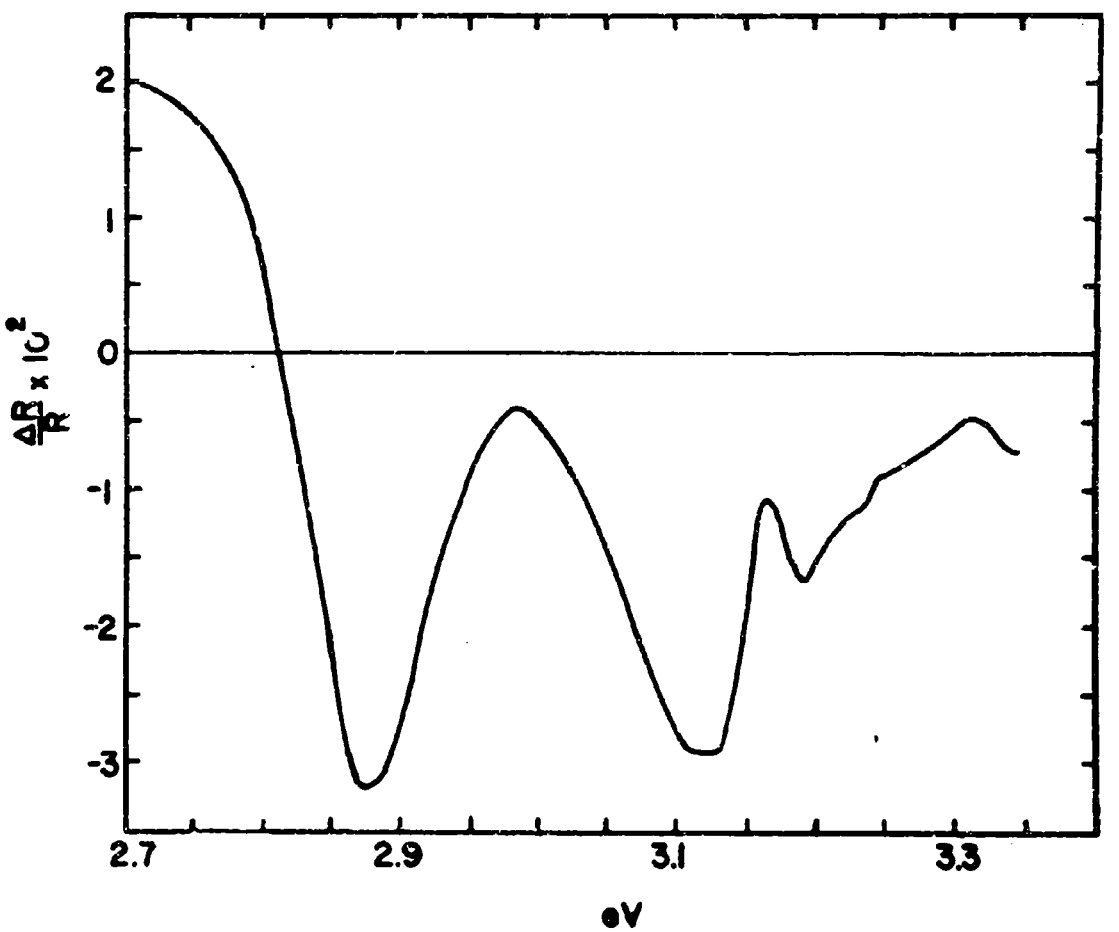

Figure 2. $\Delta R/R$ is shown as a function of reflected photon energy for semi-insulating GaAs at a beam density of .5 A cm^{-2}.

photoconductor detector was placed in the specimen holder, below the specimen. The incident light bandwidth was limited by the long wavelength cutoff of quartz and short wavelength cutoff of a germanium filter. The primary purpose of the experiment was to find the dependence between excess carrier concentration and beam density at a fixed voltage. In high resistivity germanium a linear relationship was found up to the highest density measured of .1 amp/cm^2 at 10 kv.

The modulated reflectance technique was applied to gallium arsenide. Figure 2 shows the modulated reflectance spectrum obtained near the E_1 and $E_1 + \Delta$ critical point transitions. The negative peaks approximate the transition energies and agree with similar results in electroreflectance[3]. The shape of the spectrum, however, is the same as in thermoreflectance[5]. The amplitude is almost two orders of magnitude greater. Thus the electron beam modulation technique produces thermoreflectance spectrum with rather high efficiency.

References

1. J. H. McCoy and D. B. Wittry, Appl. Phys. Letters, 13, 272 (1968).
2. R. E. Nahory and J. L. Shay, Phys. Rev. Letters, 21, 1569 (1968).
3. B. O. Seraphin, J. Appl. Phys. 37, 721 (1966).
4. B. Batz, Solid State Commun. 5, 985 (1967).
5. E. Matatagui, A. G. Thompson, and M. Cardona, Phys. Rev. 176, 950 (1968).

1.1.3.3 Diffusion Lengths in P-Type GaAs

T. Rao-Sahib and D. B. Wittry

Diffusion lengths of electrons in p-type GaAs have been measured by means of the voltage dependence of cathodoluminescence[1] using a defocussed electron beam and selected area technique (described in the previous report). Experimental results with accelerating voltages

in the range 5 - 50 kV indicate values of electron diffusion length ranging from 3.2 μ at low carrier concentration ($6.9 \times 10^{16} cm^{-3}$) to 0.6 μ at high carrier concentration ($3.76 \times 10^{19} cm^{-3}$). The results obtained with four specimens of p-type GaAs are summarized in Table I on the following page. All measurements were carried out at room temperature. For specimens 1, 3 and 4, the electron beam diameter was 144 μ with a selected area of 5 μ x 5 μ; photon counting techniques were used to measure the cathodoluminescence intensity. In the case of specimen 2, the beam diameter was 180 μ, the selected area was 27 μ x 27 μ, and intensity was determined by measuring the current from the photomultiplier tube.

For all the specimens, good agreement was obtained between experimental results and the theoretical curves which had been calculated by numerical integration of the distribution of excess carriers assuming a Gaussian approximation to the distribution of excitation with depth[2]. The results obtained show that the method of voltage dependence of cathodoluminescence can be used to measure diffusion lengths in specimens where the intensity of cathodoluminescence is not linearly proportional to the specimen current (e.g., p-type GaAs). The results have been submitted to the Journal of Applied Physics.

It is planned to study the variation of intensity with current as a function of temperature. Such a study would be useful in providing more information on the recombination mechanisms responsible for the observed behavior.

References

1. Wittry, D. B. and Kyser, D. F., J. Appl. Phys. 38, 375-382 (1967).

2. Kyser, D. F. and Wittry, D. B., Proc. IEEE, 55, 733-734 (1967).

TABLE I: Electron diffusion length L, reduced surface recombination velocity S, and d/L in p-type GaAs at room temperature. An exponent of n = 1.7 has been assumed in the electron range-energy relation, and the exponent m relates observed infrared intensity to specimen current i at constant V x i.

Specimen	$p_o(cm^{-3})$	Hall mobility (holes) $cm^2/V\text{-}sec$	power level $\times 10^3 W$	m	L(μ)	d/L	S	$d^{(a)}$ obs. (μ)	$d^{(b)}$ calc. (μ)
1	3.76×10^{19}	63.5	10	1.0	0.57	0.02	50	0.011	0.0042
			40	1.2	0.65	0.02	50	0.013	
2	3.65×10^{18}	121	5	1.0	0.74	0.033	10	0.026	0.013
			50	1.2	0.75	0.033	10		
3	7.88×10^{17}	197	80	1.4	2.6	0.05	50	0.13	0.028
4	6.9×10^{16}	247	50	1.8	3.2	0.05	20	0.16	0.1

(a) Calculated from L and $\frac{d}{L}$

(b) Calculated by assuming a 0.5 eV barrier and complete depletion.

1.1.3.4 Slow Transients in Cathodoluminescence

P. A. Sullivan and D. B. Wittry

Previous studies[1] of cathodoluminescence in CdSe shows a slow time dependence of the emission which reached a peak when the electron bombardment dose was approximately 1×10^{-6} coulombs for current densities of 0.002 to 0.1 A/cm^2. This effect was irreversible and was affected by different gases introduced into the vacuum chamber. Kyser[1] suggested that the slow decrease in intensity was due to an increase in the surface recombination velocity.

We have continued these studies using platelets and also polished bulk samples of CdSe. In some cases an initial decrease before a rise to maximum intensity was observed. After the high intensity peak is reached, the intensity decreases, in most cases irreversibly.

There appear to be two or more competing mechanisms which affect the radiative efficiency. One process causes an increasing intensity and a second, with a longer time constant causes the intensity to decrease. Since the primary intensity decrease is irreversible, it cannot be accounted for by temperature changes. However, temperature may be a contributing factor to a reaction process. The electron beam induced change in surface state density and distribution may be a significant factor, particularly due to adsorbed layers. Bube[2] has measured the reduced surface conductivity of CdSe due to adsorbed oxygen (acceptor states). He also found that the oxygen could be photo-desorbed at high temperatures and photo-adsorbed at room temperature. Work is in progress to prepare cleaner surfaces on CdSe for examination. Photo-induced sorption effects will be studied and compared with the slow transient observations.

References

1. Kyser, D. F., "Electron-Beam Excitation of Semiconductors and a Study of Cathodoluminescence with an Electron Microprobe," Ph.D. Thesis, University of Southern California, January 1968.

2. Bube, R. H., "Oxygen Sorption Phenomena on Cadmium Selenide Crystals," J. Chem. Phys., 27, 496 (1957).

1.1.4 Quantitative Electron Microscopy

GK 3904, National Science Foundation

R. Gauldin and D. B. Wittry

An electron spectrometer has been designed for use with the Hitachi HU 125 electron microscope. This spectrometer consists of a magnetic prism used below the camera chamber. The entrance and exit boundaries are inclined to provide two dimensional focussing. Because of space limitations, the distance from source to prism and image to prism are unequal.

Electronic equipment for digitally recording the transmitted electron signal has been ordered. This includes a teletypewriter and teletype scanner which will be used for transferring the data stored in the CAT 1000 to paper tape for computer processing.

1.1.5 Radiative Recombination in Semiconductors

AF-AFOSR 69-1622, Joint Services Electronics Program

GK 1764, National Science Foundation

NGL-05-018-044, Sup. #2, National Aeronautics and Space Administration

DA-ARO-D 31-124-G1054, U.S. Army Research Office

M. Gershenzon

In order to obtain efficient solid-state visible electroluminescent display devices we have been growing and characterizing two new wide-bandgap semiconductors (gallium nitride and aluminum phosphide) and studying luminescent mechanisms in two well-established semiconductors (zinc sulfide and silicon).

The installation and calibration has been completed on equipment to measure fluorescence, electroluminescence, photoconductivity, photoexcitation and absorption spectra with very high resolution from

2,000 to 25,000 Å between 4.2°K and room temperature. A pulsed ultraviolet molecular nitrogen laser has recently been set up and a pulsed organic dye and a cw gallium arsenide laser are currently being assembled for fluorescence measurements ranging from steady-state to 10 n sec time-resolved spectroscopy.

Small platelets of aluminum phosphide, suitable for optical measurements, have been grown by a closed-tube halide transport process. These crystals are stable in air.

We have shown that without resorting to high pressure techniques, the solubility of nitrogen in gallium at temperatures up to 1200°C is too small to allow gallium nitride to be readily grown from gallium solution. Instead, we have been investigating several vapor growth techniques involving reaction of a volatile gallium species with ammonia. The resulting crystals are still barely too small for normal characterization.

The movement of the Fermi level in doped and undoped zinc sulfide as a function of temperature and sulfur overpressure is being studied using resistivity as a diagnostic at present. This investigation is aimed at establishing quantitatively the feasibility of preparing p-type zinc sulfide.

Using up to 10 Joule pulses of near bandgap ultraviolet radiation we have still been unable to saturate the copper green emission in copper-activated (aluminum, chlorine co-activated) zinc sulfide in an attempt to clarify the mechanism of this efficient green luminescence. Our detection techniques are being refined to continue this program.

The search for isolated donor-acceptor pair luminescence in silicon has been delayed while high resolution detectivity in the 1-2 μ range was optimized.

1.1.6 Thin Film and Interface Phenomena

AFOSR 69-1622, Joint Services Electronics Program

C. R. Crowell, V. L. Rideout, G. I. Roberts

This program is comprised of device oriented studies related to current transport and charge storage in metal-semiconductor (Schottky Barrier) contacts.

1.1.6.1 Capacitance-Voltage Relationship in Schottky Barriers

C. R. Crowell and G. I. Roberts

The theoretical work reported in the previous report on surface state and interface effects on the capacitance-voltage (C-V) relationship in Schottky barriers was given final revision and has been accepted for publication. In the course of this work it was recognized that, for light semiconductor doping with shallow donors, the effect of deep lying impurities can have an appreciable effect not only on the slope but also on the intercept of a plot of $1/C^2$ versus V. Further theoretical analysis has clarified the role of deep lying impurities and suggests that the C-V data near zero bias can be used in a spectroscopic fashion to deduce an impurity energy level profile. More details of this treatment will be given in the next report.

1.1.6.2 Current Transport in Schottky Barriers

C. R. Crowell and V. L. Rideout

A normalized calculation of the current-voltage characteristic including effects of image force is nearing completion. Details of this work and experimental work being initiated will be given in the next report.

1.1.6.3 General Normalized Current Voltage Characteristic of Quasi-Ohmic Contacts

C. R. Crowell

A preprint of a paper on this work was delivered at the October 1968 Electrochemical Society Symposium on Ohmic Contacts. Since no reprints will be available, the following is a complete text of the paper.

The expected current density, J, versus voltage, V, characteristics of quasi-ohmic contacts where thermionic field or thermionic emission is the mechanism of current flow are shown to be of the form:

$$J = J_s \exp(qV/nkT)[1 - \exp(-qV/kT)]$$

where J_s and n are diode parameters which in general are temperature dependent. Accumulation contacts which are thermionic-emission limited (on lightly doped semiconductors) are characterized by $n \gtrsim 1$ when $J \to -J_s$, while tunneling contacts (on heavily doped semiconductors) are characterized by $n \gg 1$. When $n > 2$, a diode behaves as a backward diode. Since the "ohmic" contacts to both the p and n side of p-n junction devices must operate at reverse bias when the device is forward-biased, a backward diode with $n \gg 2$ provides an added margin of safety over the thermionic-limited accumulation contact.

A summary of results of theoretical calculations of thermionic-field emission for a 1-band approximation in a uniformly doped Schottky barrier is provided in the form of linear equations for the bias limits of applicability and a graph from which the relationship between the semiconductor doping and n can be found. A second graph permits the relationship between the barrier height and n and J_s to be determined explicitly. The useful range of analytic approximations to these results and the application of the theory to a variety of experimental results is discussed.

The term ohmic contact is frequently applied to semiconductor device contacts even though it is often apparent that it is very difficult to make an accurate characterization of a contact independent of the device itself. This article presents a few simple guidelines to assit such a separation of contact from device. An outline is given of some of the general features of the current-voltage characteristic of a metal-semiconductor contact when current transport is dominated by Maxwell-Boltzmann type tails of the energy distribution of charge carriers in the metal and the semiconductor. Simple criteria for validity of and graphs for use of a more explicit model in which thermionic-field (T-F) emission is assumed[1] are subsequently presented.

It is particularly appropriate to use the more general case of T-F emission rather than field emission because it provides a natural contrast of the properties of barrier contacts produced by an accumulation layer (or thermionic-limited contact) and by a tunneling contact. Figure 1 shows an energy band diagram for an accumulation layer contact at a semiconductor-metal interface on the p side of a p-n junction, and a tunneling contact produced by a heavily doped region in contact with the metal on the n side of the junction. The current-carrying ability of the accumulation contact is determined by the thermal excitation of holes near the semiconductor valence band edge at the semiconductor-metal contact. Unless the valence band edge is very close to the Fermi energy in the metal, such a contact will have poor current-carrying capabilities at low temperature. Current transport at the tunneling contact on the other hand will not be strongly temperature-dependent and will have the additional property of suppressing minority carrier transfer across the metal-semiconductor boundary.

The configuration in Figure 1 has another interesting property. When forward bias is applied to the p-n junction (see Figure 2), the contacts are both reverse biased (using the convention for Schottky barriers that forward bias corresponds to the injection of charge carriers into the

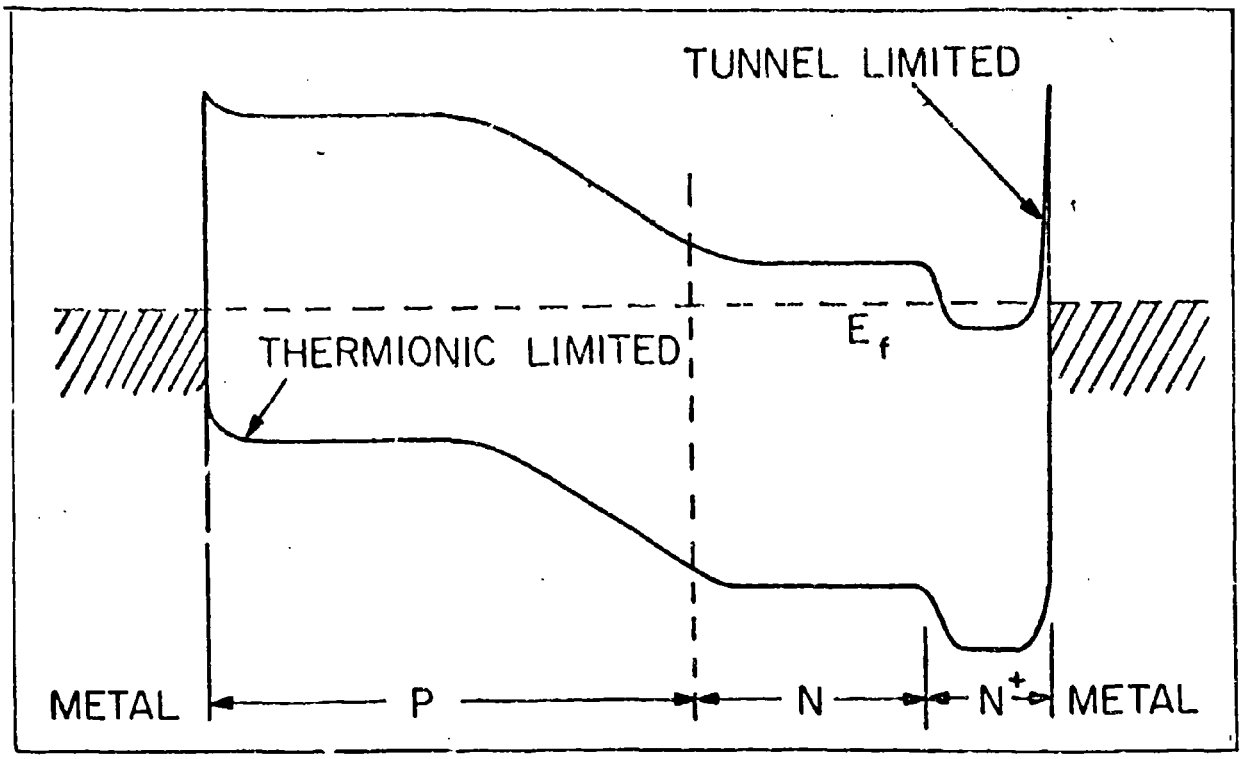

Figure 1

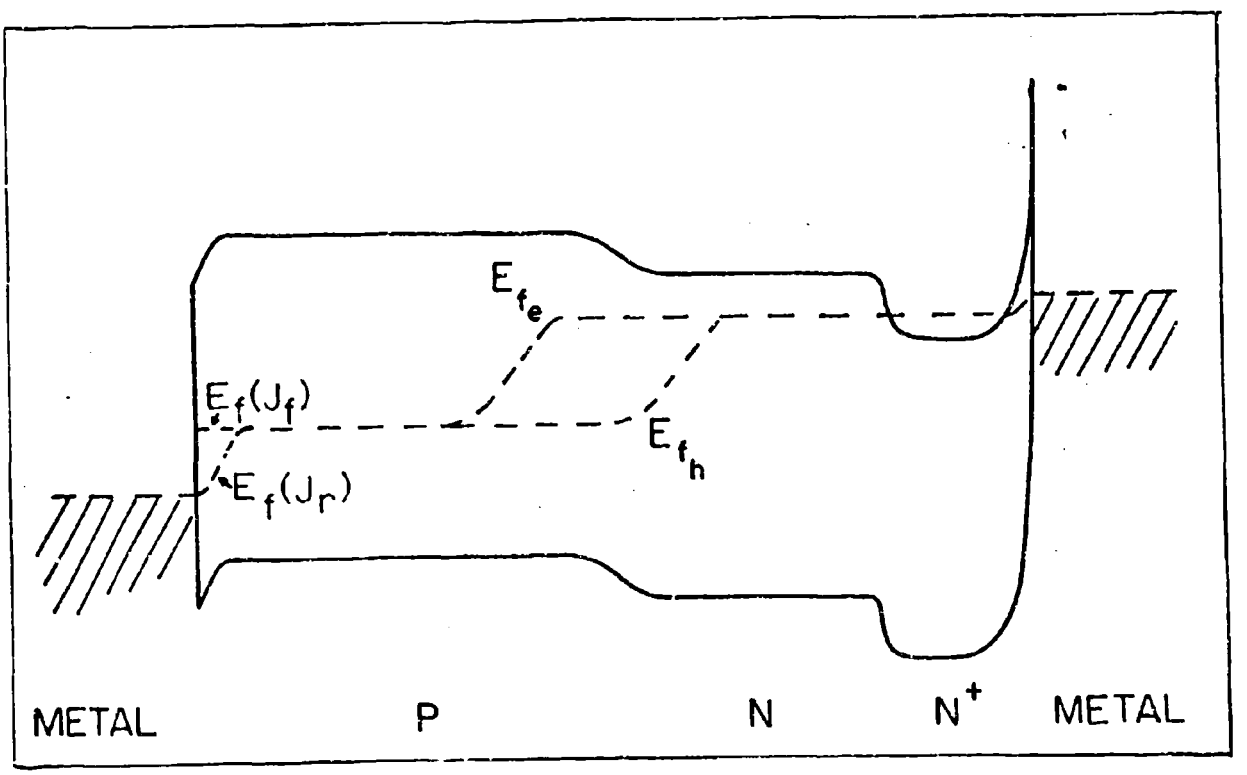

Figure 2

metal). Since many recent investigations of Schottky barriers have concentrated on the forward current-voltage characteristic, it is apparent that the relationship between the forward and reverse characteristics is of considerable practical importance. This is especially true if device current requirements in effect demand that a contact be operated in a nonlinear mode (i.e., somewhat outside the range of the zero bias resistance).

1. General Theory

The general shape of the current density, J, or dynamic resistance, R, versus applied forward bias, V_f, can be deduced by considering the currents associated with the flux of carriers J_f which tunnel toward, and J_r which tunnel away from, the metal surface. From experience of the near linearity of $\ell n\ J$ versus V_f for $V_f >> kT/q$, it is reasonable to express J_f versus V_f in the form

$$\ell n\ J_f = \ell n\ J_s + qV_f/nkT \qquad (1)$$

where J_s and n are empirical parameters which are slowly varying functions of V_f and may or may not be strong functions of temperature. If J_f and J_r are dominated by the current from the tails of the carrier distribution in the metal and semiconductor,

$$\ell n\ J_f = \ell n\ J_r + qV_f/kT \quad . \qquad (2)$$

This relationship is required because the corresponding incident fluxes (i.e., before tunneling), J_{fi} and J_{ri}, must satisfy the condition

$$dJ_{fi}/dE = (dJ_{ri}/dE) \exp (qV_f/kT) \qquad (3)$$

where E is any energy in the Maxwell-Boltzmann carrier distributions. Since

$$J_f = \int_0^\infty \tau(E)(dJ_{fi}/dE)\, dE \tag{4}$$

the transmission coefficient, $\tau(E)$, is independent of the direction of incidence, and a corresponding relationship holds for J_r, Equation (2) must hold. At zero bias Equation (3) reduces to an illustration of the principle of detailed balance. Thus

$$J = J_f - J_r = J_s \exp(qV_f/nkT)[1 - \exp(-qV_f/kT)] \tag{5}$$

In addition

$$R_c \equiv \left.\frac{dV_f}{dJ}\right|_{V_f = 0} = \frac{kT}{qJ_s} \tag{6}$$

and

$$\frac{R}{R_o} = \frac{n \exp(-qV_f/nkT)}{1 + (n-1)\exp(-q\,V_f/kT)} \tag{6a}$$

where $1/R$ is the diode conductance per unit area. R exhibits a maximum at a voltage V_{fm} given by[2]

$$V_{fm} = \frac{2kT}{q} \ell n\,(n-1) \tag{7}$$

In Figure 3 $|J|/J_s$ is shown as a function of V_f/kT.* Note that when $n = 2$, the $J\text{-}V_f$ relationship is symmetrical. When $n > 2$, the direction of easy current flow becomes the reverse direction. When $n \gg 2$, the forward direction exhibits near saturation and the reverse characteristic

---

* The asymptotic log plots for both forward and reverse polarities extrapolate to unity at $V_f = 0$. The n values have been chosen in pairs which satisfy the relationship, $1/n_1 + 1/n_2 = 1$ to illustrate the mirror symmetry about $V_f = 0$ between the $J\text{-}V_f$ characteristics of normal and backwards diodes.

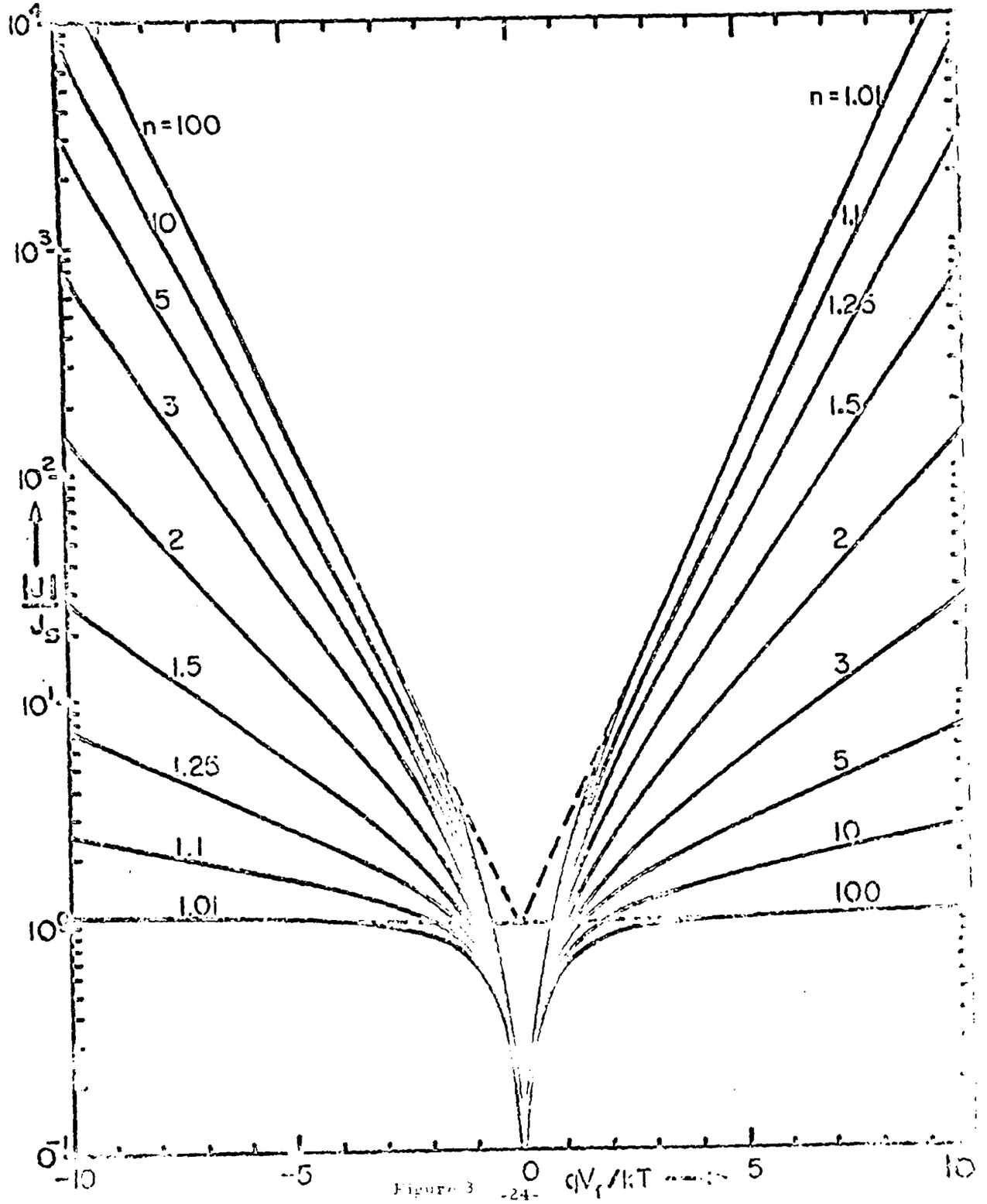
n = 100
10
5
3
2
1.5
1.25
1.1
1.01
n = 1.01
1.1
1.25
1.5
2
3
5
10
100
J_s [J]
10^3
10^2
10^1
10^0
10^{-1}
-10
-5
0
5
10
qV_f/kT

Figure 3

varies approximately as exp $(-qV_f/kT)$. This feature of exhibiting the "wrong" direction of easy current flow was first predicted from tunneling theory.[3] The thermionic-emission theory,[4],[5] which predicts the direction of easy current flow correctly for lightly doped semiconductors, was long thought to be the only correct result. Since larger n values at a given temperature can be associated with increased semiconductor doping concentrations,[1,6] both theories actually have mutually exclusive conditions under which they are applicable. From Figure 3 it is clear that, if $n >> 2$, reverse current densities much greater than J_s can be drawn without incurring a contact voltage drop much greater than kT/q. For forward biased devices, such a tunneling contact should thus prove superior to an accumulation contact from the point of view of current-carrying capability and independence of temperature.

Equations (5), (6), and (7) are of particular interest for device applications where linearity is important. Note that the zero bias resistance, R_o, is independent of n (although n and J_s may be implicitly related). For high-impedance reverse-biased Schottky barrier diodes used as varactors, Equation (6) is of particular importance. Appreciable departures of n from unity in the forward characteristic imply that for reverse voltages greater than $-V_{fm}$ the conduction mechanism will of necessity yield a rapidly decreasing resistance with increasing reverse bias.

2. T-F Emission Theory

The current-voltage relationship for T-F emission in Schottky barriers has recently been re-evaluated.[1] This work assumed a band-bending parabolic with distance within the body of the semiconductor (see Figure 4) and the WKB approximation for the tunneling probabilities for electrons incident on the barrier. Image forces are neglected and a constant tunneling effective mass is assumed (1-band approximation). The approach differs from earlier work in that the current density is computed by integration over the complete Maxwell-Boltzmann distribution of incident carriers rather than by an analytical approach which requires the assumption

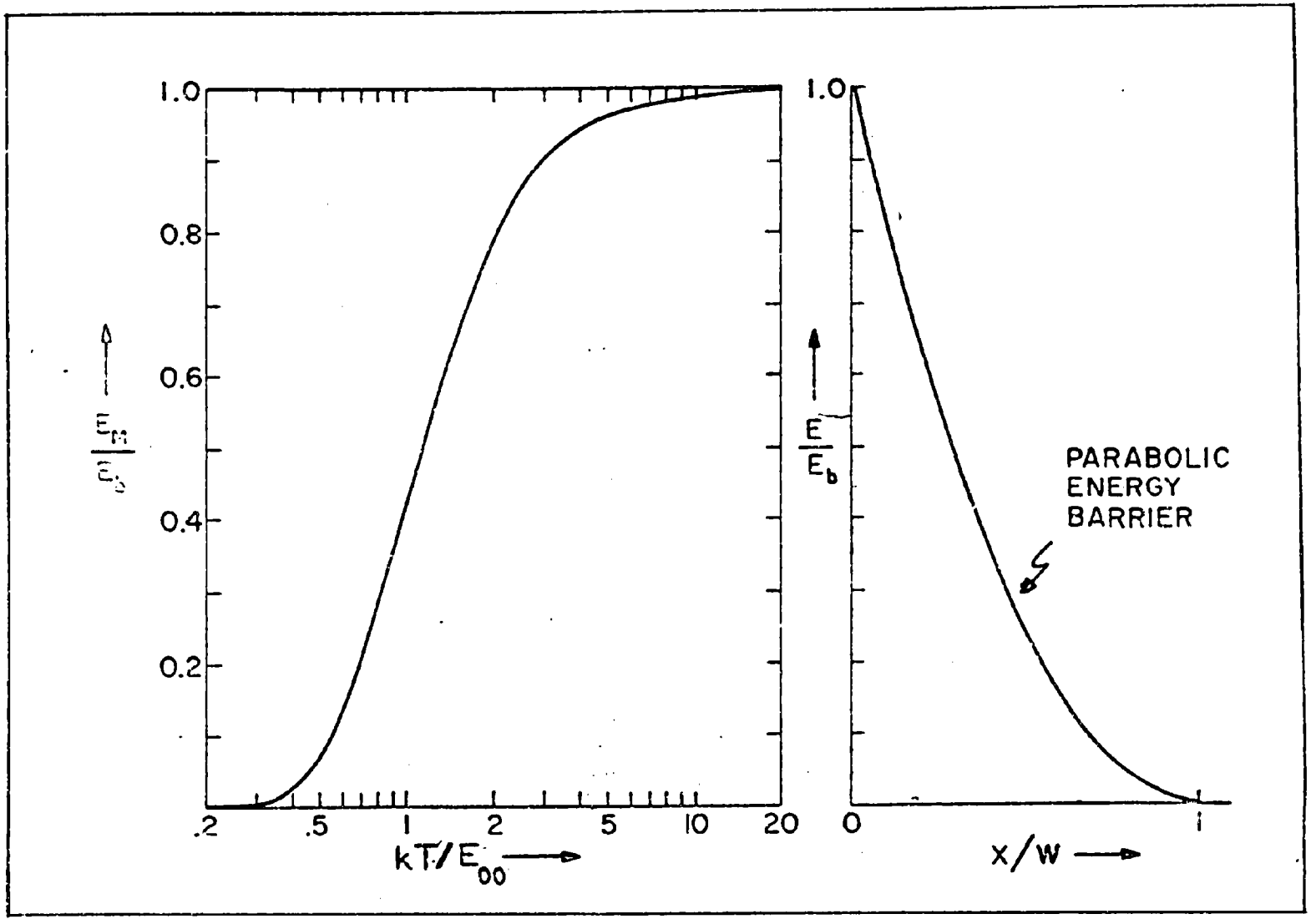
1.0
0.8
0.6
0.4
0.2
.2
.5
1
2
5
10
20
kT/E00
1.0
0
1
x/W
PARABOLIC
ENERGY
BARRIER

Figure 4

of a Gaussian distribution of emitted carriers.[6] The results are summarized here in a compact graphical form which permits relatively straightforward application. The Gaussian approach is a good approximation only when $kT \approx E_{oo}$ where

$$E_{oo} \equiv \frac{qh}{4\pi}\left[\frac{N}{m^* \epsilon}\right]^{-1/2} \tag{8}$$

is the proportionality constant between the logarithm of the WKB transmission coefficient of the barrier at its greatest width and the semiconductor band bending, E_b, i.e.,

$$\tau_{WKB}(E=0) = \exp\left(-E_b/E_{oo}\right) \quad . \tag{9}$$

N is the doping concentration in the semiconductor, m^* the component of effective mass in the tunneling direction, and ϵ the semiconductor static permittivity. The energy at which the maximum contribution to the current occurs, E_m, is shown in Figure 4 as a function of (kT/E_{oo}). Note that E_m is linearly proportional to E_b for any given value of kT/E_{oo}[1]:

$$E_m = E_b\left[\cosh\left(E_{oo}/kT\right)\right]^{-2} \quad . \tag{10}$$

The E_m versus E_b relationship leads to simple criteria for the bias limits for T-F emission. When E_m falls to the Fermi level in the metal, the maximum reverse bias $V_{r\,max}$ has been reached. Since

$$E_b = q(\varphi_b - V_f - \varphi_s) \quad , \tag{11}$$

where $q\varphi_b$ is the barrier energy relative to the Fermi energy in the metal and $-q\varphi_s$ is the Fermi energy in the semiconductor relative to the bulk conduction band edge,

$$V_{r\,max} = \varphi_s + \varphi_b\left[\sinh\left(E_{oo}/kT\right)\right]^{-2} \quad . \tag{12}$$

If the semiconductor is degenerate (negative φ_s), the forward bias limit, $V_{f\,max}$, for T-F emission will be reached when E_m falls to the Fermi energy in the semiconductor. From this criterion

$$V_{f\,max} = V_{r\,max} \sinh^2(E_{oo}/kT) \tag{13}$$

The current density J is expressed in units of J_m, the "flat-band" Maxwell-Boltzmann current density incident on the barrier from the bulk of the semiconductor. The parameters n and (J_{ma}/J_m) were computed for a range of values of E_b/kT and kT/E_{oo}. The quantity J_{ma} is the apparent flat band value of J_f when ℓnJ_f versus E_b is extrapolated linearly to $E_b = 0$: the defining equation for J_{ma} is thus

$$\frac{J_f}{J_m} = \left[\frac{J_{ma}}{J_m}\right] \exp(-E_b/nkT) \tag{14}$$

The saturation current density in Equation (1) can then be expressed as

$$J_s = \left[\frac{J_{ma}}{J_m}\right] J_m \exp\left[-q(\varphi_b - \varphi_s)/nkT\right] \tag{15}$$

where

$$J_m = A^*T^2 \exp - q\varphi_s/kT \tag{16}$$

and A^* is the Richardson constant for the semiconductor majority carrier.[5], [7]

The correlation of experimental and theoretical results can be simply accomplished from Figures 5 and 6. In Figure 5 the quantity (n-1) has been chosen as the ordinate because the departure of n from unity in general provides information about the departure of the diode from the ideal thermionic-emission model. Since n is not a rapidly varying function of E_b/kT, it is possible to determine kT/E_{oo} from Figure 5. Thus the relationship between n and the semiconductor doping is predicted [see Equation (8)].

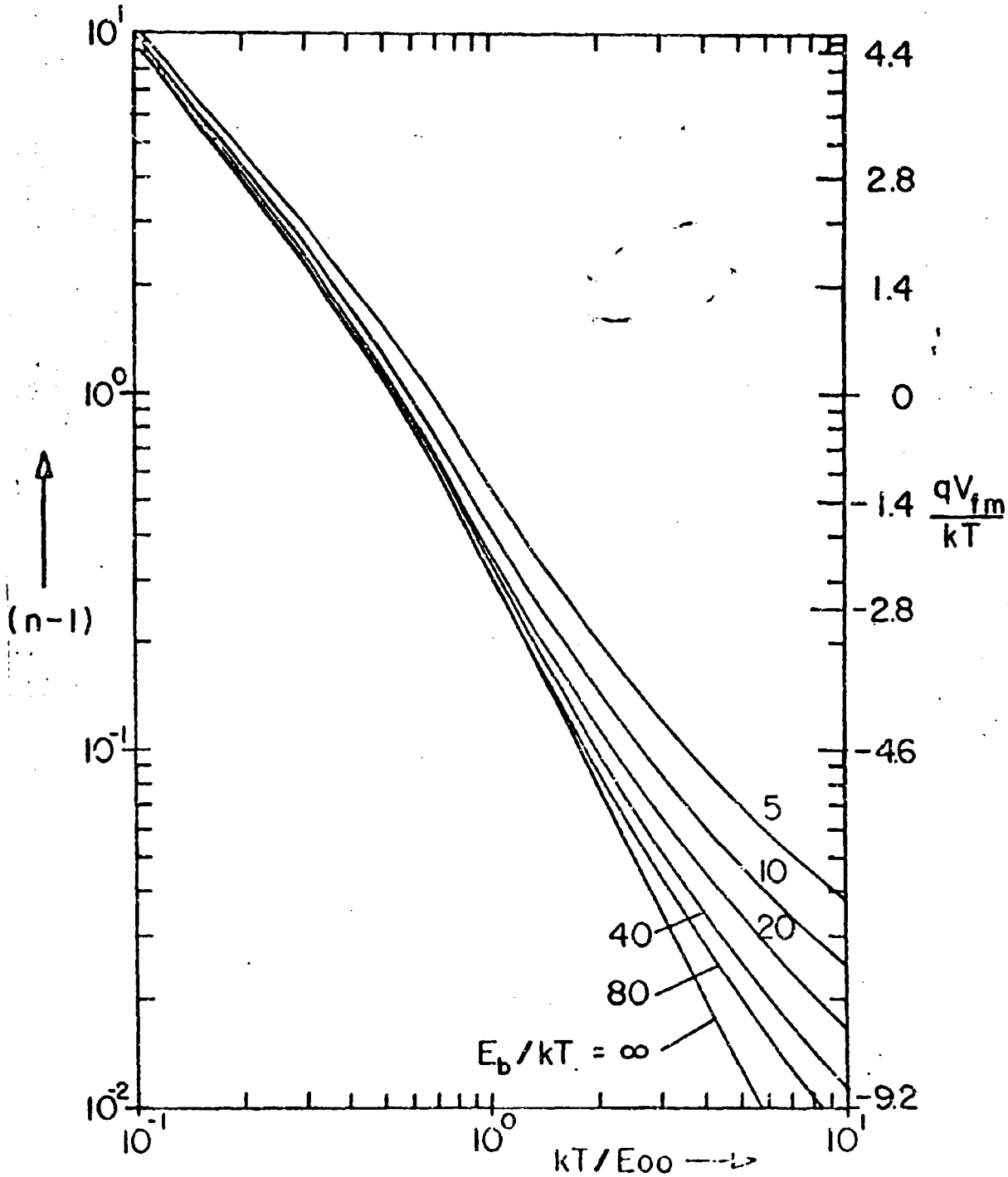
10^1
10^0
10^-1
10^-2
10^-1
10^0
10^1
kT / Eoo
(n-1)
4.4
2.8
1.4
0
-1.4
-2.8
-4.6
-9.2
qV_fm / kT
5
10
20
40
80
E_b / kT = ∞

Figure 5

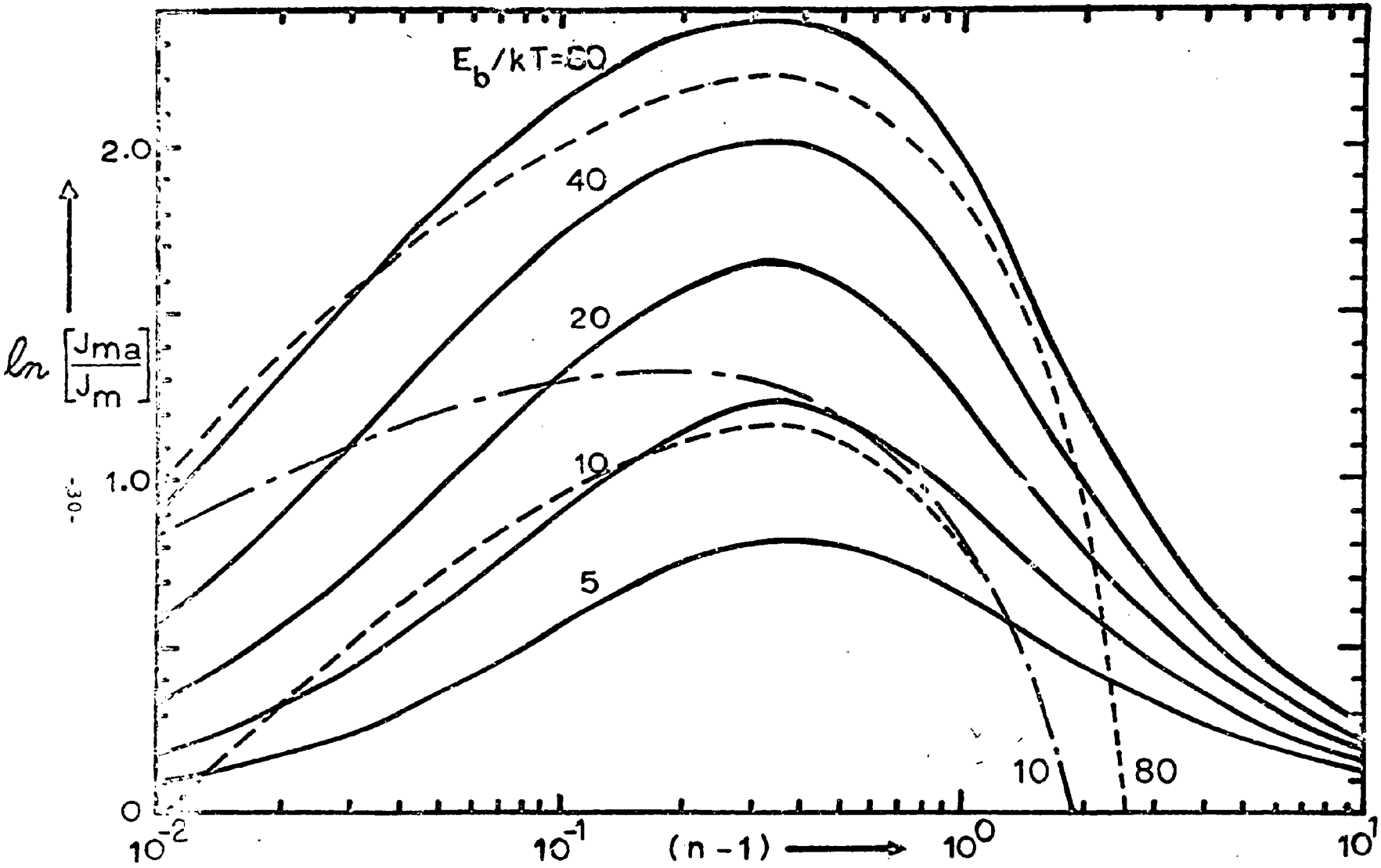
$E_b/kT=\infty$
40
20
10
5
2.0
1.0
0
$\ln\left[\frac{J_{ma}}{J_m}\right]$
10
80
10^{-2}
10^{-1}
$(n-1)$
10^{0}
10^{1}

Figure 6

In Figure 6 $\ell n\ (J_{ma}/J_m)$ is shown as a function of (n-1) for selected values of E_b/kT rather than as a function of kT/E_{oo} and E_b/kT [1]. This has been done to eliminate the determination of kT/E_{oo} as an intermediate step in relating the barrier height and the J-V characteristic:

$$\varphi_b = (1-n)\,\varphi_s + \frac{nkT}{q}\,\ell n\left[\frac{A^*T^2}{J_s}\left(\frac{J_{ma}}{J_m}\right)\right] \quad . \tag{17}$$

3. Analytic Approximations

The curve for $E_b/kT \to \infty$ in Figure 5 is that derived using the assumption of a Gaussian distribution of emitted carriers [6]:

$$n = \frac{E_{oo}}{kT}\coth\left(E_{oo}/kT\right) \quad . \tag{18}$$

This result is a reasonable approximation when $kT \lesssim E_{oo}$ for a wide range of values of E_b/kT.*

---

*This result can also be used to approximate the maximum n value, n_M, associated with T-F emission in a given diode. This value occurs at the low temperature limit, T_m, below which T-F emission vanishes from the J-V characteristic (i.e., when $V_{max} = 0$ in Equation (12)). Then

$$\sinh\left(E_{oo}/kT_m\right) = \left(-\varphi_b/\varphi_s\right)^{\frac{1}{2}} \tag{18a}$$

and

$$n_M = \frac{\varphi_b - \varphi_s}{\varphi_b}^{\frac{1}{2}}\sinh^{-1}\left[\left(\frac{-\varphi_b}{\varphi_s}\right)^{\frac{1}{2}}\right] \tag{18b}$$

This relationship shows how the range of n values between field emission and thermionic emission (where $n \approx 1$) decreases when the semiconductor doping is increased.

The dashed curves in Figure 6 for $E_b/kT = 10$ and 80 are derived from Equation (18) and from the semi-empirical relationship

$$\frac{J_{ma}}{J_m} = \left\{\pi \left[\frac{E_b}{kT}\right]\left[\frac{E_{oo}}{kT}\right] \tanh (E_{oo}/kT)/\cosh^2(E_{oo}/kT)\right\}^{1/2} \qquad (19)$$

A value of J_{ma}/J_m a factor of $\sqrt{2.718}$ less than this is the actual prediction based on an assumed Gaussian energy distribution of the tunneling carriers. There are appreciable errors in Equation (18) for the n versus kT/E_{oo} relationship when $kT > E_{oo}$ and there are also appreciable errors in the (J_{ma}/J_m) versus kT/E_{oo} relationship under the same conditions.[1] Analytic approximations should thus be used with care in the high temperature range and in particular should not be used to determine kT/E_{oo}. There is, however, a considerable compensation of errors in Equations (17) and (18) when the J_{ma}/J_m versus (n-1) relationship is calculated. A relationship analogous to Equation (19)[6] (the dashed line for $E_b/kT = 10$ in Figure 6) lacks the term in $\tanh (E_{oo}/kT)$ and thus becomes a progressively poorer fit as the temperature is increased. Both analytic approximations to (J_{ma}/J_m) fail badly when $n \gtrsim 3$ and in the limit as $n \to 1$. Note that the computer-based values of J_{ma}/J_m approach unity at high and low values of kT/E_{oo}. These values are expected because thermionic emission dominates at high temperature and the barrier becomes essentially transparent when E_{oo} becomes very large.

4. Application and Discussion

The general and specific equations for T-F emission have not as yet been subject to a detailed experimental verification. Equation (4) has, in effect, been used to calculate barrier heights as a function of applied electric field for the case of thermionic emission.[8] The authors did not, however, perform independent barrier height measurements. J-V characteristics roughly equivalent to Equation (4) have also been reported,[6] but no measurement was made near zero bias. The region

near zero bias has also been studied in detail, but the results were not correlated with the asymptotic forward and reverse characteristics. Application of the present theory to these measurements on Au-GaAs diodes and measurements on W-GaAs[10] have, however, reduced the discrepancy between barrier heights deduced from the J-V characteristics and from capacitance-voltage and photo-response characteristics.[1] The measurements which at present come closest to representing a detailed study of an "ohmic" contact under approximately practical operating conditions ($T \gg 0^{\circ}K$) are those taken recently[11] on chromium-n-type silicon Schottky barriers at $77^{\circ}K$; these data subsequently fitted by Equation (6) are shown in Figure 7. For this system the criterion for T-F emission is only satisfied at zero bias above $\approx 120^{\circ}K$. Thus an exact fit is not expected. For $V_f \gtrsim 2kT/q$, however, the R versus V_f characteristic can be represented by Equation (6) using single values of n and J_s. The barrier height and doping concentration which correlate with n and J_s are also in reasonable agreement with the barrier height measured on more lightly doped silicon and the doping concentration measured by Hall effect measurements (7×10^{18} cm^{-3}). For comparison a $0^{\circ}K$ theoretical prediction using the Murphy and Good approach is also shown in Figure 7. This prediction shows more structure in the R versus V_f characteristic than the T-F result and about the same ratio of the maximum dynamic resistance to the zero bias resistance.

The present approach should not, however, be applied to extremely heavily doped contacts such as would be required for devices operating at high current densities. Equation (12) implies that the maximum doping for which the theory should apply to silicon at $300^{\circ}K$ is $\approx 5 \times 10^{19} cm^{-3}$. Then $J_m \approx 6 \times 10^7$ amps/cm^2 and $E_{oo} = 0.076$ eV. For a barrier height ≈ 0.6 eV, $n \approx 3$, and the average transmission of the barrier is $\approx 10^{-3}$. This would imply that $J_s \approx 6 \times 10^4$ amps/cm^2.

The above may be a somewhat pessimistic prediction of J_s for the following reasons:

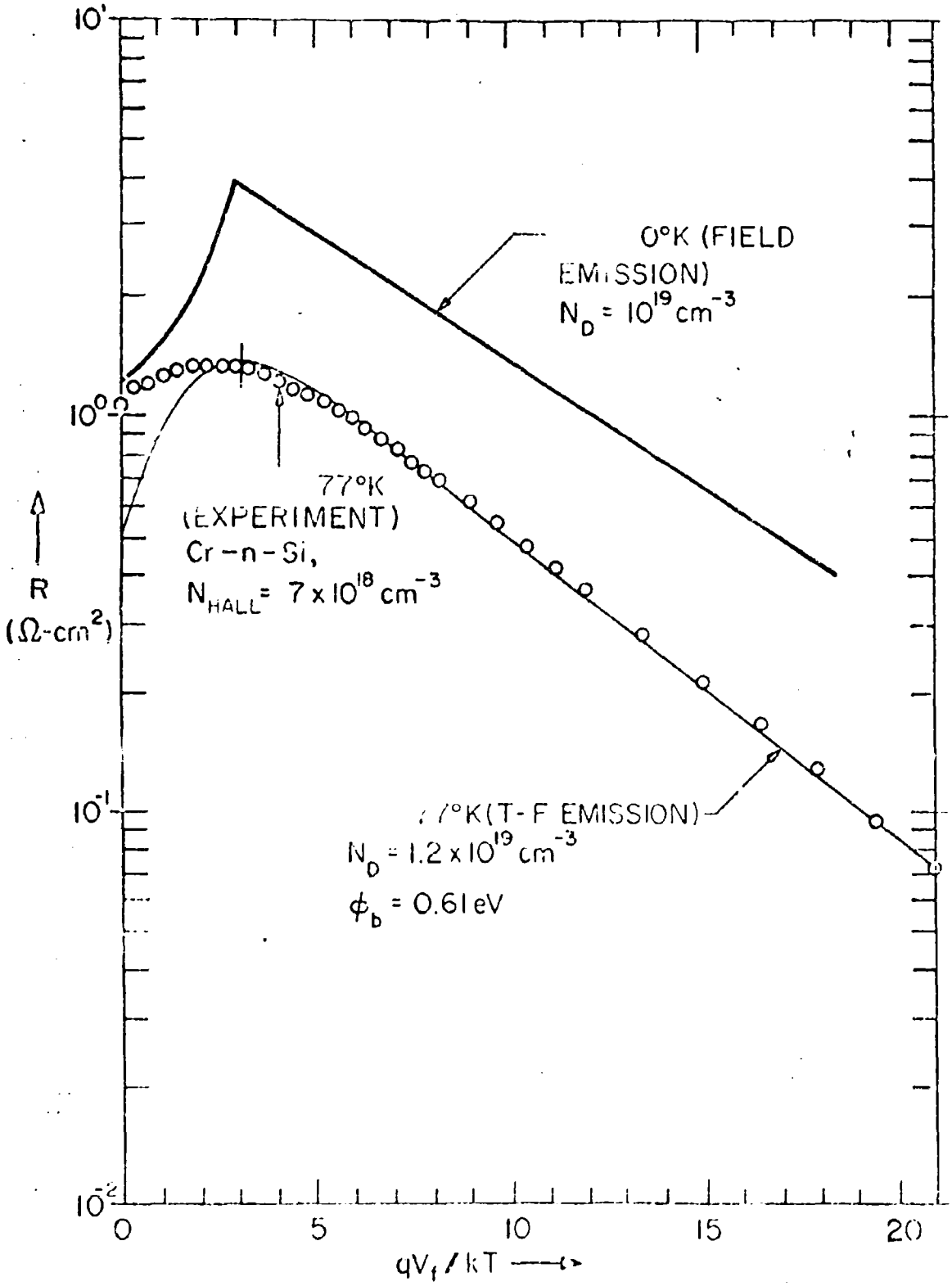
10'
10^0
10^-1
10^-2
R
(Ω-cm^2)
0°K (FIELD
EMISSION)
N_D = 10^19 cm^-3
77°K
(EXPERIMENT)
Cr-n-Si,
N_HALL = 7 x 10^18 cm^-3
77°K (T-F EMISSION)
N_D = 1.2 x 10^19 cm^-3
φ_b = 0.61 eV
0
5
10
15
20
qV_f / kT

Figure 7

1. Image force effects have been neglected. Preliminary results[12] indicate that, as this doping is approached, the image force lowering becomes an appreciable fraction of the band bending and the barrier width is also reduced appreciably. The importance of this latter factor appears not to have been previously appreciated. The transition from thermionic emission to field emission also occurs over a smaller range of temperature than for lightly doped semiconductors. The role of the image force is of considerably lesser importance for lightly doped semiconductor .

2. Lack of barrier pinning due to interface effects[8] has also not been considered. At very heavy doping, however, the interface layer needed to produce such lowering may itself restrict the saturation current density.

There is an additional factor which should contribute to a decrease in J_s. At heavy doping, Nw^3, the number of impurity atoms contained within a cube with edge dimensions equal to the nominal depletion layer width, w, becomes comparable to or less than unity. The barrier then cannot be truly described by a 1-dimensional model. The electron wavelength transverse to the barrier is then, however, usually large in comparison with w. Thus, the average barrier seen by a tunneling electron does tend towards the 1-dimensional picture.

References

1. C. R. Crowell and V. L. Rideout, Solid State Electronics 12, 89 (1969).
2. C. R. Crowell and V. L. Rideout, Appl. Phys. Ltrs., 14, 85 (1969).
3. A. H. Wilson, Proc. Roy. Soc. (London) A136, 487 (1932).
4. H. A. Bethe MIT Radiatior Laboratory Report 43/12 (1942).
5. C. R. Crowell, Solid State Electronics, 8, 395 (1965).
6. F. A. Padovani and R. Stratton, Solid State Electronics, 9, 965 (1966).

7. C. R. Crowell, Solid State Electronics 12, 55 (1969).

8. C. R. Crowell and S. M. Sze, Solid State Electronics 9, 1035 (1966).

9. F. A. Padovani, Solid State Electronics, 11, 193 (1968).

10. C. R. Crowell, J. C. Sarace, and S. M. Sze, Trans. Metal Soc. AIME 233, 478 (1965).

11. A. N. Saxena, Appl. Phys. Ltrs., 14, 11 (1969).

12. V. L. Rideout and C. R. Crowell, to be published.

1.1.7 Growth and Evaluation of GaAs and $Ga_{1-x}In_xAs$ Thin Films

DA-31-124 ARO-D-450, Army Research Office, Durham

GK 2908, National Science Foundation

J. M. Whelan

1.1.7.1 General

During the period of this progress report, work has continued on the growth and evaluation of GaAs and $Ga_{1-x}In_xAs$ thin films and related technology.

Films were grown on GaAs substrates from a Ga solution at 800-825°C. This technique is called liquid phase epitaxial growth. The Ga melt which is saturated with undoped GaAs is contained in a quartz crucible. The GaAs substrate is lowered into the melt and the temperature is lowered to grow the film. Close control of the furnace temperature allows accurate control of film thickness. Suitable thickness control in the range of 1-15 μm has been demonstrated. More details on this technique and experimental results may be found in Ralph Dawson's Ph.D. Thesis, reference).

It is anticipated that this technique will be of considerable importance in the fabrication of devices using GaAs material. In particular,

preliminary work was begun to investigate the feasibility of using this technique for the fabrication of Schottky barrier diodes, Gunn oscillators, bipolar and field effect transistors, light emitting diodes and solar energy converters.

The above technique has been applied to the growth of $Ga_{1-x}In_xAs$ thin films on a GaAs substrate. The results of this work are summarized in section 1.1.7.2.

Related to the problem of growing good thin films is the problem of making good ohmic contacts. Considerable progress has been made in this area. A new technique has been developed for making ohmic contacts to n^+ GaAs material. The results of this work are given in detail in section 1.1.7.3, as well as a summary of the preliminary work on a GaAs junction field effect transistor.

A new apparatus for growing films was designed and fabricated. One of the features of the new apparatus is the provision for growing three layered structures. Other convenience features were incorporated which make it easier to operate.

Work was begun on a new type of apparatus to quantitatively analyze the trace amounts of impurities in the GaAs films by using a sputtering technique and spectroscopic analysis.

Reference

1. L. R. Dawson, "Growth of Thin Epitaxial GaAs Films From Ga Solutions", Ph.D. Thesis, University of Southern California, Electrical Engineering.

1.1.7.2 Hetero-epitaxial Growth of Alloy Films from Solution

C. T. Li and J. M. Whelan

The effects of H_2 gas ambient on a GaAs substrate surface at 850°C were investigated. In order to protect the highly polished substrate surface from pitting by erosion or decomposition, an equilibrium

As vapor pressure is needed over the GaAs substrate as well as an O_2 free H_2 gas ambient.

A modified, more leak-tight apparatus was designed and constructed, into which near equilibrium As vapor can be introduced into the H_2 gas stream before it enters the growth zone. Better and smoother GaAs epitaxial films were grown in this new apparatus.

The same apparatus was used to grow hetero-epitaxial $Ga_{1-x}In_xAs$ alloy thin films on $<\bar{1}\,\bar{1}\,\bar{1}>$ GaAs substrates. Smooth and uniform alloy films were grown at 850°C with In content up to 5.1% and thickness in the range of $10\mu \sim 25\mu$. Attempts to grow higher In content alloy films resulted in erratic, twinned and uneven growth.

Because the nucleation difficulty in growth from a metallic rich solution as in case of Ga + In + As system, attempts were made to grow films from a pseudo-binary solution of two pure III-V compounds. The GaSb + GaAs system was chosen due to available GaAs substrates, low Sb vapor pressure, and compatible with the temperature setting of our furnace. Uniform hetero-epitaxial alloy films were grown on $<\bar{1}\,\bar{1}\,\bar{1}>$ and <111> GaAs substrates at 860°C and at 810°C. Lower Sb content of alloy films grown on <111> GaAs than grown on $<\bar{1}\,\bar{1}\,\bar{1}>$ GaAs at same temperature was found. The Sb content is 8.2% in the alloy film grown at 810°C on $<\bar{1}\,\bar{1}\,\bar{1}>$ GaAs substrates.

Alloy compositions were estimated by Vegard's law. The lattice constant of alloy film was determined by measuring the separation of alloy x-ray diffraction peak to GaAs peak. Since alloy films thickness are in the range of $10\mu \sim 25\mu$, both GaAs and alloy peaks can be obtained and well separated in {444} x-ray diffraction pattern. Laue back diffraction patterns also were taken, and indicated the growths of perfect hetero-epitaxial alloy films on the GaAs substrate.

A few of the samples were sent to other U.S.C. laboratories and to outside laboratories to make an independent composition analysis using an electron beam microprobe. New instrumentation is being

constructed in this laboratory to analyze the alloy composition using spectroscopic techniques.

1.1.7.3 Ohmic Contacts to GaAs and Fabrication of GaAs Junction Field Effect Transistor

L. T. Yuan and J. M. Whelan

Since ohmic contacts play an important role in the performance of sophisticated GaAs devices, a good ohmic contact not only requires the linear current-voltage relationship but also requires low contact resistance, planar interface and shallow penetration. During this period of research, a simple method of making ohmic contacts to n-type GaAs has been developed which gives reliable and reproducible results. The method described here makes use of the chemical reaction in a chemical cell to transport tin onto a gold-plated GaAs sample. The chemical cell consists of a molten salt mixture ($SnCl_2$, KCl, NHaCl) as the electrolyte, an Au-Sn alloy as one electrode and the Au-plated GaAs as another electrode. By short-circuiting the two electrodes in the chemical cell at a temperature of 267°C, tin is transported onto the Au-plated GaAs sample until equilibrium of the cell is reached. Immediately after tin-transport, the Au-tin coated sample is nickel-plated and then followed by alloying in nitrogen atmosphere at 375°C for two minutes. The temperature for tin-transport was so chosen that the Au-Sn alloy forms two phases; namely, the $AuSn_2$ solid and A Sn liquid, thereby preventing the Au from melting off in the tin solution. While the alloying temperature was chosen such that it was high enough to melt the Au-Sn alloy into liquid to give good melting, the nickel is merely a protection layer which prevents the Au-Sn alloy from balling up during alloying.

Ohmic contacts to n^+-GaAs with specific contact resistance within the order of $10^{-5}\ \Omega\ cm^2$, penetration depth less than 0.2 μm and planar interface were obtained on a reproducible basis. Using the same method, ohmic contacts were also successfully made to high resistivity

n-type GaAs of 126 Ω-cm.

On the p-type contacts, electroplated Ni-Au-In was found to be ohmic for p^+ GaAs, which is therefore applicable for the p^+ gate contacts in the n-channel junction field effect transistors.

During this same period, a mesa process has been developed for the fabrication of junction field effect transistors, which was able to control the channel width with accuracy by chemical etching techniques. Device configurations were much better defined by use of photolithographic techniques.

We anticipate that in using these techniques in the fabrication of field effect transistors and Gum oscillators, the device performance will be greatly improved.

1.2 QUANTUM ELECTRONICS AND LASERS

1.2.1 Quantum Electronic Investigation of Cross-Relaxation in Rare-Earth Crystals

NGR-05-018-044, National Aeronautics and Space Administration

L. G. DeShazer, L. M. Hobrock, M. M. Mann, E. A. Maunders, D. K. Rice

Knowledge of relaxation processes in laser media is currently of great importance in understanding the interaction of radiation with optically pumped media. We are studying relaxation effects in laser amplifiers and oscillators, particularly the mode-locked operation of laser oscillators. We have concentrated our examination on neodymium crystals and neodymium glass as the laser media. This work is directed towards development of models for the operative relaxation mechanisms, and determination of rate equations for the spectral flux and spectral inversion density.

Details of this investigation for the semiannual period are described in four publications from this laboratory and are briefly summarized below:

1. Spectral broadening of rare-earth ions in laser media.[1,2,3]

The processes responsible for the broadening of spectral lines are also those processes involved in relaxation phenomena. This program is studying classical experimental procedures of determining line broadening parameters of rare-earth ions in solid hosts. Systematic spectroscopic studies were made on trivalent neodymium ions in various laser glasses. Analysis of the absorption and fluorescence spectra and their temperature dependence (from 4 to 300°K) determined the energy levels and linewidths of neodymium. The complete splitting of the low-lying multiplets showed that neodymium ions occupied sites of low symmetry in glass. The magnitude of the splittings correlate closely with those determined from Nd_2O_3 crystals. There was no thermal variation of

linewidths, indicative of inhomogeneous broadening.

Due to the complexity of neodymium spectra, spectral broadening of europium ions in glass was studied to support these results on neodymium glass. The spectrum of europium contains many simple features greatly assisting this analysis; in particular, the transition between the singlet $^5D_0$ and $^7F_0$ levels is isolated from adjacent fluorescence or absorption. The absorption and fluorescence spectra of europium ions in two different glass hosts were studied in the range 4000 to 9000 Å as the sample temperature was varied from 4 to 310°K.

The primary broadening mechanism for the europium ion in glass is inhomogeneous arising from the heterogeneity of the ion environment. A secondary broadening mechanism is the asymmetric broadening resulting from the ion occupying two preferential sites of low symmetry. The $^5D_0$ -- $^7F_0$ line was found to consist of two inhomogeneous lines closely spaced and giving an asymmetry to the overall lineshape on the short wavelength side. A marked asymmetry occurs in the other fluorescence and absorption lines. Each component of the $^5D_0$ -- $^7F_0$ line was studied as a function of temperature; the results show that the linewidth, oscillator strength, and peak wavelength are independent of temperature in this range. Verification of multiple site occupation was obtained by studying the fluorescence and absorption spectra of single crystals of $Eu:Gd_2O_3$ at 4°K. The results show that the europium ion occupies three preferential sites in this crystal. The important result of this research is the demonstration that the rare-earth ion appears to have a crystalline local environment.

2. Cross-relaxation processes between ions in a laser amplifier.[4]

The laser injection oscillator experiments demonstrated their feasibility in studying ionic relaxation. Now a new experiment is being constructed utilizing amplification of saturating giant-pulse laser radiation. No results from this experiment have as yet been obtained. Experimental determination of the local anisotropy in glass as suggested above is possible from this laser experiment by measuring the functional dependence of the

saturation of a polarized amplified signal.

References

1. L. G. DeShazer and M. M. Mann, "Low-Temperature Suppression of Absorption from Excited Levels", J. Opt. Soc. Am. 59, no. 4 (1969).

2. M. M. Mann and L. G. DeShazer, "Energy Levels and Spectral Broadening of Neodymium Ions in Laser Glass", Phys. Rev., to be published.

3. D. K. Rice and L. G. DeShazer, "Spectral Broadening of Europium Ions in Glass", to be published.

4. L. G. DeShazer and E. A. Maunders, IEEE J. Quan. Elect. QE-4, 642 (1968).

1.2.2 Intensities of Crystal Spectra of Rare-Earth Ions

AF-AFOSR-69-1622, Joint Services Electronics Program

M. M. Mann, T. S. LaFrance, and L. G. DeShazer

In this program the mechanisms which give rise to parity-forbidden transitions in the spectra of rare-earth ions in crystals are being investigated. The parity-forbidden transitions are the most commonly occuring transitions in rare-earth ions, and all presently observed laser action in rare-earth crystals is due to these transitions. The present theories of laser action in rare-earth crystals treat transition probabilities in a phenomenological manner. In order to develop a more fundamental description, it is necessary to have a suitable model for the transition probabilities. Thus, it is hoped that this study will lead to a more fundamental understanding of laser processes in rare-earth crystals. Also, this understanding will hopefully help choose the "best" laser host for rare-earth ions, a very illusive host at present.

1. Atomic radiation in anisotropic media.

The anisotropy of the crystalline host must be known to permit comparison of the intensity measurements with existing theoretical

predictions. Other investigations have not considered the anisotropy effects on crystal spectra; therefore, a theoretical analysis of atomic radiation in anisotropic media was made for non-resonant, linear and lossless media.[1,2] The derived expressions provide an analytical means of relating oscillator strengths to measured intensity data. This analysis is being extended to biaxial media.

It also has been shown that the multipole intensity distribution sensitively reflects microscopic dielectric properties of the host.[3] No general expression can be given for the local field parameters; a suitable analytical model must be chosen for each case. Such models have been formed for Eu:$LaCl_3$ and Eu:YVO_4.

2. Enforced electric dipole transitions of rare-earth ions.

Both the initial and final states associated with the emission transitions of interest belong to the same electronic configuration. Then, two types of radiation in crystal spectra must be considered: a) magnetic dipole and electric quadrupole which also occur in the free ion spectra, b) electric dipole which does not occur in the free ion spectra but does in the crystal spectra. This parity-forbidden electric dipole radiation is called enforced electric dipole radiation, and occurs due to the interaction of the rare-earth ion with the electric field of the crystal. Judd[4] and Ofelt[5] have shown that the parity restriction is removed and that a substantial admixture of 4f and 5d wavefunctions occurs when the rare-earth ion is not located at an inversion center. We have studied the fluorescence oscillator strengths of the transitions of europium in YVO_4 crystals, and are presently fitting the Judd-Ofelt model to this data. The interest in Eu:YVO_4 stems from the three-parameter model for the D_{2d} symmetry.

References

1. M. M. Mann and L. G. DeShazer, "Atomic Multipole Radiation in Anisotropic Media", Phys. Rev., to be published.

2. M. M. Mann and L. G. DeShazer, "Atomic Multipole Radiation in Anisotropic Media", paper presented at the Meeting of the Optical Society of America, San Diego, California, March 11-14, 1969.

3. M. M. Mann and L. G. DeShazer, "Spectroscopic Determination of Local Field Parameters", Phys. Rev. Letters 22, 404 (1969).

4. B. R. Judd, Phys. Rev. 127, 750 (1962).

5. G. S. Ofelt, J. Chem. Phys. 37, 511 (1962).

1.2.3 Experimental Studies in Nonlinear Optics

AF-AFOSR-69-1622, Joint Services Electronics Program

G. L. McAllister, L. Huff and L. G. DeShazer

This experimental program is investigating the nonlinear effects in the propagation of light in organic liquids. The main emphasis in this program is on self-focusing effects and saturated absorption effects.

We have investigated shaping of the time contour of intense light pulses propagating through several materials having nonlinear refractive indices.[1,2] This effect, which occurs for peak powers below the level required to form trapped light filaments within the material, is a consequence of the dynamical self-focusing of intense optical beams. Previous measurements of optical self-focusing phenomena have relied upon determination of the input power threshold for the onset of stimulated inelastic scattering. By observing the pulse shaping the nonlinear response of the medium can be constructed. The measurements are independent of filament formation mechanisms and can be compared directly with numerical solutions of the nonlinear wave equation thought to describe self-focusing. We have investigated several nonlinear materials and have found critical powers for self-focusing by fitting the curves to the computer solutions. For nitrobenzene, the measured critical power was 19.5 kW.

The absorption of high power laser radiation by many organic materials reduces with increased laser power. This effect is due to saturation of optical transitions and/or photochemical changes induced by the laser radiation. Saturated absorbers have been investigated in the past for use in laser systems as passive light switches and modulators.

An experimental study was made to determine the transmission of several materials as a function of incident laser intensity.[3] Studies were conducted on several new classes of organic compounds, including indanthrone dyes and the amylose-iodine-iodide complex.[4]

The nonlinear absorption behavior of indanthrone was studied in detail.[5] This compound exhibits the interesting property of becoming opaque at intensities near ten megawatts per square centimeter. Consequently, this material is a candidate for use as a passive optical limiter. Asymmetric temporal shaping of the laser pulse transmitted by the indanthrone was investigated.

A theoretical analysis of rate-equation models was performed to explain these nonlinear absorption effects. For the materials in which the lifetimes were much less than the duration of the laser pulse, the steady-state solution of the equations was applicable. Analytical results for this case were obtained and fitted to the experimental data for cryptocyanine and the amylose-iodine-iodide complex.

References

1. G. L. McAllister, J. H. Marburger and L. G. DeShazer, "Observation of Optical Pulse Shaping by the Self-Focusing Effect", Phys. Rev. Letters 21, 1648 (1968).

2. G. L. McAllister and L. G. DeShazer, "Optical Pulse Shaping by the Self-Focusing Effect", to be presented at 1969 IEEE Conference on Laser Engineering and Applications, Washington, D.C., May 26-28, 1969.

3. L. G. DeShazer and L. Huff, "Saturated Absorption and Transmission of Laser Radiation by Organic Compounds", Meeting of the Optical Society of America, San Diego, Calif., March 11-14, 1969.

4. L. Huff, L. G. DeShazer and F. W. Schneider, "Laser Saturation of Optical Transitions in a Starch Component: the Amylose-Iodine-Iodide Complex", Science 163 (1969).

5. L. Huff and L. G. DeShazer, "Nonlinear Optical Behavior of Indanthrone Dyes", to be submitted.

1.2.4 Theory of Self Focusing of Intense Optical Beams

AF-AFOSR-69-1622, Joint Services Electronics Program
DA-ARO-D 31-124-6920, U.S. Army Research Office (Durham)

J. Marburger, E. Dawes, W. Y. Chen, N. Kadamoto,
R. Johnson

Prior to this reporting period, we had developed efficient computer programs which enabled us to analyze the dynamical behavior of intense optical beams traveling through media with an intensity dependent refractive index. The results of this analysis permitted for the first time a detailed quantitative comparison between theory and experiment. The experimental work was also performed at U.S.C. under the direction of Prof. L. DeShazer with whom we are working closely. To obtain a tractable theory it was necessary to discuss the optical intensity only at axial distances prior to the focal region. This work is reported in previous semiannual reports.

During this period we have begun to extend our theoretical analysis into the focal region in which many of the simplifying assumptions valid in the pre-focal region are severely violated. Preliminary experiments performed here and at the University of California at Berkeley indicate that the physical phenomenon which most influences the self focusing process near the focal region is stimulated inelastic (Raman and Brillouin) scattering. Since both of these processes lead to backward scattered radiation, the set of coupled wave equations describing the situation has "streaming derivatives" in both forward and backward directions as well as the radial dependence leading to self focusing and diffractive effects. This system of equations is much more difficult to solve numerically than that for the pre-focal region which had only two independent variables. Nevertheless a similar problem has been successfully analyzed numerically by W. Y. Chen under the direction of W. G. Wagner (see elsewhere in this report) and we have used the experience gained in that effort to obtain an efficient numerical solution scheme for the present problem.

While this analysis is not yet completed, we can present a picture of the behavior we expect on the basis of simple preliminary calculations. As always a quantitative theory can be obtained only for known incident intensity distributions. We assume that a single "giant pulse" of radiation from a ruby laser operating in single transverse and longitudinal modes enters a medium such as liquid CS_2 in which self focusing is known to occur. As the beam propagates, its transverse intensity distribution changes in a smooth way described by our previous work, and verified by experiment, until the intensity near the axis becomes large enough to cause appreciable scattering into Raman and Brillouin modes. These scattering processes determine the subsequent drain of power from the primary beam. Much power is lost to backward scattering causing the self focusing force to diminish. The ultimate size of the focal spot seems likely to be determined by the backward scattering rate although this must be verified by the more detailed calculation. Beyond the focus the beam diffracts out in a complicated manner determined by its new transverse distribution and the nonlinear properties of the medium. There is no reason to expect self "trapping" to take place in the manner envisaged by Chiao et al. Only a very special transperse distribution leads to stationary trapping of this type. Reported observations of "filaments" of light probably refer to unresolved pictures of the focal spot as it moves axially in response to the changing peak power during the laser pulse. The filament like phenomenon predicted by our previous analysis of saturation of the nonlinear index is expected to be modified appreciably in the presence of strong stimulated Raman and Brillouin scattering.

1.2.5 Relaxation Oscillations in Stimulated Inelastic Light Scattering

AF-AFOSR-69-1622, Joint Services Electronics Program
DA-ARO-D 31-124-6920, U.S. Army Research Office (Durham)
J. Marburger, R. Johnson

In a previous semiannual report we discussed numerical solutions of rate equations describing stimulated forward and backward Raman scattering from a plane wave pump beam. We found that in the absence of other effects the scattering was always nonstationary in that for sufficiently long active medium lengths all three beams showed strong oscillations with a period roughly inversely proportional to the input intensity. This is in sharp contrast to previously reported nonstationary behavior in light scattering which depends upon the existence of dispersion or relaxation in the active medium.

During this period we analyzed this phenomenon more thoroughly, taking into account possible gain asymmetry for scattering into forward and backward modes, and considering as well the effects of finite driving pulse time T and active medium length L on the period of oscillation. As expected, oscillations did not occur for L or CT somewhat less than the distance required for the backward wave to be amplified to an intensity comparable with the input. In addition, the period of oscillation was found to depend sensitively on the forward backward gain ratio, with minimum period occurring for equal gains.

1.2.6 Estimation of Nonlinear Refractive Indices from Light Scattering Data

AF-AFOSR-69-1622, Joint Services Electronics Program
DA-ARO-D 31-124-6920, U.S. Army Research Office (Durham)
J. Marburger, E. Bochove

In self focusing situations in which stimulated inelastic scattering plays a negligible role, such as focusing with picosecond pulses, the relaxation and saturation properties of the active medium determine the behavior of the optical field in the focal region. While several theories of the saturation of the nonlinear index have been developed, there is no experimental evidence to suggest that the predicted magnitudes of this phenomenon are correct. In fact the available evidence on "filament" or spot sizes in the focal region is not consistent with any of the proposed theories.

We are attempting to relieve this situation by developing theories which allow more reliable determination of the saturation properties of the nonlinear index. R. W. Hellwarth at Hughes Research Laboratory has recently demonstrated the existence of a relation between the nonlinear refractive index (or Kerr coefficient) and the total depolarized Rayleigh scattering cross section. The validity of this relation depends only upon very general assumptions concerning the electrical properties of the interacting molecules. In particular the relation does not depend upon the detailed molecular distribution function of the active medium.

We have found similar general relations between other light scattering phenomena and the first saturation term in the expansion of the refractive index in powers of the intensity. It is not yet clear whether the scattering effect in question, the static field dependence of depolarized scattering in a Kerr cell, can be determined with sufficient accuracy to allow extraction of the saturation parameter from the data. Apparatus required for observation of light scattering in a strong static electric field has already been constructed by the experimental group of Prof. S. Porto here at U.S.C.

1.2.7 Coherent Optical Devices

AF-AFOSR 69-1621, Joint Services Electronics Program

W. H. Steier, J. P. Campbell

I. Introduction

This work concerns the development and study of devices for the control and modulation of coherent energy in the visible and infrared wavelength regions. The devices currently under study are described below.

II. Frequency Shifter Using $LiNbO_3$

A single side band modulator or frequency shifter using $LiNbO_3$ has been designed and is being constructed.

A. Selection of Modulator Parameters

Lithium niobate is normally a uniaxial crystal, but application of an electrical field E normal to the c-axis induces birefringence. The resulting phase difference (retardation) Γ between a pair of orthogonally polarized waves passing through a length L of the crystal along the c-axis is

$$\Gamma = 2\pi L n^3 r_{22} E/\lambda$$

where n is the ordinary refractive index (2.29 for $LiNbO_3$), r_{22} is an electro-optic coefficient (3.4×10^{-12} meters/volt for $LiNbO_3$ under high-frequency modulating fields), and λ is the wavelength. In the single-sideband modulator, half-wave retardation ($\Gamma = \pi$) will be induced by a field whose direction (in a plane normal to the c-axis) rotates at half the

desired modulating frequency. In a crystal of square cross section with side d, the peak voltage required to achieve half-wave retardation at a wavelength of 6328 Å is

$$V = 7750\, d/L \text{ volts} .$$

The voltage attainable will be limited by losses in the crystal. The power dissipated is related to the loss tangent, tan δ, by

$$P = \tfrac{1}{2} V^2 \omega \epsilon L \tan \delta$$

where ω is the modulation frequency, and ε is the permittivity of the crystal. For $LiNbO_3$ the relative permittivity ϵ/ϵ_o is 43 (in a direction perpendicular to the c-axis), and tan δ is 0.08 at a frequency of 100 MHz. If an upper limit on P is chosen, based on available modulator power or on tolerable heating of the crystal, then the achievement of half-wave retardation requires crystal dimensions satisfying the inequality

$$(L/d) \geq (3.0 \times 10^7)\, \omega \epsilon d \tan \delta / P$$

Choosing P as 40 watts and ω as 2π (100 MHz),

$$(L/d) \geq 14.2\, d \quad (d \text{ in millimeters})$$

Taking one millimeter as a practical minimum for d, L/d can be conservatively chosen to be 20. The selected crystal dimensions were 1mm x 1mm x 20mm. The peak voltage across the crystal required for half-wave retardation is then 387.5 volts.

B. Modulation Circuitry

An electrode will be placed on each of the long (1mm x 20mm) faces of the crystal. For single-sideband modulation, one pair of electrodes (on opposite faces) will have a modulating waveform applied, whose peak-to-peak amplitude is the half-wave voltage. The other pair of electrodes will receive the same waveform, delayed in phase by 90°. This

will produce a rotating electric field of constant magnitude in a region near the central axis of the crystal.

To produce these modulating signals in the 50 MHz to 100 MHz range, circuitry for impedance transformation and phase shifting is being designed. The phase shift will probably be introduced by a quarter-wavelength transmission line. The impedance transformation is necessary for efficient transfer of power from the power oscillator, which operates into a standard 50-ohm impedance, to the modulator crystal. The impedance of the crystal consists of the electrode-to-electrode capacitance C, in parallel with a resistance R determined by crystal losses.

Expected values are:

$$\left.\begin{aligned} C &= \omega \epsilon L = 7.6 \text{ picofarads}, \\ (\omega C)^{-1} &= 210 \text{ ohms} \\ R &= [\omega C \tan \delta]^{-1} = 2600 \text{ ohms} \end{aligned}\right\} \quad \text{(at 100 MHz)} .$$

C. Heat Removal

The crystal will be mounted on a small copper block, which will serve as a heat sink. If a total power P is dissipated uniformly within the crystal, and heat removed through one face to a constant-temperature (T_o) heat sink, then the equilibrium temperature distribution in the crystal (neglecting end effects) will be a function only of the perpendicular distance x from the cooled face:

$$T(x) = T_o + [(x/d) - \tfrac{1}{2}(x/d)^2] P/kL ,$$

where k is the thermal conductivity (0.042 watt/cm deg. for $LiNbO_3$). Hence the temperature difference ΔT across the crystal will be

$$\Delta T = P/2kL \simeq 6.0P^{\circ}C \quad (P \text{ in watts})$$

During modulation, the power P must approach 40 watts to achieve half-wave retardation. To avoid extreme temperature gradients

in the crystal, it will therefore be necessary to pulse the modulating waveform. Pulsing at a 0.5% duty ratio (e.g., one-millisecond pulses at 0.2-second intervals) would result in a temperature difference ΔT of only $1.2^{\circ}C$.

E. Lithium Niobate Crystal

An $LiNbO_3$ crystal rod of the selected dimensions has been procured. Its optical quality was checked and found satisfactory in two ways: (1) A single-mode laser beam was passed through the crystal, and showed no visible degradation; (2) The interference figure of the crystal was observed and showed no indication of residual strain.

III. Hi-Accuracy Optical Phase Measurements

A Machzender interferometer has been set up with a rotating half-wave plate in one arm. The rotating plate acts as a frequency converter so that the interference patterns observed at the output of the interferometer occur at twice the frequency of the plate rotation. The device can be used for high accuracy measurements of the shape of optical phase fronts coming through any optical element or system placed in the interferometer.

The interferometer has been set up with a plate rotating at 57 cps to give an interference pattern at 114 cps. The phase of the detected 114 cps signal was detected by observing lissajou patterns on the oscilloscope. The pattern was relatively insensitive to mechanical vibrations of the inteferometer if the phase was measured relative to the phase of the 114 cps signal detected at the complementary output of the interferometer. A spurious 60 cps signal was observed to cause distortion in the lissajou pattern.

Considerable work remains before high accuracy phase measurements will be attempted. The source laser is being modified to provide a clean single mode output. The detection electronics are being improved and an electronic phase meter is on order.

IV. Intra-Cavity Laser FM Modulation

A single side band modulator using KD*P has been built and placed inside the cavity of an He-Ne laser. To a first approximation the KD*P modulator looks like the rotating wave plate modulators described earlier. The modulator is arranged so that the frequency shifted energy is deflected from the laser cavity by a Wollasten prism. This technique has several advantages: (a) it can provide an FM modulated laser beam; (b) it requires less modulation drive power than single side band modulators outside the cavity; and (c) it may give linear coupling modulation at frequencies near the cavity longitudinal mode spacing.

With the modulator in the cavity, the laser still oscillates with a power output of about 1 mw. The r-f circuitry for applying the rotating electric field is being designed.

Analysis shows that unlike a true rotating wave plate this KD*P modulator will produce small sideband frequency components in the polarization that remains inside the laser cavity. These components will affect the modulation linearity when the modulation frequency approaches the axial mode spacing of the laser. Measurements will be attempted to determine the effects of this mode coupling.

The laser in this work is relatively long and hence has many output frequencies. For a practical system with modulation frequencies greater than the axial mode spacing, the laser should be made to operate at a single frequency. Consideration is being given to making the laser single frequency either by placing a neon discharge tube in the cavity or by replacing one end mirror with a mode selective interferometer.

1.2.8 Optical Experiments with Laser Sources

DAHC-04-69 C-0003, U. S. Army
AF-AFOSR 69-1622, Joint Services Electronics Program

W. L. Faust

We are continuing work on a large CO_2 laser which employs a diffraction grating, spinning about its normal, to achieve Q-switched operation on a single vibrational/rotational line. The oscillating line is chosen by adjustment of the spin axis (to which the grating normal is always parallel). This scheme has a number of advantages over previously demonstrated schemes, some of which have only recently been appreciated.

Advantages pointed out in earlier reports are: i) Low optical loss, relative to other schemes for the same effects; ii) A mechanically simple and practicable structure for the device, in several respects (again relative to other schemes); iii) We easily provide for a net output beam fixed in the laboratory, despite changes of the operating wavelength.

Advantages realized more recently, since the device has been operating are: i) the lineup for this geometry is completely trivial, as it turns out (essentially no lineup procedure is done, except on the opposite laser mirror ...); ii) This scheme has a great advantage over the usual "flopping mirror" Q-switch technique in that we are able to achieve large pulse repetition rates, perhaps ten times as great.

There is a certain "dwell time" τ_d, during which the resonator lineup is adequate for high Q, (for all these rotating-optics schemes).[1,2] The laser gas insists upon a certain time τ_D for amplification of a signal developing from noise to reach a measurable level, and further time τ_p to saturate the transition.[2] For a well-formed pulse we require $\tau_d \geq \tau_D + \tau_p \simeq 300$ nsec.[2] For flopping-mirror Q switches, this limits the shaft speed to 150 to 200 rps, and thus the repetition rate also, since the two are inseparable. In our scheme we could use a grating blazed at 6° ($\sin 6^\circ \simeq 0.1$) at a shaft speed of 2000 rps (again, the mechanical balance

situation, etc., are favorable) to give a τ_d equivalent to a flopping-mirror at 200 rps. We would get similar pulses, but ten times as often (for confirmation of the validity of this, one must consult values for such other parameters as the "inversion-regeneration" time; but, the numbers are very favorable . . .). On the adverse side, a small blaze angle might worsen problems of inadequate spectral resolution (see below).

The shape of the laser pulse seems to be consistent with a theory of B. A. Lengyel and W. G. Wagner[1] (see also ref. 2). Values of parameters obtained by direct observation and/or from a best fit to Lengyel and Wagner's table are: $\tau_d \simeq 600$ ns (at 4000 rps); $\tau_D + \tau_p = 300$ ns; rise time t_r and fall time t_f are in the ratio $t_r/t_f = 0.52 \pm 0.02$; the initial inversion N_i and the high-Q threshold N_p are in the ratio $N_i/N_p = 6.0 \pm 0.5$; the peak photon density is $(0.27 \pm 0.02)\, N_i$; $t_r \simeq 120$ ns; the photon lifetime $T \approx 230$ ns, and the corresponding loss coefficient $\approx 13\%$; the output coupling coefficient $\sim 6\%$. Our observed average power of 1.5 watts can be used to infer $N_i = 5.4 \times 10^{14}\ cm^{-3}$, in good agreement with Meyerhofer's value for the maximal inversion density $N_i = 5.9 \times 10^{14}$. The peak power is about 9 kw.

In the previous report we described a problem with insufficient spectral resolution to isolate a single rotational line (for the weaker lines). We have since eliminated that problem by using a 20 meter radius mirror instead of the 10 meter mirror used initially. The bore is now somewhat small for such a geometry, and a few lines are missing. We feel that the best solution is to use a generous bore size and to provide the necessary aperture limitation in one dimension only by adjustable slits* (a compromise between high spectral resolution and low resonator loss). Another variant of our general scheme would employ a grating with one groove face at 45° to the one side of the grating normal and the other groove face at 45° to the other side of the normal. Such a grating would give <u>two</u> pulses per revolution. It would give good resolution; and, running at 300 rps, it would give 600 pulses/sec. Actually, we have essentially observed this

mode of operation, with a Bausch and Lomb grating not explicitly designed for this mode of operation.

We have designed a very pleasing structure in which the grating and motor are operated within the vacuum envelope, to eliminate Brewster windows. The machine work for its fabrication has essentially been finished. We are reassembling our laser with a larger bore (tapered, as before, in three steps of diameter to accommodate the fundamental trans-verse mode) and with this in-vacuo-grating structure. Adjustable slits* are provided just in front of the grating. We feel that this structure should find use in many laboratories if it can be marketed under a satisfactory arrangement.

Heretofore we have not employed water cooling, on the basis of a prejudice that it should not enhance R lines, in which we have a specific spectral interest. In an exploratory setup we have found that R lines, as well as P lines, are enhanced by cooling; so our new tube will be cooled, perhaps with tubing wrapped around. Also we will reduce the number of discharge sections (but not the net length) from three to two, to facilitate a possible try of excitation pulsed synchronously with the spinning grating.

Because of the extreme expense of commercial cryogenic infrared detectors, we have built our own. It is a Ge:Hg unit (material supplied by W. P. Allred of the Materials Science Department), liquid hydrogen cooled, with a very fast integrated-circuit preamplifier built-in. For direct observation of Q-switched pulses, such a sensitive unit is not necessary or even desirable. On the other hand, we are now in a position to observe heavily attenuated laser signals, or weak fluorescence.

We are continuing work to observe Raman scattering from impurity local vibrational modes in GaP, with a repetitively-pulsed ruby laser. The sample is a rectangular parallelopiped about 1 x 5 x 10 mm. The 1 x 5 face is illuminated, over most of its area, by a cigar-shaped spot. This pattern of illumination is formed by a deliberately astigmatic

and somewhat defocussed optical system. It enables us to use most of the energy available from our laser at a 1 sec^{-1} repetition rate, without destroying the crystal. The 1 x 10 face is to be imaged onto the entrance slit of a Jarrell-Ash one meter Czerny-Turner spectrograph. We have built a sample dewar in which the crystal is to be bathed in liquid nitrogen below the boiling point, to avoid bubbling. The Raman frequencies we seek are in the range 400-600 cm^{-1}, giving relatively large frequency separation of the scattered light from the exciting light. Our present belief is that a series of dielectric fillers and a spectrograph will give entirely adequate rejection of the ruby light, for the 90^{o} scattering which we wish to observe.

References

1. B. A. Lengyel and W. G. Wagner, Proc. Int. Conf. Quantum Electronics III, Paris, 1964, p. 1427.

2. D. Meyerhofer, Jour. Quantum Electronics 4, 762 (1968).

1.2.9 Interaction of High Intensity Light Beams with Matter

AF-AFOSR-69-1622, Joint Services Electronics Program

W. G. Wagner

The topic of our investigations is the interaction of very intense electromagnetic beams, generated by lasers, with fluids. These interactions at high intensities are governed by nonlinear responses which produce a number of qualitatively striking phenomena. Early studies concerned themselves with the prediction of novel effects in terms of material characteristics, and turned out to be qualitatively illuminating, but quantitatively deficient to a very significant degree, in large part because of the neglect of nonlinear distortion of the beam. Therefore, we have concentrated our efforts on the problem of nonlinear beam propagation; only when the characteristics of propagation are reasonably well calculable can reliable extraction of nonlinear coefficients be made from various

experiments.

During the past period we have initiated a detailed numerical study of the distortion of a laser beam resulting from the density changes induced in a fluid by the deposition of thermal energy which ultimately results from the absorption of laser radiation by the medium. A program for the solution of a system of partial differential equations has been written. This analysis has been restricted to those cases characterized by cylindrical symmetry so that there are three independent variables (r, z, t); the number of dependent variables is six--electromagnetic field amplitude, phase, density of the fluid, temperature, and raidal and longitudinal components of the fluid velocity. The techniques have been chosen to eliminate as far as possible computer generated instabilities, and we appear to have been successful in this attempt at low beam powers. For higher powers where the nonlinear effects become more pronounced, we are having difficulties with cumulative round-off errors, which generate a spurious second pulse.

During the next period, work will continue on this problem directed toward eliminating at high powers spurious mathematical instabilities, so that we can then arrive at a clear description of thermal absorption on the shape of a laser beam.

1.2.10 Multiple-Phonon-Resonance Raman Effect in CdS

GP7804, National Science Foundation

M. V. Klein and S. P. S. Porto

Multiple-LO-phonon structure was observed by Leite and Porto in the Raman scattering spectrum of CdS at room temperature for exciting light in the region of the fundamental absorption edge.[1] This report presents several new experimental aspects of this phenomenon and suggests a way of looking at the theory of the effect.

Light incident normal to the polished surface of a CdS

single crystal was focused to a spot about 50 μ in diameter. The 180° back-scattered light was analyzed with the usual combination of a double-grating monochromator and photomultiplier. We found that in the region of strong absorption necessary for the resonance Raman effect the laser power had to be limited to less than about 20 mW to avoid sample-heating effects.

The scattered light spectrum shows a mixture of fluorescent emission and Raman scattering. In the room-temperature spectra of Fig. 1, the peak of the broad fluorescent emission is at about 5070 Å (2.447 eV), independent of the wavelength of the exciting light. The superimposed sharp lines represent Raman scattering of the incident light; the frequency separation $\omega_L - \omega_R$ is an integral multiple of ω_0, the $k \approx 0$ LO-phonon frequency at 304 cm^{-1}.[2]

The observed fluorescent emission is believed to be intrinsic and hence not caused by recombination of excited electron-hole pairs at impurity centers. The photon-created carrier density estimated from the light intensity was several orders of magnitude larger than the estimated impurity concentration. The position of the emission peak seems consistent with what is known from absorption and emission of CdS[3]; at room temperature it is about 25 meV below the position of the (n=1, A) exciton ($E \perp c$ axis). This is to be expected if the emission is composed of an unresolved superposition of this exciton line plus replicas shifted by multiples of ω_0. Scattering spectra for $E \| c$ have also been taken. Results are similar to those shown in Fig. 1, except that both the fluorescent emission and the most intense Raman line peak at about 16 meV lower energy, as expected for the (n-1, B) exciton.

The emission peak shifts to higher energy at lower temperatures, as may be seen in Fig. 2. The 25-meV separation between the A exciton and the emission peak reduces somewhat as the temperature is lowered.

The following facts characterize the data shown here and a

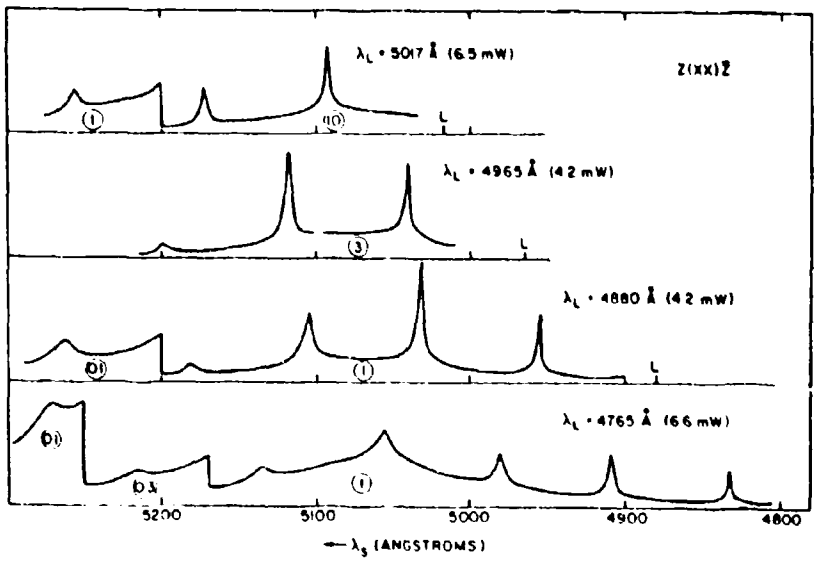

FIG. 1. Spectra of light back-scattered at room temperature from a CdS crystal for various wavelengths λ_L of incident laser light (also indicated by an "L" on the horizontal axes). The incident laser power is indicated in parentheses. The vertical axis represents electrometer current from the photomultiplier; the circled numbers give the full-scale reading in nanoamperes. The combined response of monochromator plus photomultiplier is flat in this region–the current is directly proportional to the light intensity. The $z(xx)\bar{z}$ notation is that of Ref. 2.

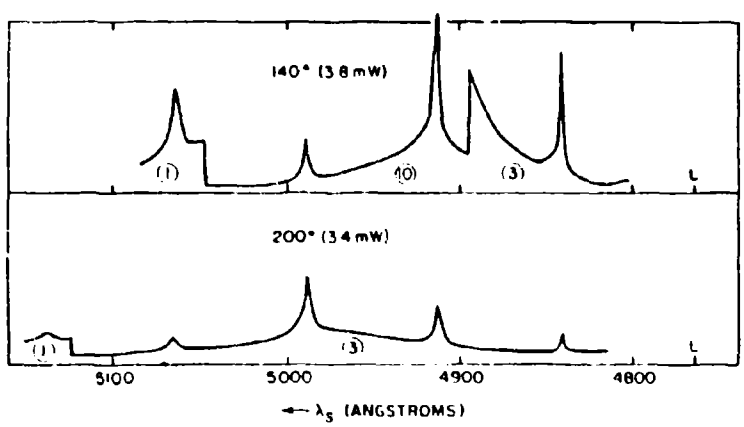

FIG. 2. The scattered light spectrum at two different temperatures for 4965-A laser excitation. The remarks in the caption for Fig. 1 apply here also.

considerable amount of additional data taken at temperatures between 112°K and room temperature.

(1) The multiple-phonon Raman spectrum closely follows the fluorescent emission. There is not a simple proportionality between the area under a given Raman line and the nearby emission intensity, but where there is no emission, there is no resonance Raman effect, and the most intense Raman line (in terms of integrated intensity) is the one closest to the emission peak and hence, approximately, closest to the exciton.

(2) The intensity of the entire scattered spectrum (Raman plus emission) increases as the laser frequency approaches the exciton frequency. This can be seen in Figs. 1 and 2. When $\omega_L < \omega_{ex}$, as is the case for $\lambda_L = 5145$ Å, the entire intensity falls off again. Because we do not have a continuously tunable laser, we are not sure exactly where the intensity peaks as a function of ω_L; it could be near ω_{ex} but not exactly at it. There seem to be two broad resonances, one for $\omega_L \approx \omega_{ex}$ and one for $\omega_R \approx \omega_{ex}$. There is no evidence for an intermediate frequency ω', $\omega_L > \omega' > \omega_R$, also resonating with ω_{ex}, as would be predicted by the cascade process illustrated in Fig. 3(a) of Ref. 1.

(3) The selection rules for this resonance Raman effect are not the usual rules of Loudon.[4] The ordinary prediction is that for back scattering of light propagating along the z (c) axis, there are interactions with A_1 - LO phonons with a dynamic polarizability tensor $\Delta\alpha$ having non-zero components $\Delta\alpha_{xx} = \Delta\alpha_{yy}$, and $\Delta\alpha_{zz}$. Hence one should see LO phonons in a $z(xx)\bar{z}$ experiment, and we do. For back scattering along the x axis ($\perp$ c), the LO phonons have E_1 symmetry and usual section rule gives $\Delta\alpha_{xz} = \Delta\alpha_{zx}$ as the only nonzero components of $\Delta\alpha$. Thus there should be no coupling to a single LO phonon in an $x(yy)\bar{x}$ experiment. Figure 2 shows that there is indeed such coupling. It is about as strong as that in a $z(xx)\bar{z}$ experiment. Far below resonance, say for $\lambda_L = 5462$ Å, the usual Loudon selection rules apply; several different $k \approx 0$ phonons are then seen in first order in an $x(yy)\bar{x}$ experiment, but no first-order LO phonon.

(4) We have studied the depolarized light scattered in geometries such as $x(yz)\bar{x}$ and $x(zy)\bar{x}$. The combined (fluorescence plus Raman) spectrum is asymmetric, i.e., the yz and zy results are not equivalent. These spectra are evidence that interband (A ⇌ B) exciton processes are important; nevertheless we would like to ignore such processes in a first approximate discussion of this effect.

Apart from these A ⇌ B interband effects and apart from shifts in the emission peak due to A - B energy difference, our results show that the resonance Raman tensor $\Delta\alpha$ couples to LO phonons, regardless of their direction of propagation, even in first order, and has diagonal components $\Delta\alpha_{\perp\perp}$ along axes perpendicular to the propagation direction of the photon. As pointed out by Kleinman,[5] such would be the form of the Raman tensor for light in a dielectric continuum interacting with a longitudinal polarization wave. This is what one would expect if the interaction with LO phonons is via the orbital part of a large-radius Wannier exciton. Then continuum polarization effects would dominate over the short-range forces which usually determine the symmetries of the scattering tensor.

The above considerations suggest strongly that the resonance Raman effect of LO phonons goes through an exciton as an intermediate state.[6] Assume a single exciton band for simplicity; multiple bands may be treated by the methods of Segall and Mahan.[7] Consider the three processes shown in Fig. 3 of Ref. 1. Our data suggest broad resonances at $\omega_L \approx \omega_{ex}$ and $\omega_R \approx \omega_{ex}$ with no other resonances at intermediate frequencies between ω_L and ω_R. This seems to rule out the cascade process in Fig. 3(a).[8] The remaining processes, (b) and (c), will have resonance factors in perturbation theory of the form $(\omega_L - \omega_{ex}^0)^{-1}(\omega_R - \omega_{ex}^0)^{-1}$ that describe the propagation of the exciton just after creation and just before annihilation. Absorption and emission data indicate a strong broadening of the exciton line due to phonon interactions. Thus it is a much better approximation to replace the bare-exciton frequency ω_{ex}^0 in the propagators by the experimental exciton frequency ω_{ex} plus a large imaginary

part $i\Gamma(\omega, T)$. This will give the type of broad resonance we need to explain our data, including temperature dependences of the type shown in Fig. 2.

It is necessary to assume no additional strong frequency dependences beyond those already accounted for. This might tend to favor the processes in Fig. 3(c) of Ref. 1 over those of Fig. 3(b), but this will require further study. Due to the exciton's kinetic energy, the integrals over the k vectors of the intermediate states of processes such as that of Fig. 3(b) of Ref. 1 should provide additional smoothing of the ω_L dependence beyond the substantial amount already provided by large exciton linewidths represented by $\mathrm{Im}\Sigma$.

In a more complete paper to be submitted shortly we shall discuss many more experimental details and hope to say more about the theory of this effect including how the above arguments relate to a more detailed treatment of the exciton-photon interaction.[9]

We are pleased to acknowledge several profitable discussions with R. W. Hellwarth, J. H. Marburger, and especially D. A. Kleinman.

References

1. R.C.C. Leite and S.P.S. Porto, Phys. Rev. Letters 17, 10 (1966).

2. B. Teil, T. C. Damen, and S.P.S. Porto, Phys. Rev. 144, 771 (1966).

3. See the contributions by E. Gutsche and J. Voigt, in Proceedings of of the International Conference on II-VI Semiconducting Compounds, Providence, R.I., 1967, edited by D. G. Thomas (W. A. Benjamin, Inc., New York, 1968), p. 337; C. E. Bleil and J. G. Gay, ibid., p. 360.

4. R. Loudon, Advan. Phys. 13, 423 (1964).

5. D. A. Kleinman, private communication.

6. J. L. Birman and A. K. Ganguly, Phys. Rev. Letters 17, 647 (1966); A. K. Ganguly and J. L. Birman, Phys. Rev. 162, 806 (1967).

7. B. Segall and G. D. Mahan, Phys. Rev. 171, 935 (1968).

8. If the LO branch has noticeable dispersion, then the multiple-phonon lines due to processes (b) and (c) in Ref. 1 will be much broader than the single-phonon line because the multiple phonons have a distribution of k values. In process (a) only $k \approx 0$ phonons are emitted. Our data show no broadening of the multiple-phonon lines beyond that due to phonon lifetimes, but this does not favor process (a), since there is apparently little dispersion in the LO branch of CdS: Reference 2 gives the frequency of the 2-LO-phonon line as very close to twice that of the one-phonon line.

9. E. Burstein, D. L. Mills, A. Pinczuk, and S. Ushioda, Phys. Rev. Letters 22, 348 (1969).

1.3 MAGNETISM

1.3.1 Investigation of Vibronic Spectra of Rare Earth Ions in Fluorite Lattices

AF-AFOSR 69-1622, Joint Services Electronics Program

J. P. Hurrell

Prior to arrival at U.S.C., the author had started an interpretation of the vibronic spectra of rare earth ions in fluorite lattices (BaF_2 and SrF_2), obtained by Dr. E. Cohen at Bell Telephone Laboratories. To proceed with this work, detailed knowledge of the phonon dispersion curves was necessary and neutron data for BaF_2 was collected by Dr. Shirane's group at Brookhaven. The author has now performed a shell model calculation to fit this neutron data and is in the process of applying this calculation to the original problem of the vibronic spectra.

These spectra consist of absorption (or emission) side bands on sharp electronic absorption (or emission) lines, whose width is comparable with the host crystal Debye temperature. They are caused by simultaneous absorption (or emission) of lattice phonons with electronic excitation. The interaction between the rare earth ion and phonons proceeds via the electric fields produced by the latter at the ion site. While an absolute magnitude calculation is prohibitively difficult, a calculation of the shape of the sidebands is more tractable and this has determined the scope of the work.

The potential has been expanded in multipole moments and the interaction Hamiltonian becomes a sum of products of potential multipoles with charge distribution multipoles of the rare earth ion; this procedure is valid for zero overlap of the impurity ion wavefunctions with the ligand wavefunctions. The assumption is made that this series should be rapidly convergent so that only 2 or 3 terms are necessary for a good approximation. This seems to be verified by the results of a cluster calculation, valid for the higher multipole moments; they are seen to

make a negligible contribution. Consequently, efforts have been concentrated on the dipole, quadrupole and octopole terms. These are being calculated by performing exact lattice sums on a computer for a series of k-vectors and using the appropriate eigenvectors of the corresponding phonons for the perfect lattice to estimate the contribution of each phonon to the multipole moment in question. A projected density of states for the dipole moment has been calculated and the results are very encouraging. The electronic transitions impose certain selection rules on the sideband and by comparing different transitions, the contributions from the different multipoles can be partially separated. In particular the dipole contribution can be completely separated and compared directly with the calculation.

To put these calculations in context, it is necessary to note that there exists many examples of defects interacting with lattice phonons producing for example: reduction in thermal conductivity, defect induced I.R. absorption and Raman scattering, sidebands in I.R. absorption by local modes and the present problem. In every case a different interaction mechanism is involved and the shape of the bands is different. However, they all purport to yield information concerning the host crystal and the localized properties of the defect. Vibronic spectra are one of the cases where little calculation has been done and only one spectrum has been analyzed to any appreciable extent (Timusk and Buchanan, Phys. Rev. 164, 345 (1967)) even though there exists a proliferation of experimental results in the literature.

It is hoped that the present investigation will yield a useful contribution to the understanding of the interaction between rare earth ions in crystals and lattice phonons. In particular the role of resonance modes, or the change in lattice dynamics, produced by the defects should become apparent when the calculations are fully compared with experiment.

1.3.2 Optical Absorption and Faraday Rotation of the Co^{2+} Ion in Tetrahedral Coordination

AF-AFOSR 69-1622, Joint Services Electronics Program

W. K. Ng and J. Smit

Magneto-optical rotation and optical absorption of a light beam with a wavelength between 0.5 and 1 μ passing through single crystals of Cs_3CoCl_5, Cs_3CoBr_5, $Cs_3Zn_{1-x}Co_xCl_5$ and $Cs_3Zn_{1-x}Co_xBr_5$ were measured at low temperatures between 4.2° and 30°K. In the presence of a static magnetic field parallel to the direction of propagation, a large rotation of the plane of polarization of the incident beam is observed near the absorption band edge located at about 0.7 μ. This absorption band is associated with the $^4A_2 \rightarrow {}^5T_1(P)$ transitions of the Co^{2+} ions in tetrahedral sites. At 4.2°K only the lowest Kramers doublet is significantly populated; the Faraday rotation is found to be proportional to the magnetization of the sample. The optical rotation of Cs_3CoCl_5 and Cs_3CoBr_5 as a function of an applied magnetic field at 4.2°K and at λ = 8630 Å are given in Figure 1. From absorption measurement data on Cs_3CoCl_5, the attenuation of the incident beam at this wavelength is 16 db/cm. Therefore, at a saturating applied magnetic field the rotation per db absorption is approximately 560 degrees. This ratio is comparable to the highest value known for ferromagnetic materials. No attempt has yet been made to take into account losses due to reflection at the surfaces.

Far outside the absorption region, the wavelength dependence of the Faraday rotation at 4.2°K is shown in Figure 2 for both Cs_3CoBr_5 and Cs_3CoCl_5. The rotation is found to fit the expression

$$V = \frac{C}{\lambda_t^2 - \lambda^2}$$

where V is the Faraday rotation in degrees/cm gauss, C is a constant proportional to the strength of the optical transition causing the rotation and λ_t is some average wavelength of the absorption band. This is found

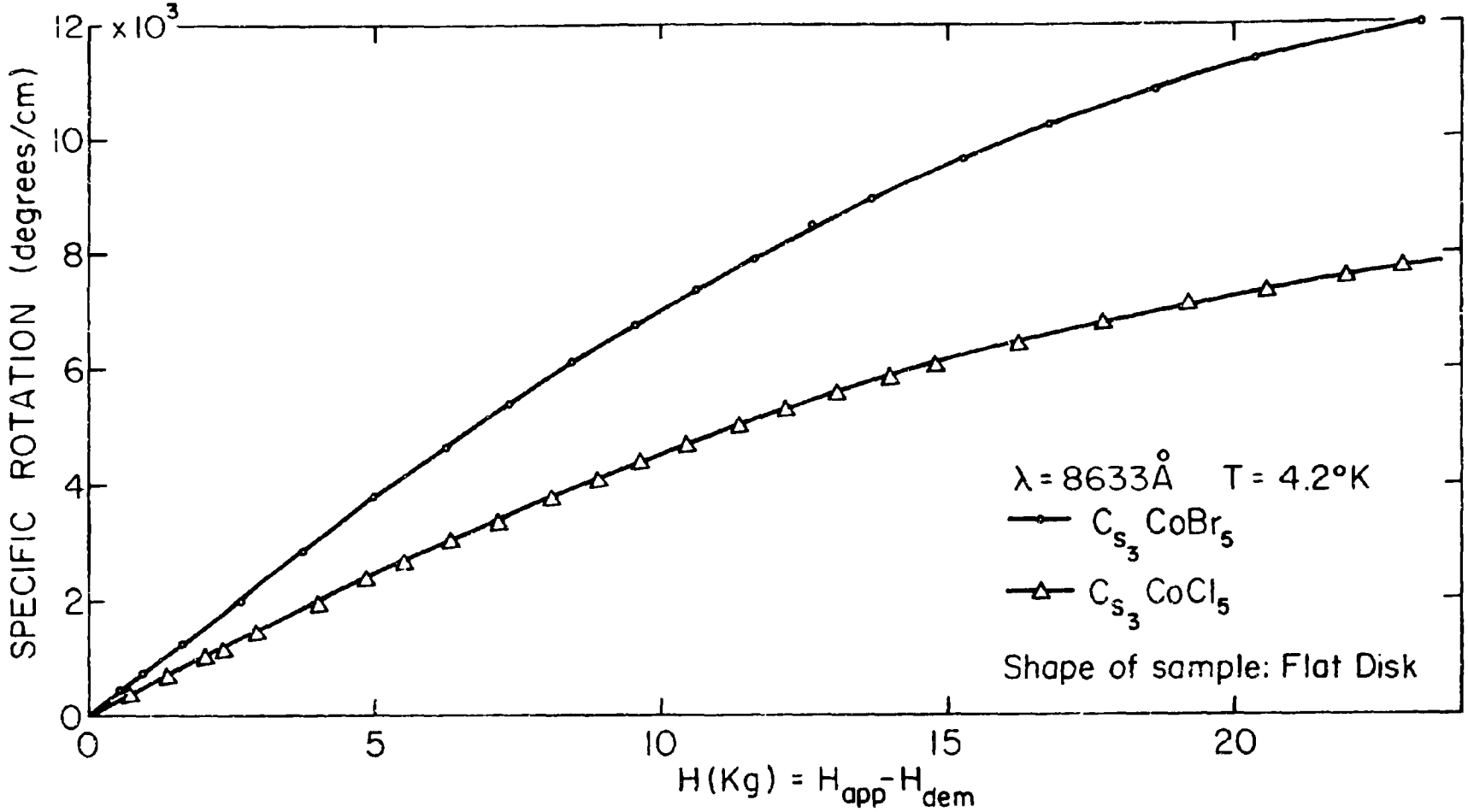
12
x10^3
10
8
6
4
2
0
SPECIFIC ROTATION (degrees/cm)
0
5
10
15
20
H(Kg) = H_app - H_dem
λ = 8633Å T = 4.2°K
Cs3 CoBr5
Cs3 CoCl5
Shape of sample: Flat Disk

Fi re 1

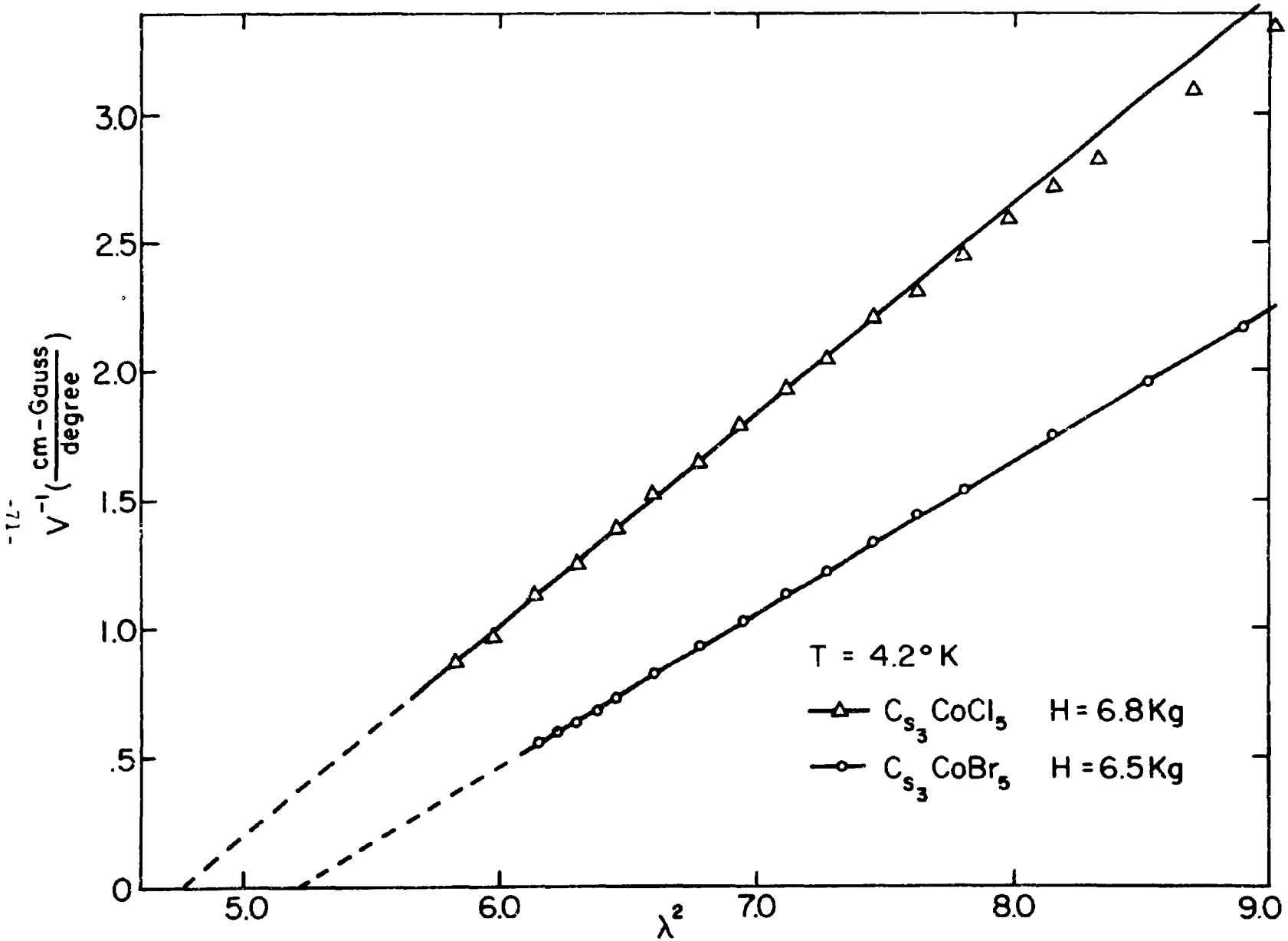
3.0
2.5
2.0
1.5
1.0
.5
0
5.0
6.0
7.0
8.0
9.0
λ²
V⁻¹(cm-Gauss/degree)
T = 4.2° K
Cs₃CoCl₅ H = 6.8Kg
Cs₃CoBr₅ H = 6.5Kg

Figure 2

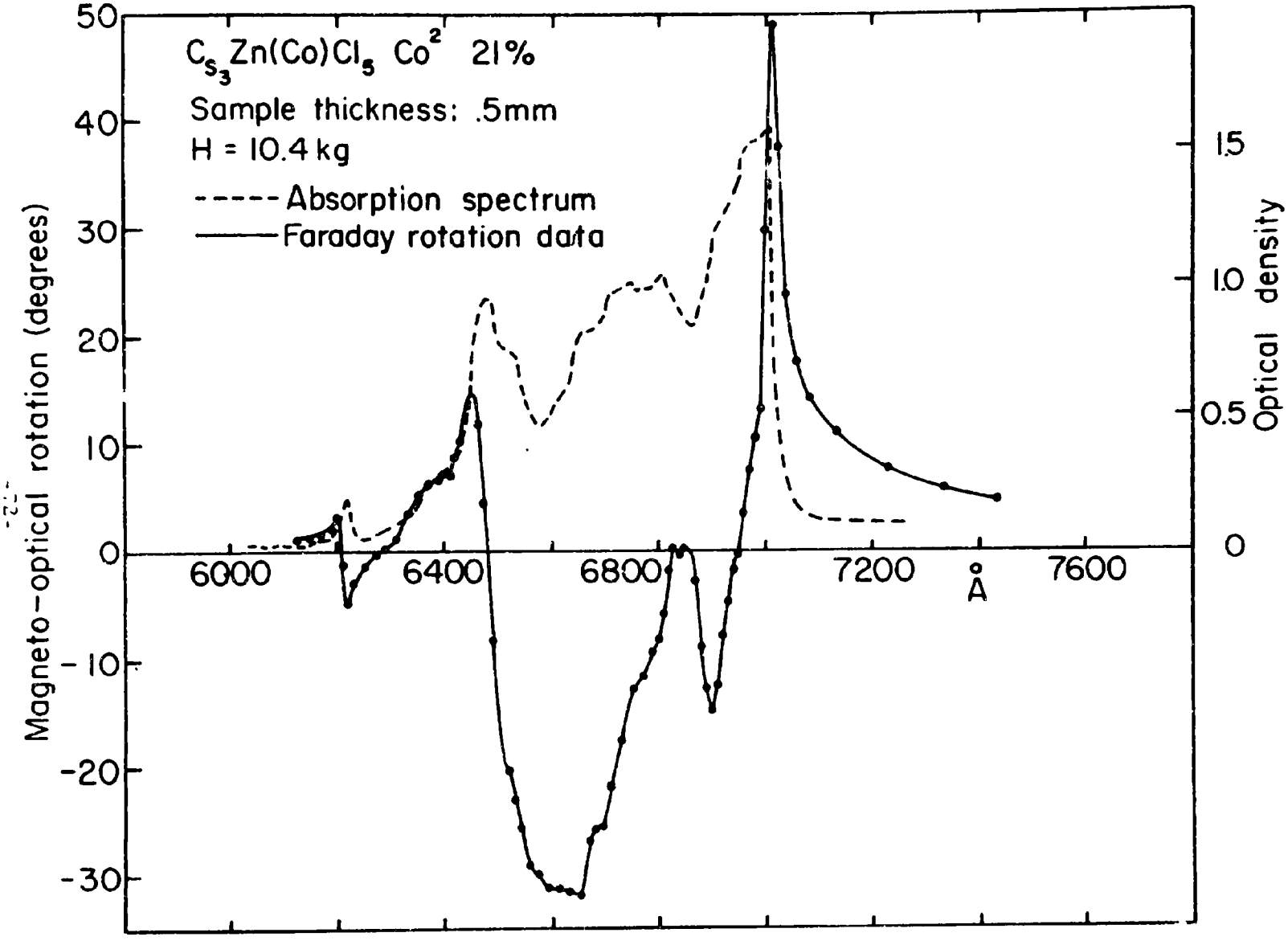
$C_{s_3}Zn(Co)Cl_5$ Co^2 21%
Sample thickness: .5mm
H = 10.4 kg
Absorption spectrum
Faraday rotation data
Magneto-optical rotation (degrees)
Optical density
50
40
30
20
10
0
-10
-20
-30
1.5
1.0
0.5
0
6000
6400
6800
7200
Å
7600

Figure 3

to be λ_t = 6800 Å for Cs_3CoCl_5 and λ_t = 7200 Å for Cs_3CoBr_5. Comparison of the slopes of the two straight lines in Figure 2 indicates that the strength of Faraday rotation is larger for Cs_3CoBr_5 than for Cs_3CoCl_5.

The absorption spectrum and the Faraday rotation of $Cs_3Zn_{1-x}Co_xCl_5$ in the region of the absorption band are given in Figure 3. The absorption spectrum shows three main peaks which are found to be much sharper in $Cs_3Zn_{1-x}Co_xBr_5$. These peaks are interpreted as due to the effect of the tetragonal distortion of the Co^{2+} ion site which splits the $^4T_1(P)$ state into an orbital singlet and a lower lying doublet. This doublet in turn is split by spin-orbit interaction. A more detailed analaysis of these data and further measurements on other compounds are in progress.

1.3.3 Localized Moments in Metals

GU 1559, National Science Foundation

M. D. Daybell

An atom that normally possesses a magnetic moment, such as iron or vanadium, may or may not retain that moment when it is alloyed into a normal metal, like copper or gold. Over the past two years, it has been learned that whether or not it does so depends on the temperature of the material when the measurement of its moment is carried out. Below a certain temperature T_K for each alloy, called the Kondo temperature, the moment disappears in all cases so far investigated. The variation of T_K from alloy to alloy is apparently such that log T_I is proportional to the number N of magnetic electrons in the dopant atom. This logarithmic dependence of T_K on N is reasonably well established only for iron group dopants in gold. However, the other properties of these dilute magnetic systems have nearly all been established by experiments in copper based alloys, which are now fairly well understood in many cases[1]. Unfortunately, the relative difficulty of preparing some of the copper based alloys (for example, vanadium as a dopant in copper)

has resulted in a lack of data on the systematic variation of log T_K with N in these systems. A knowledge of T_K for titanium and vanadium in copper has prevented any convincing proof of the ln T_K vs. N conjecture to be obtained in any host material other than gold. We are trying to obtain such information by measuring T_K for vanadium in copper.

We expect the Kondo temperature of vanadium in copper to be higher than 300° Kelvin, and in this range the simplest, and perhaps the only way of measuring T_K is to look for a peak in its thermoelectric power, which should occur near T_K. The solubility of vanadium in copper is known to be quite low, probably less than 0.3%. The problem thus centers around the preparation of the alloy, and this is being attacked using our newly acquired arc melter. Attempts to prepare the alloy by vacuum furnace and induction melting failed, in part because the long running times at high temperatures necessary were not available. This will be remedied if the arc-melting leads to problems.

Reference

1. M. D. Daybell and W. A. Steyert, Reviews of Modern Physics, 40, 380 (1968).

1.3.4 Very Low Temperature Physics

GU 1559, National Science Foundation

M. D. Daybell

Since the end of 1966, it has been possible to continuously cool experimental samples to temperatures within three hundredths of a degree of absolute zero, using a sophisticated refrigerator that relies on the fact that heat is absorbed when the light isotope of helium is dissolved into ordinary liquid helium.[1] Much use has been made of this "dilution refrigerator" by J. C. Wheatley and collaborators at the University of Illinois (and later at the University of California at La Jolla), and by M. D. Daybell and W. A. Steyert at Los Alamos Scientific Laboratory.

Until quite recently, the first group concentrated on perfecting the design of the refrigerator itself, while the Los Alamos group has concentrated on using it to carry out a sequence of experiments in solid state[2] and more recently, nuclear physics. An improved version of the Los Alamos design is nearing completion here in the Electronic Sciences Laboratory for the general use of our new low temperature group.

One significant advance in dilution refrigerator design was made in building the U.S.C. version. Perhaps the most critical part of these refrigerators is the heat exchanger used to cool the incoming light isotope of helium, He^3, by flowing it through porous high purity sintered copper plugs, which are in turn cooled by metallic conduction over to similar plugs through which helium from the coldest portion of the refrigerator is returning. Bonding these fragile copper plugs to their holders has been a recurring problem in the past, since the bond must be one that retains a high thermal conductivity at very low temperatures. The best earlier solution was to heat shrink the plugs into a common copper sleeve, but the conductivity of the plug-sleeve interface always limited the thermal contact that could be obtained. After some effort, we have developed a technique for sealing the sides of the porous disk with solid copper before heat shrinking, and the conductivity of the plug-sleeve interface is now better than that of the porous copper itself. This should lead to improved cooling capacity for our design at very low temperatures.

Because the specific heats of most materials are quite small at the temperatures where dilution refrigerators are most useful, it is important to prevent stray energy from reaching the samples being investigated. One of the harder sources of such energy to eliminate is vibrational heating. We have designed a support for the experimental dewar which isolates it from the mechanical environment by tying it to a large granite mass supported on servo-controlled air diaphrams. This special design was built by a local supplier for about five thousand dollars. A duplicate of the system has since been ordered by Los Alamos to supplant an earlier in-house mount design costing several times as much, but

giving no better performance.

References

1. J. C. Wheatley, O. E. Vilches, and W. R. Abel, Physics 4, No. 1.

2. M. D. Daybell and W. A. Steyert, Proceedings of the 14th International Conference on Magnetism and Magnetic Materials (to be published in Journal of Applied Physics.)

1.4 DEFECTS IN CRYSTALS

1.4.1 Defect Chemistry of CdS

GK 4056, National Science Foundation

1.4.1.1 High Temperature Hall Effect Measurements

F. A. Kroger, G. Hershman

Measurement of the Hall effect of CdS in equilibrium with cadmium vapor at pressures between 0.07 and 1 atm and temperatures between 60 and 1000°C keep giving consistent results which can be interpreted on the basis of an Al content of $\approx 8 \times 10^{16} cm^{-3}$ varying with temperature as a result of precipitation, and an amount of doubly ionized native donors (Cd_i or V_S) varying with temperature and $p_{Cd}^{1/3}$.

1.4.1.2 Cadmium Self Diffusion

F. A. Kroger, V. Kumar

The self diffusion coefficient of Cd in CdS under known Cd-pressures was measured between 700 and 1000°C. D_{Cd} was found to be independent of p_{Cd}. The measurements are extended to sulfur atmospheres. Also, sulfur self diffusion will be studied.

1.4.2 Electrochemistry of Solids

AF-AFOSR-68-1405A, Air Force Office of Scientific Research

1.4.2.1 Zirconia as an Oxygen Pump

F. A, Kroger and D. Yuan

The work has been written up for publication, and the manuscript has been accepted by the Journal of the Electrochemical Society.

1.4.2.2 The Activity of Dilute Solutions of Na in Liquid Sn

F. A. Kroger and D. Yuan

This work has been written up as a publication which has been accepted by the Journal of Physical Chemistry.

1.4.2.3 Pyrex Glass as Oxygen and Sulfur Electrodes

F. A. Kroger and D. Yuan

Cells of the type

$$Na \mid Pyrex \mid O_2 \qquad (a)$$

$$Na \mid Pyrex \mid S' \qquad (b)$$

$$O_2 \mid Pyrex \mid S \qquad (c)$$

are being investigated.

Cells (a) give an emf following the Nernst formula

$$E = E_o + \frac{RT}{4F} \ln pO_2$$

E_o is determined by the activity of Na_2O in the glass; E_o varies with polarization but returns to the same value after removal of the polarizing field.

Cells (b) give a stable emf. The sulfur pressure dependence is being investigated.

Cells (c) give an emf decreasing with time.

1.4.2.4 Polarization Studies on AgCl

F. A. Kroger and Y. van der Meulen

Polarization studies have been carried out with cells Ag |AgCl|C and C, Cl_2 | AgCl | C using both "pure" AgCl and Cd-doped AgCl. The results show both electron and electron hole currents for AgCl in equilibrium with Ag at $T \geq 380^{\circ}C$, but only hole currents in AgCl in contact with Cl_2. The results are being analyzed.

1.4.2.5 I-V Characteristics of Zirconia Cells

F. A. Kroger and H. Yanagida

Symmetrical cells of the type

$$Pt,\ O_2 \mid ZrO_2 \cdot \delta CaO \mid Pt,\ O_2$$

are being investigated for their electrode kinetics by measuring the I-V characteristic as f(p_{O_2} and temperature). The cells show non-ohmic behavior indicating surface rate limiting steps connected with the ionization of absorbed oxygen.

At high oxygen pressures the conduction is mainly ionic (due to $V_O^{\bullet\bullet}$); at low oxygen pressures electronic conduction becomes appreciable. At high voltages the characteristic becomes time dependent due to the migration of F centers created by polarization.

1.4.3 Defect Chemistry of Al_2O_3

N00014-67A-0269-0007, Office of Naval Research

1.4.3.1 High Temperature Conduction of Al_2O_3

R. J. Brook, J. Lee and F. A. Kroger

Measurements of electrical conductivity and ionic transport number are being made on single crystals of aluminum oxide; the crystals are either flux-grown (at U.S.C) or pulled from the melt (at Union Carbide). Conductivity and transport number data (measured using a volume guard to prevent leakage around the specimen either across the surface or through the gas phase) are interpreted in terms of a model of complete ionic conduction involving $Al_i^{\bullet\bullet\bullet}$ (triply ionized aluminum interstitials) as the charge carriers. In air, the compensating defects are believed to be V''_{Al} (doubly ionized aluminum vacancies).

It is found that Mg and Co as additives enhance the conductivity and that Ti suppresses the conductivity; both of these results are in accordance

with the model.

Measurements are now to be made on a function of oxygen pressure.

1.4.3.2 Valency Variation of Transition Elements in Al_2O_3

F. A. Kroger and J. Chang

A beginning is made with the measurement of optical absorption and electron spin resonance of annealed crystals of $Al_2O_3 \cdot Co$ as a function of the oxygen pressure and the temperature of annealing. It is the intention to obtain concentrations of Co^{2+} and Co^{3+} and explain the results on the basis of a detailed defect model. Also, the association of Co^{2+} with compensating Al_i^{3+} will be studied.

1.4.4 Defect Chemistry of SiO_2

Supported by TRW

Th. G. Mills and F. A. Kroger

SiO_2 is important as an insulating layer in Si-based semiconducting devices, but its application is hindered by migration of native and/or foreign ions. Foreign ion-free films of SiO_2 will be grown on Si, and its defect structure will be studied by polarization studies and thermoelectric power measurements on cells

$$Si \mid SiO_2 \mid Si \qquad (a)$$

and

$$Pt, O_2 \mid SiO_2 \mid Pt, O_2 \qquad (b)$$

Attempts will be made to find electronic contributions to the current. Similar studies will be carried out on donor or acceptor-doped layers, both with and without monovalent ions being present.

1.4.5 Grain Growth in Ceramics

GK 1487, National Science Foundation

R. J. Brook

The analysis of normal and abnormal grain growth in porous and in impure ceramic systems has continued. Since it is known that the technique of sintering ceramics to final density (zero porosity) depends on preventing the separation of the grain boundaries from the pore phase, the possible interactions between pores and boundaries have been studied. While results depend on the specific assumptions made, a typical situation is shown in figure 1 where it has been assumed

(i) that pores migrate by surface diffusion

(ii) that the interpore spacing is equal to the grain size.

Boundary control and pore control denote microstructural conditions (i.e., of pore size and grain size) where the pores and boundaries remain attached, the migration of the composite being controlled by the boundary and pore fractions respectively. Separation denotes detachment of the pores from the boundaries.

The progress of any firing cycle can be traced on the graph since it can be represented as a combination of sintering (reduction in pore size) and of grain growth. Final densities can be achieved provided that the separation region is avoided. The role of impurity additives in aiding sintering is seen from the figure to be that of reducing the area of the separation region and thus of enhancing the possibility of avoiding it under a given set of firing conditions.

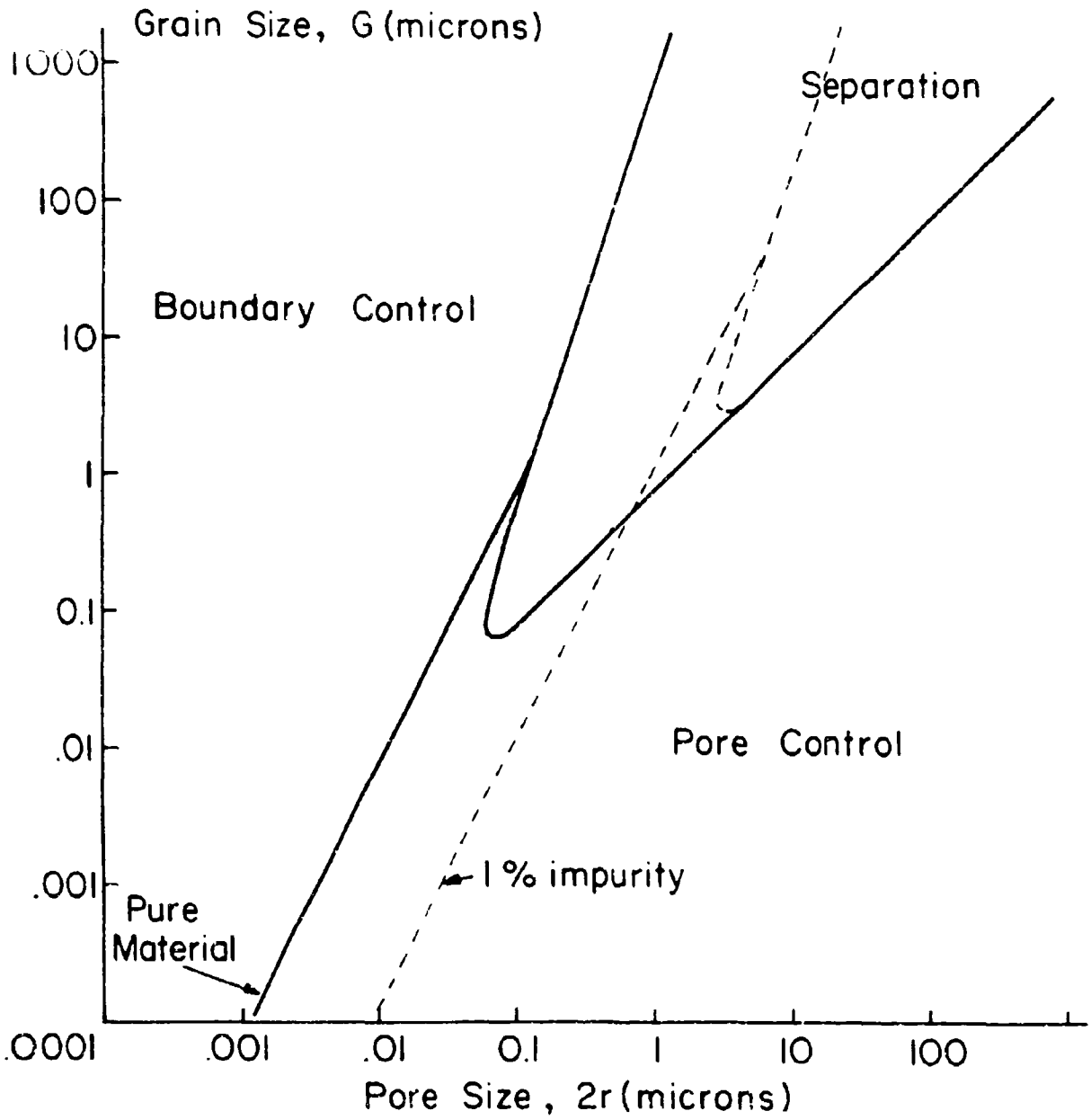
Grain Size, G (microns)
1000
100
10
1
0.1
.01
.001
.0001
Separation
Boundary Control
Pore Control
1% impurity
Pure
Material
.001
.01
0.1
1
10
100
Pore Size, 2r (microns)

Figure 1

1.5 METALS

1.5.1 Experimental Studies of Fermi Surface Topology in Metals

AF-AFOSR-69-1622, Joint Services Electronics Program

M. H. Halloran, J. Brewer, R. Parker

This area of research is primarily concerned with the determination of Fermi surface information which can be used to further the understanding of the electronic band structure of pure metals and interactions of the conduction electrons with phonons, magnons, foreign atom impurities and lattice defects. Materials of particular interest are the transition and rare earth metals, and several intermetallic compounds.

During the past six month period the effort and progress has been channeled into two specific projects--low field deHaas-van Alphen (dH-vA) measurements of the intermetallic compound $AuGa_2$ and the installation of a high field superconducting magnet facility for experiments in fields up to 100 kOe.

The low field dH-vA measurements in $AuGa_2$ were obtained using a torsion balance at fields up to 28 kOe. Results have been obtained for both the (100) and (110) planes and are in agreement with earlier results[1] which exhibited some qualitative similarities but quantitative disagreements with the free electron model. Recent APW band calculations[2] appear to provide a better model for comparison, and in particular a specific Fermi surface sheet predicted by the free electron model is absent in the new APW model. The data thus far obtained can be interpreted in favor of either model and further results with higher fields and better samples are required. In addition, experiments on the dH-vA effect in $AuGa_2$ under pressure or with dilute impurities are being considered as possible ways to resolve the band structure problem. The missing Fermi surface sheet in the APW model is due to a band just at or below the Fermi energy, and such experiments could shift that band above the Fermi energy where it can be readily observed.

The installation of the high-field superconducting magnet facility is nearing completion. This is the second time this installation was made, as the original facility failed to meet specifications and the new facility was delivered in January, 1969. The new solenoid has been operated up to magnetic fields slightly over 100 kOe, and has been operated in the persistent mode where the homogeneity over a 1 cm sphere was verified to be better than 4 parts in 10^4. Modifications to provide for field modulation and sample rotation are being installed at the present and high field dH-vA experiments should commence shortly. The first experiments will include those mentioned above in $AuGa_2$, and related experiments in the similar compounds $AuIn_2$ and $AuAl_2$, and initial studies of the transition metal vanadium. The vanadium samples are presently being prepared with an electron beam zone refiner recently obtained. The results in vanadium will be of interest for comparison with results obtained previously[3] in niobium and tantalium which with vanadium form a group of transition metal elements which calculation indicates should have similar band structures and therefore similar Fermi surfaces.

Other experiments being planned include high field experiments on ultra-high purity mercury samples doped with specific impurities in order to investigate (via the Dingle broadening of the Landau levels) the scattering of the Fermi surface electrons from different impurities. Finally experiments on other metallic intermetallic compounds such as the tungsten bronzes or transition metal oxides and sulfides are being considered for utilization of the high field facilities.

References

1. M. H. Halloran, J. H. Wernick, Bull. Am. Phys. Soc. 10, 350 (1965); J-P. Jan, W. B. Pearson, Y. Saito, M. Springford, and I. M. Templeton, Phil. Mag. 12, 1271 (1965).

2. A. C. Switendick, Bull. Am. Phys. Soc. 14, 360 (1969).

3. M. H. Halloran, J. H. Condon, T. E. Graebner, F.S.L. Hsu and J. E. Kunzler (to be published); G.B. Scott, M. Springford and J. R. Stockton, Physics Letters 27A, 655 (1968); M. H. Halloran, F.S.L. Hsu and J. E. Kunzler, Bull. Am. Phys. Soc. 13, 59 (1968).

1.5.2. Fundamental Studies of Explosive Shock Loading and High Velocity Perforation by Transmission Electron Microscopy

NGR-05-018-044, National Aeronautics and Space Administration

AF-AFOSR 69-1622, Joint Services Electronics Program

L. E. Murr, J. V. Foltz*, R. J. Horylev and W. N. Lin

The purpose of this research program is the basic study of very high pressure (shock) deformation and associated ballistic impact and perforation of metals and alloys of importance in engineering-technology applications.

During the current report period, we have concluded portions of the originally proposed work, namely the characterization of residual defect microstructures in planar shock loaded Inconel 600.[1,2] Several errors were corrected in our original interpretations, particularly the fact that we had erroneously assumed the precipitates in this material to be Al-Ti compositions. A more careful evaluation indicated the precipitates to be carbides of the general form $M_xC (x \tilde{=} 6)$. Our conclusions of the dislocation mechanisms, etc., are not changed since the precipitates are coherent, initially, as previously noted.

A "serendipity experiment" has been completed which, for the first time, illustrates in a very detailed manner the precise nature of deformation at a perforation in metal sheet. Specifically, we have observed the residual defect substructure at a .22 caliber bullet hole in stainless steel and Inconel sheets in the electron microscope. Figure 1 illustrates the typical results and the experimental implications. The technique has applications in armor evaluation, investigations of meteor perforation in thin skinned vehicles, etc.[3,4]

Dr. Foltz has devised a new technique for the direct observation

---

*Visiting Research Associate. Permanent address: Ballistics Division, U.S. Naval Weapons Laboratory, Dahlgren, Virginia.

Fig. 1 Microstructural features associated with a .22 caliber bullet hole in 304 stainless steel. The location of the zones is indicated. Zones 1-5 correspond to residual Vickers microhardnesses of 400, 300, 220, 200 and 181 respectively (100 gm load). The substructure in Region 1 is characterized by deformation twins. Region 2 shows dense dislocation arrays and stacking faults, with the dislocation density decreasing in Regions 3 and 4. Region 5 shows the typical structure of the undeformed material. The bright-field transmission electron micrographs were obtained with a 125 kilo-volt electron beam.

of residual defect structures in cylindrically shock-loaded metals and alloys which we have shown to be feasible. Preliminary studies in thin-walled stainless steel cylinders indicated a somewhat different microstructure than that previously observed for 304 stainless steel shock-loaded using a planar (flying-plate) shock pulse.[5] The techniques and a comparison with plane-wave loading are given elsewhere.[6,7]

We have begun the follow-up to shock-loading of Inconel; namely, the design of an experiment to simultaneously shock deform materials nominally strengthened with precipitates (coherent) and inclusions or dispersions which are incoherent; and to relate the residual shock response to the unstrengthened base metal or matrix. The preliminary analysis has included the measurement of initial hardnesses for pure nickel, nickel containing 2% ThO_2 (TD-Ni) as an incoherent dispersion, 80/20 NiCr, Ni-Cr alloy containing a ThO_2 dispersion (TD-NiCr: 2% ThO_2, 20% Cr, balance Ni); and of course the Inconel 600 alloy (76% Ni, 16% Cr, 7% Fe--containing fine coherent precipitates).

The unique feature of each comparative microstructure for these materials is illuatrated in the transmission electron micrographs in Figs. 2 and 3. The corresponding microhardness is indicated in the figure captions.

We have also noticed, in the preliminary investigations of the TD-Ni and TD-NiCr that the dispersion sizes change for these materials, i.e., it appears the particle spacing may be affecting the initial strength (as hardness--compare the hardness for TD-Ni in Fig. 2(b) with that of TD-NiCr in Fig. 3(c)). In addition, anomalous contrast features at the ThO_2 particles has been investigated and found to be due to crystallographic or geometrical features and diffraction contrast (extinction) effects. These features prove the particles to be single crystals and indeed incoherently dispersed.[8]

References

1. L.E. Murr and J.V. Foltz, "Shock Deformation of Inconel 600 Alloy: Effect of Coherent Precipitates on Explosive-Shock Hardening", J. Appl. Phys., August, 1969.

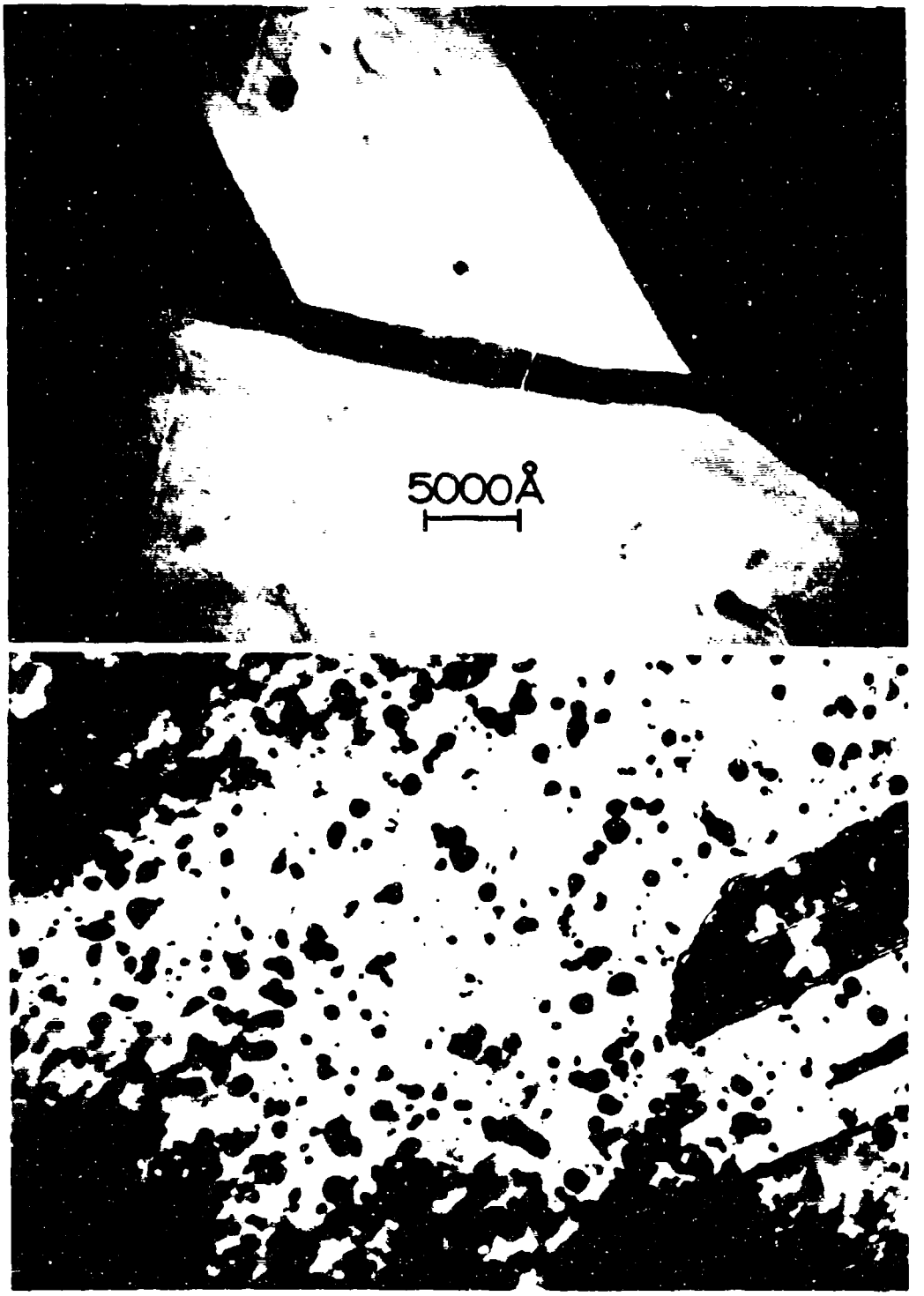

Fig. 2 Bright-field electron transmission images showing the undeformed substructure in (a) pure nickel having an average hardness of VHN 135, and (b) TO-Ni (2% ThO_2) having an average hardness of VHN 214. The "black" particles in (b) are ThO_2 dispersed particles.

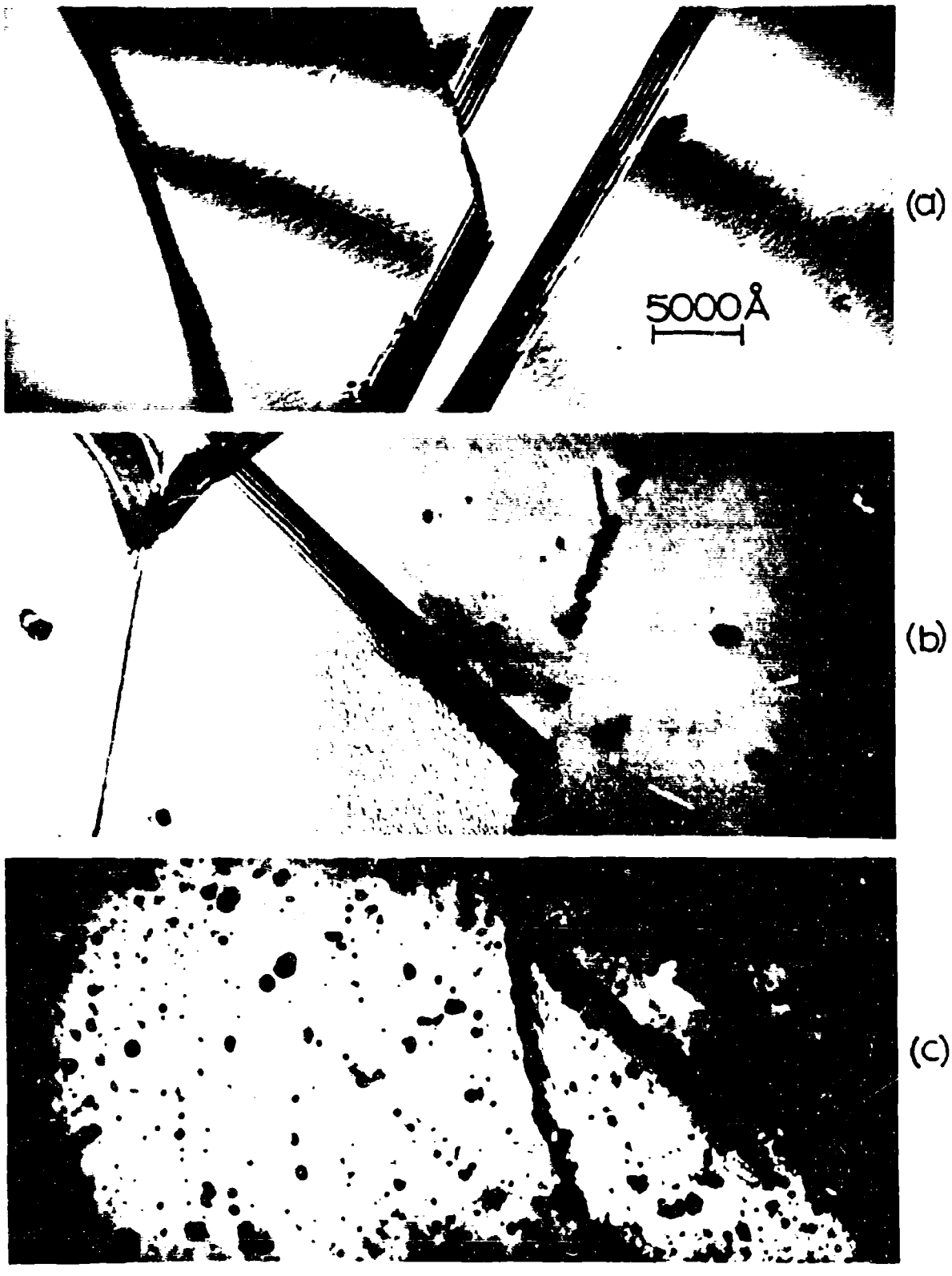

Fig. 3 Bright-field electron transmission images showing the undeformed substructure in (a) 80/20 NiCr having a hardness of VHN 222, (b) Inconel 600 (76% Ni, 16% Cr) having a hardness of VHN 229, and (b) TO-NiCr having a hardness of VHN 349. (b) and (c) show coherent and incoherent inclusions respectively.

2. L. E. Murr and J. V. Foltz, "Residual Deformation Twin Structure in Planar Shock-Loaded Inconel 600", paper to be presented to Electron Microscopy Society of America, August, 1969.

3. L. E. Murr and J. V. Foltz, "Direct Observation of Deformation Microstructures Surrounding a Bullet Hole in Stainless Steel Sheet", ibid.

4. L. E. Murr and J. V. Foltz, "A Terminal Ballistics Application of Transmission Electron Microscopy: The Anatomy of a Bullet Hole", to be published.

5. L. E. Murr and F. I. Grace, Exp. Mechanics (SESA), April (1969).

6. J. V. Foltz and L. E. Murr, "Comparison of Deformation Microtwins in Planar and Cylindrical Explosive Loaded Type 304 Stainless Steel", paper to be presented to Electron Microscopy Society of America, August, 1969.

7. J. V. Foltz, F. D. Altman and L. E. Murr, "A New Technique for the Direct Observation of Residual Defect Structures in Cylindrical Shock-Loaded Materials", to be published.

8. R. J. Horylev and L. E. Murr, "Characteristic Geometry and Diffraction Contrast of Dispersed ThO_2 Crystals", paper to be presented to Electron Microscopy Society of America, August, 1969.

1.5.3 Measurement of Interfacial Free Energies in Solid Metals and Alloys

N00014-67-A-0269-0010, NR 031-735, Office of Naval Research

L. E. Murr, J. V. Foltz*, R. J. Horylev and W. N Lin

This research program has as its goal the characterization of interfacial energies in metals and alloys, the development of techniques to measure these energies, and the utilization of this information in the design of materials, particularly with regard to strength of materials and their response, for example, in a corrosive environment.

*Visiting Research Associate. Permanent address: Ballistics Division, U.S. Naval Weapons Laboratory, Dahlgren, Virginia.

The initial approach involves the characterization of interfacial structure and crystallography, as well as the measurement of relative interfacial free energy ratios γ_{tb}/γ_{gb} at twin boundary-grain boundary intersections using modifications of the technique previously outlined by Murr[1,2]. Preliminary studies now indicate that a definite variation exists for grain boundary energy with crystallographic misorientation. Studies in support of this conclusion are underway in Cu, Ni, Cu-Al alloys, and 304 stainless steel. The coincidence of low-angle boundaries has been observed to be appreciable even in "equilibrated" stainless steel and nickel, and we are continuing work in this area.[3]

While Fig. 1 illustrates the nature of a twin/grain boundary junction in copper, from which the ratio, γ_{tb}/γ_{gb}, can be determined as indicated above; it also shows the anomalous formation of widely extended stacking faults. This same effect has been observed in nickel; and aside from being the first such reported observations in Ni, it points up a very interesting phenomenon which is presently being pursued in more detail. It has also indicated that a thorough evaluation of the significance of stacking-fault energy is needed; and we are also proceeding along these lines. In particular, the stacking-fault energy in 304 stainless steel and Inconel is presently being measured using the electron microscope. These measurements will then be compared with the apparent stacking-fault energies in the anomalous cases of very wide splitting of the partial dislocations. It is presently believed that this anoamlous splitting in many thin film materials is due to peculiar stress distributions due in large part to the surface image forces, which may in effect create local anisotropic behavior.

A detailed study of metal and alloy interfaces, i.e., grain boundaries, twin boundaries and stacking faults is also in progress which will attempt to clarify the procedures we will utilize in our experimental work, as well as aid us in the characterization, hopefully, of the geometrical, crystallographic, and structural nature of these interfaces which we will eventually co-ordinate with the relative energies of formation.

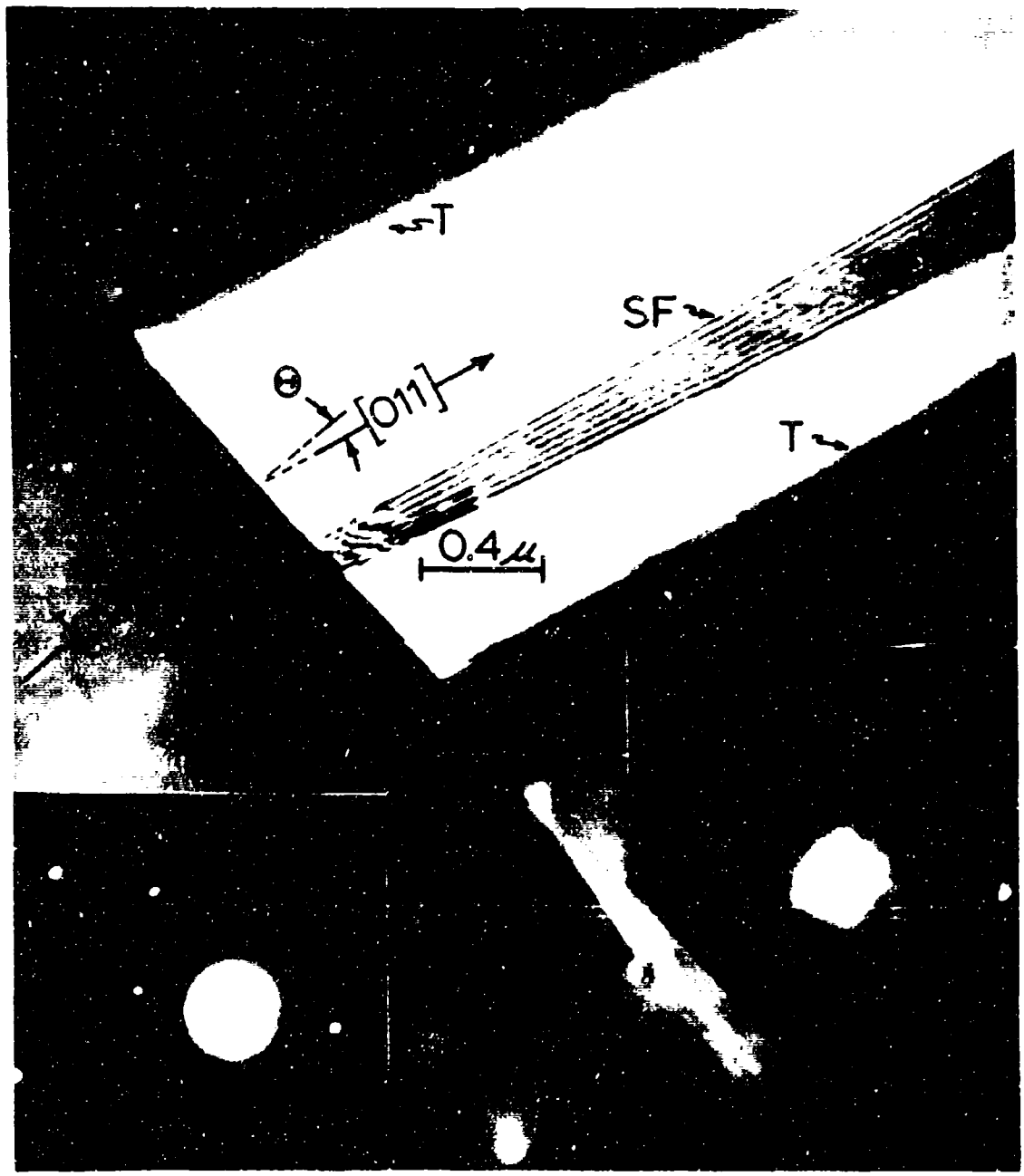

Fig. 1 Twin-grain boundary junction in copper annealed 0.5 hr at 700°C). The grain boundary misorientation, Θ is indicated between the [011] directions inferred from the selected-area electron diffraction patterns and the {111} traces. Note the stacking-fault contrast (SF) as distinct from the twin interfaces (T). The grain surface orientation of grains A and B is approximately (100).

References

1. L. E. Murr, Acta Met., 16, 1127 (1968).

2. L. E. Murr, J. Appl. Phys., 39, 5557 (1968).

3. L. E. Murr, L. J. Horylev and W. N. Lin, "The Role of Crystallographic Misorientation in the Measurement of Relative Twin/Grain Boundary Energy Ratios", Scripta Met., to be published (June, 1969).

1.5.4 Rare Earth Metastable Solid Solutions

AF-AFOSR 69-1622, Joint Services Electronics Program

R. Wang

The terminal solid solubility limits in binary alloy systems can be greatly extended after forming metastable solid solutions by a rapid quenching technique[1]. Experiments performed by different workers already show that the ranges of existing limited solid solutions could be amplified, in general, from 2 X up to 150 X[1,2,3]. A feature of great attraction is that the non-soluble elements could possibly form limited solid solutions which are impossible by conventional quenching methods[2,3].

Research in rare earth metastable solid solutions is initiated as follows:

1. The solubility and stability of metastable solid solutions of Calcium, Indium and Tin in Cerrium

According to the classical theory, Ca, In and Sn are expected to have high solubility in cerium which is not true in the real case. The high cooling rate will be possible to retain some of the high solubilities in room temperature or in liquid nitrogen temperature.

2. The age-hardening properties and its particle dispersion of some highly super-saturated rare earth solid solutions.

3. Search of the high temperature allotropes of Ho, Er and Tm under a high cooling rate with additional small amount of solute such as Mg, etc.

4. Defects in rare earths quenched from the liquid state.

Since the cooling rate has played an important role in the formation of defect structure. Very high and uniform densities of defects observed in the splat foil of pure aluminum[4] indicate that very large super-saturation of vacancies are retained by rapid quenching from the melt. The defect structure of Gd[5] and La[6] were recently reported. It is intended to study the defect structure obtained first from pure rare earth elements and then extended to their alloys.

References

1. P. Duwez, Progress in Solid State Chem. 3, 377 (1966).
2. B. C. Giessen, Private Communication MIT, Cambridge, Mass., 1968.
3. C. Jansen, B. C. Giessen and N. J. Grant, Presentation in Fall Meeting of AIME, Detroit, Michigan, 1968.
4. G. Thomas and R. H. Willens, Acta Met. 12, 191 (1964).
5. O. N. Srivastava, Phil. Mag. 18, 503 (1968).
6. J. Silcox, Trans. Met. Soc. AIME 242, 579 (1968).

1.5.5 Preparation of Rare Earth Magnets

AF-AFOSR 69-1622, Joint Services Electronics Program

R. Wang

The promising magnetic properties of rare earth-cobalt compounds require the preparation of these materials as small, ideally single-crystalline particles which have to be aligned with their easy axes parallel to each other packed so densely as possible and permanently held in the position by a non-magnetic matrix. The conventional mechanical grinding process usually causes plastic deformation effects which may severely reduce the magnetic properties to achieve to their theoretical limits. Even though it is possible to cast massive magnets by substitute

some of the cobalt by copper and iron[1]. And a rapid freezing of the compounds from the molten state will lead those small crystallines in this cast aligned directionally normal to the cold surface[2]. These direction effects appear to be associated with the directionally magnetic properties.

Experiments have been initiated for studying the cooling rate associated with the preferred orientation and the size of the five particles by rapid quenching of several rare earth cobalt compounds from its liquid state and followed by low temperature treatments. YCO_5, $SmCO_5$ and their copper, iron substituted alloys will be subject to investigation. Intensive studies will be concentrated on YCO_5 alloys since they have higher theoretical limits than $SmCO_5$ but the laboratory achievement for YCO_5 is far behind that of $SmCO_5$ alloys.

References

1. E. A. Nesbitt, R. H. Willens, R. C. Sherwood, E. Buehler and J. H. Wernick, Appl. Physics Letters 12, 361 (1968).

2. E. A. Nesbitt, presented in the 1969 Spring meeting of the Metallurgical Society of AIME, Pittsburgh, Pennsylvania.

1.5.6 The Crystal Structure of Metastable Au_7Bi_8

R. Wang and B. C. Giessen*

In addition to the equilibrium phase Au_2Bi (C15 type) in Au-Bi system, there are three metastable Au-Bi phases, π, π' and $\phi(Au_7Bi_8)$. These phases can be produced by rapid quenching from the melt[1] to -190°C followed by thermal treatments.

While metastable π and π' have disordered, element-like crystal structure, Au_7Bi_8 belongs to a new structure type; from X-ray powder diffraction, it was found to be trigonal, space group $P\bar{3}$ ml, with lattice parameters a = 8.776 Å and c = 5.530 Å at -190°C. It was formed by a complicated sequence of transformations in the solid state as shown

*Associate Professor, Department of Chemistry, Northeastern University, Boston Massachusetts.

here for alloy with composition $Au_{0.45}Bi_{0.55}$:

$$\text{melt} \xrightarrow[-190^{\circ}C]{\text{s.c.}} \text{microcrystalline phase} + \pi + \text{traces Bi and } Au_2Bi$$

$$\xrightarrow[-60^{\circ}C]{\text{H.T.}} \pi + Au_2Bi + Bi$$

$$\xrightarrow[0^{\circ}C]{\text{H.T.}} \phi + \text{Trace } \pi' + Au_2Bi + Bi$$

$$\xrightarrow[20^{\circ}C]{\text{H.T.}} Au_2Bi + Bi$$

(s.c. = splat cooled; H.T. = heat treatment at temperature given)

The crystal structure of Au_7Bi_8 was determined by X-ray diffraction and is illustrated in Fig. 1. It is composed of 4 NiAs-type unit cells with an ordered cation vacancy which is partly filled by the surrounding Bi atoms. The structure construction is based on the valence electron concentration related to AuSn.

The phase of $Au_7(Sb_xBi_{1-x})_8$ could also be retained by splat cooling but did not decompose after 24 hours at 20°C. The greater stability of $Au_7(Sb_xBi_{1-x})_8$ may be due to the smaller size of Sb atoms. The maximum value of x was not established. Attempts to substitute Sn for Bi was not successful, i.e., no NiAs type single phase alloys were obtained by rapid quenching, possibly due to the necessary stoichiometry change from AuSn to Au_7Bi_8.

References

1. P. Duwez, Prog. in Sol. State Chem. 3, 377 (1966).

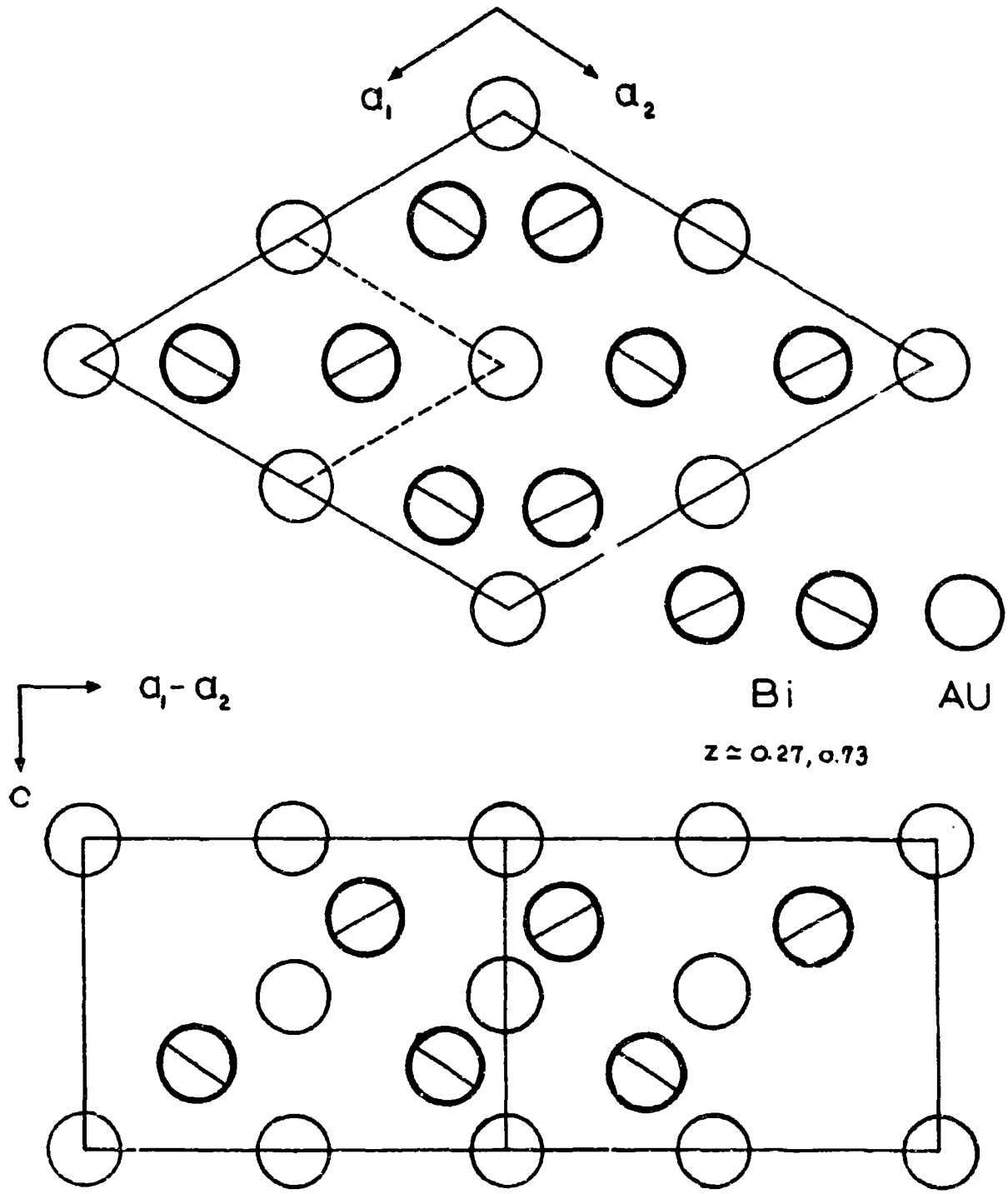

Figure 1. Unit cell of Au_7Bi_8 projected along [001] (top) and $[\bar{1}\,\bar{1}\,0]$ (bottom).

2. APPLIED ELECTROMAGNETICS AND PLASMAS

2.1 PLASMAS

2.1.1 Reflection and Transmission of Waves from Magnetized Nonuniform Plasma Slabs

GK 4066, National Science Foundation

H. H. Kuehl, B. B. O'Brien

The experimental study of microwaves reflected from and transmitted through a magnetized plasma slab appears to be complete.[1] A theoretical study of the coupling of incident electro-magnetic waves to longitudinal waves has been completed.[2] The observed reflection and transmission coefficients are in quite good agreement with the predicted values. The elctron temperature was determined from the radiation from the plasma at 3 GHz; the peak electron density as a function of time in the afterglow from double probe measurements; and the integrated value of electron density across the slab from phase shift observations of a 20 GHz inteferometer.

It appears that the resonances, e.g., in the reflection coefficient may provide a sensitive means of determining the electron density profile.

References

1. Consolidated Semiannual Progress Report No. 8, University of Southern California.

2. H. H. Kuehl, Phys. Fluids 11, 456 (1968).

2.2 MILLIMETER WAVE RADIOMETRY

2.2.1 Millimeter-Wave Radiometry for Radio Astronomy

NASA7-100, National Aeronautics and Space Administration
952 210, Jet Propulsion Laboratory
W.V.T. Rusch, A. Cooper, S. Slobin, C. Stelzried

The total integrated opacity of the atmosphere can be determined by measuring the radiation from an extra-terrestrial microwave source over a range of zenith angles. The sun is a strong source of millimeter-wave radiation that can be used for this purpose. In the interest of acquiring large amounts of atmospheric data, a semi-automated sun tracking system (STS) has been constructed. The data obtained in this manner can be correlated with ground-level atmospheric parameter data. Correlations of these two sets of data provide information useful in many types of communication systems such as, for example, satellite repeater stations. Furthermore, the present nodding subdish system[1,2], because of its beam switching capabilities, is particularly well suited for such a sun-tracking system.

The STS consists basically of the existing 90-GHz radio telescope with appropriate modifications. The antenna is tilted into its equatorial position. Accurate automatic tracking of the sun is provided by a closed-loop control system described below.

The STS was designed to keep the antenna pointed at the sun with a maximum pointing error of one minute of arc in any direction. The error sensing device consits of an optical telescope and four photoconductive cells to provide error signals for the feedback loop. The electronic circuitry consists of two identical channels: one for the right-ascension axis and one for the declination axis. Each channel consists of a detector, a logic circuit, and a power circuit. The power circuits control the stepping motors which drive the antenna. The logic circuits determine the correct sequence of voltages to be supplied to the stepping motors, and the detector circuits convert the analog signals from the photoconductive cells into

appropriate inputs to the logic circuits.

The STS has been found to perform within the design requirements of one-arcminute tracking error. The system works with a clear sky or with a light haze, but patches of clouds cause the system to lose its lock on the sun whenever any portion of the sun's limb is obscured. Under such circumstances a semi-automatic tracking mode is implemented, during which manual corrections are applied to the sidereal tracking rate. Fifteen days of solar observations were carried out during the first quarter of 1969. The data from these observations was reduced using a technique developed by Stelzried and Rusch[3], yielding the atmospheric zenith loss at 90GHz.

A. Atmospheric Loss Study. Stelzried[4] has developed a theory which may be used to relate the 90-GHz zenith loss with ground-level temperature and humidity. It may be assumed that the zenith atmospheric loss A in dB is separable into A_o, due to the total integrated oxygen content, and A_w, due to the total integrated water-vapor content. Thus:

$$A = A_o + A_w \tag{1}$$

The oxygen loss has been determined to be about 0.28 dB[5]. It may then be assumed that the water-vapor loss is related to the density of water vapor at ground level by the relation

$$A_w = A_{wr}\left(\frac{\rho}{\rho_r}\right)^{\alpha} \tag{2}$$

where A_{wr} is the water-vapor loss of a reference atmosphere of temperature T_r and hymidity H_r.

ρ is the actual ground-level density of water vapor, g/m^3.

ρ_r is the ground-level density of water vapor of the reference atmosphere.

α is a parameter relating the loss to the water-vapor content in accordance with the above equation.

Stelzried has empirically determined that in the range from 32 to 100°F the water density in saturated air is related to the temperature by

$$\rho_s = 1.8722 + 7.4970 \times 10^{-3} T + 2.7799 \times 10^{-3} T^2 - 1.2069 \times 10^{-5} T^3 + 2.7390 \times 10^{-7} T^4 \quad (3)$$

where the temperature is given in degrees Fahrenheit. The water-vapor content ρ and ρ_r are related to the content in saturated air by the relation

$$\rho = \frac{H}{100} \rho_s \quad (4)$$

where H is the humidity in percent. Equations (3) and (4) are then used to determine $\rho(T,H)$ and $\rho_r(T_r,H_r)$ for inclusion in equation (2).

The remaining parameters in equation (2), A_{wr} and α, may be determined by minimizing the variance between the theoretical and measured values. This has been done for the 15-days of solar data with the result that

$$A = 0.28 + 0.24 \left(\frac{\rho}{\rho_r} \right)^{0.4} \text{ dB} \quad (5)$$

where the temperature of the reference atmosphere has been chosen to be 60°F and the humditiy to be 40 percent. The variance obtained in the statistical determination of the above equation was 0.05 dB.

The advantage of the above result is that it does not require information concerning the water-vapor content (or temperature and humidity) above ground level. The ground-level values are easily determined with conventional instruments. It should be emphasized that equation (5), or an equivalent equation based upon considerably more data, is only valid for one particular season and geographical location and should not be expected to provide accurate information at other seasons and/or sites. However, once such an equation has been accurately determined

for a particular site, considerable advantage can be derived from its use rather than the conventional extinction-curve technique.

References

1. Consolidated Semiannual Progress Report No. 7, The Electronic Sciences Laboratory, School of Engineering, University of Southern California.

2. Giandomenico, A. and W. V. T. Rusch, "Millimeter-Wave Radiometer for Radio-Astronomy", U.S. Patent #3,417,399, Dec. 17, 1968.

3. Stelzried, C. T. and W. V. T. Rusch, "Improved Determination of Atmospheric Opacity from Radio Astronomy Measurements", Journal of Geophysical Research, Vol. 72, No. 9, May 1, 1967, pp. 2445-2447.

4. Stelzried, C. T., Private Communication.

5. Shimabukuro, F. I., "Propagation Through the Atmosphere at a Wavelength of 3.3 Mm", IEEE Transactions on Antennas and Propagation, Vol. AP-14, No. 2, March 1966, p. 228.

3. INFORMATION SCIENCES

3.1 CONTROL SYSTEMS

3.1.1 Stochastic Control Systems

AF-AFOSR 67-1029, Air Force Office of Scientific Research

D. D. Sworder

In many application problems the design of a controller devolves into a problem of selecting the best parameter setting for a control element whose structure is essentially fixed. Even in this circumstance a solution is far from easy to obtain because the nonlinearities and randomness in the mathematical model make it difficult to express the system performance measure as a function of the controller design parameters. The availability of digital computer facilities has created much interest in stochastic approximation as a means of evaluating the best controller without first displaying the performance functional. Survey papers [1] and [2], for example, provide a large number of references to work of this nature.

Of particular interest to engineers are results related to multidimensional algorithms requiring that the parameters be within a bounded region of the parameter space. In [3] this general problem is posed and conditions are derived which are sufficient to guarantee that a Kiefer-Wolfowitz procedure will converge with probability one. Utilization of this important result is limited by the difficulty one experiences in verifying the hypotheses of the theorem. It can be shown that to insure convergence, the criterion of performance must be almost equally sensitive to each component of the parameter vector.

If the nature of the performance index is known near its

minimum, it is possible to determine a linear transformation of the parameter space which converts the problem into one in which the sensitivity restriction is satisfied. Unfortunately, it is seldom the case that the information required to determine this transformation is available a priori with the result that additional computation must be performed.

In the past reporting period an investigation of a modification of the multidimensional Kiefer-Wolfowitz stochastic approximation algorithm has been made. A new algorithm which may be viewed as an analogue of the Newton-Raphson technique in deterministic problems has been developed. This iterative formalism is also related to Davidon's variable metric method for minimizing a function of several variables. It has been shown that under certain conditions this algorithm can be used to locate the minimum of a regression function in a bounded region of the parameter space and a qualitative measure of relative convergence rates with and without modification has been derived.

To show the relevance of this technique to controller design problems, an attitude control system for a space vehicle was investigated. Using classical techniques and a linear deterministic model, a nominal controller was selected which appeared to be adequate for the application. When the nonlinearities and randomness occurring in the actual system are introduced into the model, this controller was no longer satisfactory. It did, however, provide an initial point for a stochastic approximation algorithm which generated the final design.

An interesting aspect of the space vehicle problem was that the closed loop stability problem was solved implicitly by the design technique. It is expected that this same characteristic will be exhibited in many if not most applications problems. Whenever the performance measure is such as to magnify the unstable sample functions, the parameter vector will tend to move quickly into a stable region of parameter space.

For the example studied the computer time requirements were reasonable. It has been observed, however, that the time necessary to

obtain adequate results with stochastic approximation algorithms increases rapidly with the dimension of the parameter space. For this reason a judicious choice of parameter must be made. The design engineer must exercise the utmost care in the study of the linear model to find those characteristics of the compensation which most influence the system behavior.

References

1. Ya. Z. Tsypkin, "Adaptation, Training and Self-Organization on Automatic Systems," Automation and Remote Control, vol. 27, no. 1, pp. 16-51, 1966.

2. N. V. Loginov, "Methods of Stochastic Approximation," Automation and Remote Control, vol. 27, no. 4, pp. 706-728, 1966.

3. K. B. Gray, "The Application of Stochastic Approximation to the Optimization of Random Circuits," Proc. of Symposia in Applied Math., vol. 16, pp. 178-192, 1964.

3.1.2 Fuel Optimum Space Vehicle Attitude Control

NGR 05-018-044, National Aeronautics and Space Administration

H. J. Payne, V. G. Robinson

The determination of optimal controllers for systems in the presence of noise is reduced to the solution of partial differential equations of the form

$$\frac{\partial J}{\partial \tau} = \min_{\underline{u}} \left\{ d_{ij} \frac{\partial^2 J}{\partial \xi_i \partial \xi_j} + f_i(\underline{\xi}, \underline{u}) \frac{\partial J}{\partial \xi_i} + h(\underline{\xi}, \underline{u}) \right\} .$$

Successful numerical solution of this equation requires the use of stable, consistent and convergent numerical schemes. Stable numerical schemes have been developed for any equation of the above form. They involve the choice between forward or backward difference approximations for the first derivatives (the non-central points are taken

in the direction of the deterministic trajectory). These schemes are also consistent. That these schemes produce solutions which converge to the actual solution is a problem that has been left unanswered because existence of any solutions of the above equations is a yet unsolved problem.

A further problem which arises is the necessity of imposing artificial boundary conditions since numerical integration necessarily takes place over a finite region. Several forms of boundary conditions which retain stability are being investigated for their effect on the solutions. In the special case of the solution of

$$\frac{\partial J}{\partial \tau} = \min_{u} \left\{ d \frac{\partial^2 J}{\partial \xi^2} + u \frac{\partial J}{\partial \xi} + \xi^2 + |u| \right\}$$

(representing the optimal control of a single integrator), the steady-state solution is known [1], so that a means of evaluating the effect of boundary conditions is available.

Reference

1. McGhee, Payne, and Spuck, "Fuel Optimum Stochastic Attitude Control", USCEE Report 250, February, 1968.

3.1.3 Inversion of Multivariable Linear Systems

AF-AFOSR 69-1622, Joint Services Electronics Program

L. M. Silverman

Let $\mathcal{A}$ be a linear dynamical system represented by the equations

$$\dot{x}(t) = A(t)\, x(t) + B(t)\, u(t) \tag{1a}$$

$$y(t) = C(t)\, x(t) + D(t)\, u(t) \tag{1b}$$

where $x(t) \in R^n$, $y(t) \in R^p$ and the matrices A, B, C and D are of compatible order and are differentiable a finite number ($\leq n$) of times. Let $\mathcal{U}$ be the input function space over $[t_o, \infty]$ and $\mathcal{Y}$ the corresponding

output space. Elements of $\mathcal{U}$ are assumed to be at least continuous. For each initial state $x_o = x(t_o)$, $\mathcal{A}$ defines a mapping $H_{x_o}: \mathcal{U} \rightarrow \mathcal{Y}$. The present study is concerned with the problems of determining when the mappings H_{x_o} are invertible and in finding a system representation of the inverse when it exists. These problems have been studied by several authors for various classes of systems[1-4] and the applicability of a system inverse either implicitly or explicitly to numerous problems in control, filtering, decoding and network synthesis has been demonstrated[1-8].

Most previous research has centered on the linear time-invariant case where the fact that invertibility is equivalent to nonsingularity of the system transfer function matrix can be fully exploited. Brockett and Mesarovic[1,2] gave the first necessary and sufficient condition for invertibility in terms of the coefficient matrices as well as an inversion algorithm for the subcase $p = 1$. Youla and Dorato[3] derived a somewhat simpler criterion for invertibility and gave an inversion algorithm for $p > 1$. Silverman[4] showed that Brockett's[2] inversion algorithm could be generalized to the time-variable case for $p = 1$ and that it could be modified to obtain an inverse system of lower dynamic order than n.

Both the time-invariant and time-variable cases for $p > 1$ are now being studied and a new algorithm for constructing an inverse for a time-invariant system has been obtained. This algorithm has several important advantages in comparison with previous procedures. In particular, a separate test to determine non-invertibility is not required. A sequential test is incorporated into the algorithm which detects singularity quite simply. As a result, computation is reduced significantly. Moreover, considerable insight into the structure of the inverse system is gained. A minimal number of differentiations are employed and a technique for reducing the order of the inverse system, generalizing that of [3], is obtained. The total number of integrators and differentiators employed in the reduced inverse is precisely n.

The algorithm and techniques of proof for the time-invariant

case also have the advantage of generalizing directly to the time-variable case. It has been shown that if a time-variable system satisfies certain regularity conditions a necessary and sufficient test for invertibility can be given which does not require solving differential equations. For this class of systems, the method for constructing an inverse is formally the same as in the time-invariant case.

Work is continuing on applications of the inverse system theory and techniques so far developed. A particular application being considered is the problem of filtering and estimation in the presence of colored noise. While this problem has been treated in the past, a completely satisfactory solution has not been obtained. Preliminary investigations have shown that the inversion algorithm we have obtained gives new insight into the problem and should lead to a more complete solution.

References

1. R. W. Brockett and M. D. Mesarovic, "The Reproducibility of Multivariable Control Systems", J. Math. Anal. & Appl., Vol. 11, pp. 548-563, July 1965.

2. R. W. Brockett, "Poles, Zeros and Feedback: state space interpretation", IEEE Trans. on Automatic Control, Vol. AC-10, pp. 129-135, April 1965.

3. D. C. Youla and P. Dorato, "On the Inverse of Linear Dynamical Systems", Electrophysics Memo PIBMRI-1319-66, Polytechnic Institute of Brooklyn, March 1966.

4. L. M. Silverman, "Properties and Application of Inverse Systems", IEEE Trans. on Automatic Control, Vol. AC-13, to appear, August 1968.

5. P. L. Falb and N. A. Wolovich, "Decoupling in the Design and Synthesis of Multivariable Control Systems", IEEE Trans. on Automatic Control, Vol. AC-12, pp. 651-659, December 1967.

6. B.D.O. Anderson and J. B. Moore, "State Estimation Via the Whitening Filter", Proc. 1968 Joint Automatic Control Conf., Ann Arbor, Michigan, pp. 123-129.

7. J. L. Massey and M. K. Sain, "Inverse of Linear Sequential Circuits", IEEE Trans. on Computers, Vol. 17, pp. 330-337, April 1968.

8. B.D.O. Anderson, J. B. Moore and L. M. Silverman, "Network Realizations of Time-Varying Passive Impedances", in preparation.

3.1.4 Generalizations of a Theorem of Dolezal*

AF-AFOSR 69-1622, Joint Services Electronics Program

L. M. Silverman, R. S. Bucy

Let $A(t)$ be an $n \times n$ matrix function which is continuous on an interval J and whose rank is less than or equal to $r < n$ for all t in J; a question which arises in many problems is whether there is a nonsingular continuous matrix $M(t)$ such that $A(t)M(t) = [B(t): 0]$ where $B(t)$ has r columns for all t in J. If this is the case, then there is a set of continuous basis vectors which span an r-dim subspace of the null space of $A(t)$. Dolezal[1] has established the following when $A(t)$ has constant rank.

Dolezal's Theorem: Let $A(t)$ be an $n \times n$ matrix which is C^k and has rank r everywhere in the interval in $[0, \infty)$. Then there exists a $n \times n$ matrix $M(t)$ which is C^k and nonsingular for all $t \in [0, \infty)$ such that $A(t)M(t) = [B(t):0]$ where $B(t)$ is $n \times r$ for all $t \in [0, \infty)$.

In many time-variable system applications, matrices with non-constant rank are encountered. We have recently[2] examined the extent to which Dolezal's Theorem can be generalized if $A(t)$ does not have constant rank. It was shown by several examples that a complete generalization is not possible without some type of analyticity assumption on the elements of $A(t)$. If $A(t)$ is analytic, however, the existence of an analytic basis for its null space can be shown[2].

* Research performed with Department of Aerospace Engineering and also supported under grant AF-AFOSR 1244-67B, Air Force Office of Scientific Research.

References

1. V. Dolezal, "The Existence of a Continuous Basis of a Certain Linear Subspace of E_r which Depends on a Parameter", Cas. Proc. Pest. Mat. Soc. 89, 466-468, 1964.

2. L. M. Silverman and R. S. Bucy, "Generalizations of a Theorem of Dolezal," Presented at The Second Hawaii International Conference on System Sciences, January 1969.

3.1.5 Investigations on the Existence, Uniqueness, Continuous Dependence, and Differentiable Dependence of the Solutions of Certain Operator Equations

AF-AFOSR-67-1029B, Air Force Office of Scientific Research

AF-AFOSR-69-1622, Joint Services Electronics Program

L. W. Neustadt

An investigation was carried out on solutions of operator equations of the form $x = Tx$, where x is a member of the space of continuous functions from a compact interval into R^n, Euclidean n-space, and T is a continuous (not necessarily linear) operator from this space into itself. The questions that were asked were the following: Does this equation have a solution (if only in some local sense), and is this solution unique? Can a local solution be continued? Is there a maximal continuation? Do simplifications occur when T is affine? Does x in some sense depend continuously, or even in a differentiable manner, on T?

It was shown that, when T satisfied certain hypotheses, then all of the above questions have affirmative answers. The hypotheses were chosen in such a way that one obtained theorems that included, as special cases, most of the existence, continuation, uniqueness, and continuous and differentiable dependence theorems for ordinary differential equations, Volterra integral equations, and functional differential equations. Thus a very general unified theory of the subject matter was obtained.

The results also provided a new and surprisingly natural way to view optimal control problems, particularly from the viewpoint of existence theorems and necessary conditions.

One paper reporting these results is in preparation; another is planned.

3.1.6 Optimal Recursive Estimation with Uncertain Observation

NGR-05-018-044, National Aeronautics and Space Administration

N. E. Nahi

In classical estimation theory, the observation is always assumed to contain the signal to be estimated. In practice certain observations, or sequences of observations, may contain noise alone, only the probability of occurrence of such cases being available to the estimator. An example is trajectory tracking where the signal is first detected and then the estimator is allowed to process it for tracking purposes. However, any detection decision is associated with a false-alarm probability, which is the probability that the detected signal contains only noise. Minimum-mean-square estimators are derived for two different forms of this problem: 1) when it is possible that the observation at any sample time contains signal or is noise alone, independently of the situation at any other sample, and 2) when the entire sequence of observations contains signal or is only noise. The estimators derived are of recursive form.

3.1.7 Optimal Control With Dead Time Constraint

NGR-05-018-044, National Aeronautics and Space Administration

N. E. Nahi, B. Herron

Systems whose control inputs are constrained in some prescribed manner have been studied by many individuals in the last decade. In this research the case of controls which cannot change their polarity instantaneously is considered. More specifically, this implies that in order for a control function to change its polarity it must first assume the value zero (identically) on a time interval of at least τ seconds irrespective of its original magnitude or polarity prior to initiating the change. This control constraint is referred to as the polarity reversal constraint (PRC). The set of admissible controls (denoted by $U(\tau)$) is assumed to contain bounded measurable functions constrained in amplitude or energy which satisfy the PRC.

The study has been limited to control systems which are described, for all t in the compact control interval $K = [t_0, T]$, by a linear vector differential equation $x^{o}(t) = A(t)x(t) + B(t)u(t)$, with $x(t_0) = x_o$, where A and B contain continuous elements. The problem is to determine the control(s), $u \in U(\tau)$, which transfer the system from x_o to a final state, $x(T)$ at $t = T$, such that the quadratic function $(x_d - x(T))'Q(x_d - x(T))$ is minimized--the terminal control problem. The matrix Q is assumed positive semidefinite and the designated point x_d is not reachable by any control in $U(\tau)$ for $t \in K$.

The admissible control set $U(\tau)$ can be decomposed into subsets by defining four types of subintervals (in K) on which the controls must be identically zero. These intervals can be used to systematically construct the elements of each subset. By introducing the idea of an extremal control which maximizes the travel in a given direction in the state space, conditions can be determined which stipulate the requirements for a control to be extremal with respect to a given subset. The subsets of extremal control

can be shown to generate hypersurfaces (extremal surfaces) which have separation properties analogous to those of convex sets. This leads to a necessary and sufficient condition for a local minimization of the quadratic function on each of the extremal surfaces.

The relationship between extremal surfaces and portions of the boundary of the reachable set for $\tau \equiv 0$ has been established. The reachable set for constant coefficient systems with real eigenvalues and controls constrained in amplitude is found to be compact but not convex and the boundary of the set lies in the union of the associated extremal surfaces. The reachable sets for the larger class of systems originally specified (for both amplitude and energy constraints) have been investigated via representative examples and found to have the same properties as given above. From this it follows that the global minimum of the quadratic function can be found from knowledge of the local minimum on extremal surfaces.

A computational technique for determining the global minimum has been developed. The technique is a modification of a method for minimizing a quadratic function on a convex set.

3.1.8 Optimal Stochastic Regulator Problem With Observation Constraints

NGR-05-018-044, National Aeronautics and Space Administration

N. E. Nahi, T. Cooper

The usual type of stochastic regulator problem consists of finding a control for a dynamic system which is optimal in the sense that it minimizes some cost function. This cost function is usually assigned to the control and to the state of the dynamic system. The usual stochastic regulator problem also considers the possibility of random disturbances entering into the system dynamics, but assumes the vailability of all observations of the system's state which may be needed to determine the

optimal control. In some important classes of problems, however, observations may not always be available, or observations may be available only if we are willing to incur a certain cost.

The two observation constraints which are considered here are: (1) stochastic interruption of observations and (2) assignment of a cost to the act of making an observation, and requiring the controller to generate both an optimal observation function and an optimal control function. General functional equations have been derived for each of these problems which will formally permit solution by Dynamic Programming techniques. However, the application of Dynamic Programming to this particular class of problems will usually require an excessive amount of computation. Hence it is desirable to find analytic solutions to these functional equations. This has been done for some particular but very important cases.

For a linear dynamic system with quadratic costs on state and control, and with stochastic interruption of observations, the general functional equation has been analytically solved for a closed form feedback control law. This control law may be interpreted as using the least mean square estimate of the state, based upon whatever observations are available, in the feedback control law for the usual stochastic regulator problem.

For a linear dynamic system with quadratic costs on state and control and a fixed cost on the act of making an observation, the general functional equation has been analytically solved for a solution which simultaneously gives both the optimal observation function and the optimal control function. This optimal observation function depends only upon the system parameters, and is independent of the actual value of any observation. Once the optimal observation function is known, the optimal control function may be interpreted as using the least mean square estimate of the state, based upon the optimally selected observations, in the feedback control law for the usual stochastic regulator problem.

3.1.9 The Identification of Human Operator Models by Stochastic Approximation

NGR 05-018-022, National Aeronautics and Space Administration

C. B. Neal, G. A. Bekey and M. J. Merritt

The main objective of this research is the application of stochastic approximation techniques to the identification of parameters in sampled models of dynamic systems, including those which involve hypothesized discrete models of human controllers. Since the last report, the first phase of this work has been completed and C. B. Neal's dissertation[1] has been completed and issued as a report. The theoretical aspects of this work will be submitted to the 1969 Joint Automatic Control Conference for presentation as an invited paper[2] and will be submitted for publication to the IEEE Transactions on Automatic Control. The aspects of this research most particularly concerned with the description of human operators will be presented at the 1969 MIT-NASA Conference on Manual Control[3].

The abstract of C. B. Neal's dissertation follows:

Abstract

Various methods have been proposed to estimate the parameters of both open loop and closed loop sampled-data control systems. Generally speaking, these methods yielded approximate models of the system under study; the degree of approximation depending on the a priori knowledge of the system structure, state observation noise, system nonlinearities, and other factors. However, none of the methods has been applied to the problem of determining the sampling interval of either closed loop or open loop sampled-data control systems. This has been the task of the present study. Specifically, this dissertation is concerned with estimation of parameters in systems that have internal sampling, but have continuous input and output. The continuous portion of the sampled-data

system is given by the differential equation

$$\frac{dz}{dt} = f(z, p, u(t)); \quad z(t=0) = \zeta$$

where z is an n dimensional vector of state, $f(\cdot)$ is the n dimensional vector of the dynamical system, p is a constant h dimensional vector of parameters, u(t) is an r dimensional vector of piecewise continuous control functions, and ζ is the initial condition vector. For our results, $f(\cdot)$ was required to be of class C^1 in z and p. The differential equation is preceded by some form of data hold. The model-matching technique was used for parameter estimation. Methods were developed for determining not only the sampling interval, but all the other parameters and initial conditions of the sampled-data system as well.

In this investigation, three methods were employed for the estimation of sampling intervals and other parameters of a sampled-data system. In all methods, the cost function was the integral of norm-squared error, where the error function was defined as the difference between the observed state vector of the system, and the state vector of the model.

The first method employed programmed search to vary the model parameters in order to minimize the cost function.

The second method employed iterative gradient search by means of discrete sensitivity difference equations for the various model parameters. The work of Bekey and Tomovic in connection with discrete sensitivity difference equations for the sampling interval was extended to all the other parameters of the system. Gradient search was then used for parameter estimates.

The third, and most important, method used was that of stochastic approximation. This permitted observation noise. The mean-square convergence of the model parameters to the true parameters of the system was proved under the following conditions: The systems and

model agreed in form and order, the data holds were identical, the observation noise had zero mean, finite variance, and was uncorrelated with both the system state vector and model state vector, $f(\cdot)$ was of class C^1 in z and p, and the partial derivative of the cost function with respect to the sampling interval existed and was bounded.

Stochastic approximation was then applied to the practically important problem of estimating the parameters of the human operator from records of scalar input and scalar output of the human operator operating in a closed loop configuration. Parameters were estimated successfully in both continuous and sampled-data models of human operators.

References

1. Neal, C. B., "Estimation of the Parameters of Sampled-Data Systems by Stochastic Approximation", Ph.D. Dissertation, Univ. of So. California, January 1969 (Also issued as USC Electronic Sciences Laboratory Report, USCEE 333).

2. Neal, C. B. and Bekey, G. A., "Estimation of Parameters of Sampled-Data Systems by Stochastic Approximation", to be presented at Joint Automatic Control Conference, Boulder, Colorado, August 1969.

3. Neal, C. B. and Bekey, G. A., "Identification of Human Operator Models by Stochastic Approximation", to be presented at MIT-NASA Conference on Manual Control, March 1969.

3.1.10 Discrete Human Operator Models

NGR 05-018-022, National Aeronautics and Space Administration

M. J. Merritt and G. Meier

The development of mathematical models which describe discrete human operator control actions has been discussed in references 1, 2 and 3. The models utilized two basic building blocks: the Multi-State Decision Element (MSDE) and the Proportional Decision Element (PDE). Identification procedures for both elements are given in reference 5. However, the procedures for the MSDE are not satisfactory.

Consider the following manual control task in which the human operator elects to produce the discrete control actions +1, 0 and -1. Although the only direct input to the human operator is x(t), the human

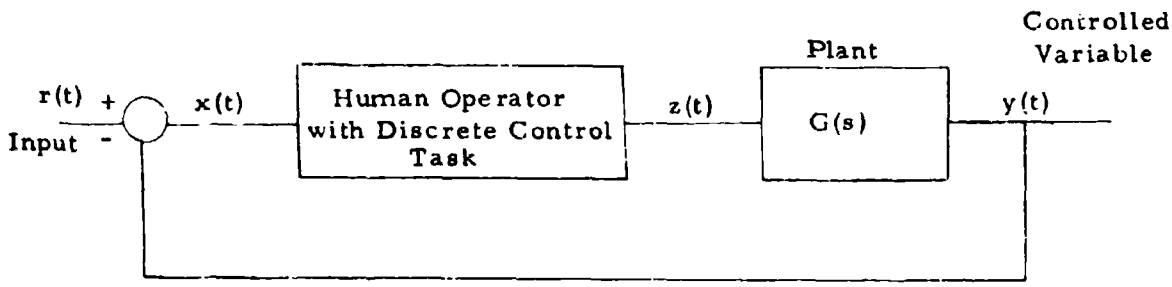

operator is capable of estimating $\dot{x}(t)$. Thus the decision policy will, in general, be a function of both x(t) and $\dot{x}(t)$. Previously, the number of input state variables was increased, through the inclusion of algebraic functions of x and $\dot{x}$, until hyper planes could be used as decision surfaces. Interpretation of the hyper plane decision surfaces in the original input space, x and $\dot{x}$ was difficult.

Under development are digital computer programs which will locate decision surfaces and volumes in multi-dimensional decision spaces and approximate them using a set of parametric figures. The dimensionality of the problem will be that of the input state space and will not be artificially increased. Interpretation of the decision boundaries will present no difficulties.

Two manual control tasks have been simulated and input-output data obtained. This data will be used to test and improve the identification procedures. The two tasks are shown in the figures below; (see Ref. 3)

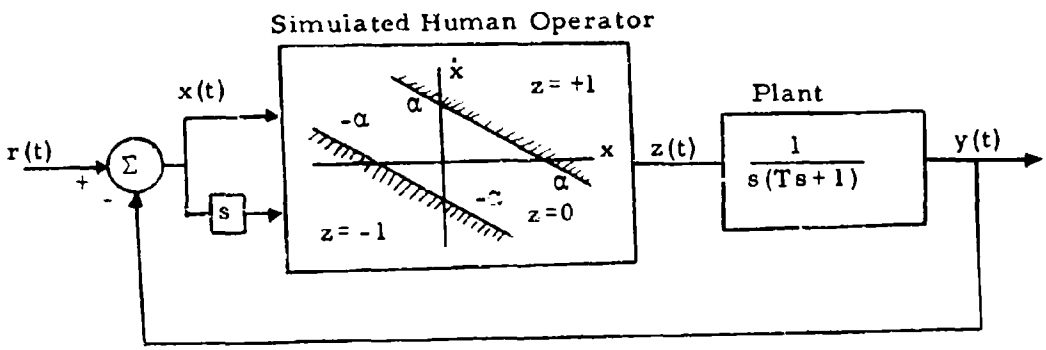

Task 1

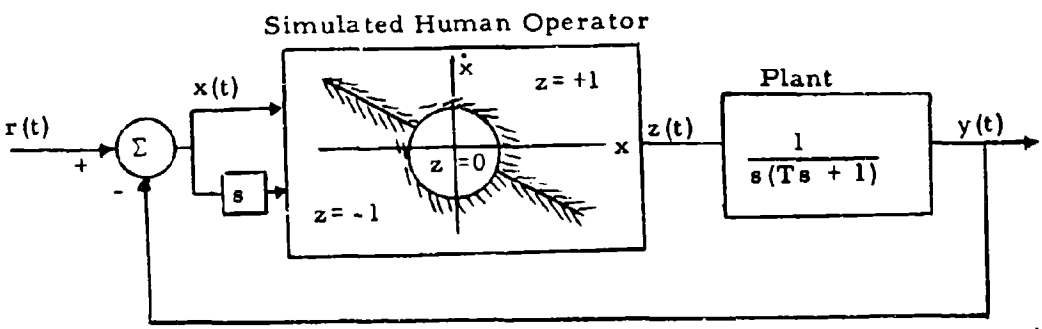

Task 2

References

1. Merritt, M. J. and Bekey, G. A., "An Asynchronous Pulse-Width, Pulse-Amplitude Model of the Human Operator", Proc. 3rd NASA-University Conference on Manual Control, NASA SP-144, pp. 225-240, 1967.

2. Merritt, M. J., "Synthesis and Identification of Mathematical Models for the Discrete Control Behavior of Human Operators", Ph.D. Dissertation, University of Southern California, 1967 (Also issued as USC Electronic Sciences Laboratory Report, USCEE 202, 1967).

3. Merritt, M. J., "The Application of Discrete Modeling Elements to the Synthesis and Identification of a Deterministic Model for the Visual Scanning Behavior of Human Operators", presented at the NASA-University of Michigan Conference on Manual Control, 1968.

3.2 COMMUNICATION AND RADAR SYSTEMS

3.2.1 A New Simulation Technique for White Noise Processes

GU 1559, National Science Foundation
DA-ARO-D-31-124-G929-SU#1, U.S. Army Research Office, Durham

J. J. Stein, C. L. Weber

A new digital simulation technique for a large class of nonlinear differential equations has been developed[1]. This technique has been shown to have the desirable property of mean square convergence. The technique has been successfully applied to the simulation of phase locked loops in cascade[2]. It has been shown that significant economics in computational time are achieved for this technique as opposed to an existing method of digital simulation[3].

References

1. J. J. Stein and C. L. Weber, "A New Simulation Technique for White Noise," presented at the Polytechnic Institute of Brooklyn-Microwave Research Institute Symposium on Computer Processing in Communications, April, 1969.

2. J. J. Stein and C. L. Weber, "Cascaded Phase Locked Loops", presented at the National Electronics Conference, Chicago, Illinois, December 1968.

3. Babuska, I., Prager, M., Vitasek, E., "Numerical Processes in Differential Equations," J. Wiley, 1966.

3.2.2 Signal Design for M-ary Noncoherent Digital Communication Systems

GU 1559, National Science Foundation

M. S. Stone, C. L. Weber

It has been inferred for some time that the optimal solution of amplitude and phase modulation time waveforms for an alphabet of size M when the receiver is assumed unable to track the r-f phase of the arriving signal was not only a much more difficult problem than that for the coherent channel, but that it was also a significantly different problem. Recently, however,[1] a concise representation for the probability of detection for an arbitrary M-ary signalling alphabet has been obtained for the incoherent channel which is sufficiently similar to that for the coherent channel so that the optimization techniques used there can be similarly employed for the incoherent channel.

From this new representation, a new and simple approximation of the probability of error for an arbitrary signal waveform inner-product matrix has been obtained. With this approximation, the global optimality of the orthogonal noncoherent signal set has been demonstrated at large signal-to-noise ratios.[2]

In addition, it has been shown that all noncoherent signal sets are of an even number of dimensions, thereby limiting the number of possible solutions for a fixed alphabet size. Dimensionality is a measure of bandwidth in this framework.

General necessary conditions that a signal set must satisfy so as to locally extremize the probability of correct decision were then determined for the dimensionality, D, such that $D \leq 2M-K$ for K even, and $K \leq M-1$. Finally, classes of signal sets which satisfy these conditions were found.[3]

References

1. C. L. Weber, "A Contribution to the Signal-Design Problem for Incoherent Phase Communication Systems", IEEE Transactions on Information Theory, March 1968.

2. M. S. Stone and C. L. Weber, "On the Globally Optimum M-ary Noncoherent Digital Communication System", Proceedings of the IEEE, Vol. 57, 1969, (in press).

3. M. S. Stone and C. L. Weber, "Noncoherent Transmitter Optimization," IEEE Transactions on Information Theory, (to be submitted).

3.2.3 Nonlinear Analysis and Synthesis of Generalized Tracking Loops

GU 1559, National Science Foundation

W. C. Lindsey

The purpose of this research is to investigate the nonlinear behavior of generalized tracking loops which are of great practical interest in the design and successful operation of telecommunication networks.

Using the theory of Markov processes, the response probability density function $p(\underline{y},t)$ of a generalized tracking system is shown to be the solution to a $(N+1)$-dimensional Fokker-Planck equation. The vector $\underline{y} = (\varphi, y_1, \ldots, y_N)$ is Markov and φ represents the system phase error reduced modulo 2π.

It is further shown that the response distributions $[p(\varphi,t), p(y_k,t), k=1,2,\ldots,N]$ of the state variables satisfy a set of second-order partial differential equations. In the steady state, this set of equations become ordinary, first-order differential equations for which the exact solutions which specify the marginal probability densities $[p(\varphi), p(y_k), k=1,2,\ldots N]$, are determined by two sets of conditional expectations. In particular, the marginal density $p(\varphi)$ of the phase error is embedded in a knowledge of the conditional expectations $\{E(\nu_k(\varphi), k=1,2,\ldots N\}$ while the marginal density $p(y_k)$ of the state variable y_k is embedded in a knowledge of the conditional expectation $E\{g(\varphi)|y_k\}$; $k=1,2,\ldots,N$. Here $g(\varphi)$ belongs to that class of nonlinearities for which $g(\varphi)$ is an odd function. The conditional expectations are approximated by two methods and, for

the case of greatest interest, i.e., $g(\varphi) = \sin \varphi$, the conditional expectation $E(y_1 | \varphi)$ is measured via computer simulation methods. Agreement of the simulation results with these obtained from theoretical considerations are within less than one percent of each other.

Synthesis procedures for effecting stochastic optimization of a generalized tracker are presented. For zero detuning it is shown that the tracker which minimizes the mean-squared value of the phase-error is obtained when $N = 0$ and $g(\varphi)$ is proportional to $\operatorname{sgn} \varphi$. For large loop signal-to-noise ratios and equal mean-squared loop phase-errors, the second-order PLL system requires a loop signal-to-noise ratio, ρ, of approximately $\rho/2$ times larger than that required in the optimum second-order tracker. At low loop signal-to-noise ratios it is shown that all trackers perform approximately the same. For second-order trackers some results are presented for the case where $g(\varphi)$ must be physically realizable.

The field of probability currents is derived and it is shown that this field is rotational when there is zero detuning in the loop. From these currents the average number of cycles slipped per unit of time is derived. With zero detuning this average is zero. Finally, the diffusion coefficient, representing the rate with which the phase-error is undergoing diffusion, is given as well as the expected value of the time interval during which the loop remains locked.

References

1. Lindsey, W. C., "Nonlinear Analaysis and Synthesis of Generalized Tracking Systems," University of Southern California, USCEE 317, December 1968, Los Angeles, California. Also accepted for publication in Proceedings of IEEE.
2. Lindsey, W. C., "Statistical Dynamics of Second-Order Phase-Locked Loops", to be presented at the International Communications Conference, June 8-11, 1969, Boulder, Colorado. Also submitted to IEEE Transactions on Communication Technology, January, 1969.
3. Lindsey, W. C., "The Performance of Phase-Locked Loops in Cascade," submitted for publication to IEEE Transactions of Communication Technology, February, 1969.

3.2.4 Nonstationary Solutions for Phase-Locked Loop Systems

GU 1559, National Science Foundation

A. Chang, J. R. LaFrieda, W. C. Lindsey

This research is concerned with the "time solutions" of nonlinear phase-locked loops. In particular, for Nth-order nonlinear tracking loops, via a method similar to the Barret-Lampard expansion for first-order Markov processes, approximate numerical solutions of a periodic two-point boundary value problem, corresponding to the time-dependent Fokker-Planck equation, are constructed for the transition probability density function of the nonstationary, Markov phase-error process. From these results, the steady-state autocorrelation and power spectral density functions of the phase-error process are obtained. In addition, for the case of Nth-order loops, approximate solutions of the time-independent Fokker-Planck equation are obtained for the phase-error process.

3.2.5 Synchronization Coding

DA-ARO-D 31-124-G929, U.S. Army Research Office

R. A. Scholtz and R. M. Storwick

In a continuing study of statistically synchronizable codes for the discrete noiseless channel[1,2], efforts have been concentrated on those whose synchronization depends upon observing a sequence which appears in only one position relative to true sync. This synchronization procedure is simply implemented by shift register constructions. Uniformity of word lengths assures maintenance of word sync, once it has been attained. It is possible to compute the probability that, for any given positive integer, synchronization requires inspection of at least that many consecutive code symbols. This probability is one possible basis for comparison of codes. Also available are simple upper and lower bounds to this

probability, both of which are partially characterized by the average sync delay.

A method for analyzing the sinc capabilities of prefix codes has been developed. Based on the structure of their code trees, this method can be used with various sync procedures which, with probability one, establish sync after observing a finite (though not bounded) number of letters. It applies to codes with unequal word lengths as well as uniform lengths, and the prefix property guarantees maintenance of sync. In particular, the average sync delay for the ultimate sync procedure is computable. Also, upper and lower bounds to the probability that the synchronization process will require inspection of at least a given finite number of code symbols are available.

It has been established that for a code to be synchronizable in this sense, a necessary and sufficient condition is that its code tree is not a full tree, and that its codeword lengths have a GCD of one. The structure of any other code tree assures, with probability approaching one as the inspected symbol sequence becomes longer, that a point will be reached where sync can be definitely determined. A simple example of such a binary code is that having the following code tree:

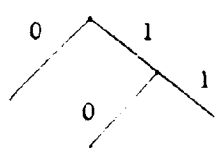

This code can be statistically synchronized by simply waiting for the first appearance of the code symbol 0, which can occur only at the end of a codeword. Note that this property holds even if the encoding is perfectly efficient.

This method of analysis applies to codes with the bounded sync delay or comma-free properties as well as those having only the statistical sync property. It may also be applied to any finite order

Markov message source.

References

1. R. A. Scholtz and R. M. Storwick, "Synchronization Coding", (Section 3.2.3, ESL Consolidated Semiannual Progress Report No. 8).

2. R. A. Scholtz and R. M. Storwick, "Statistical Synchronization Techniques", presented at the Second Hawaii International Conference on System Sciences, January, 1969.

3.2.6 Frequency Tracking

DA-ARO-D31-124-G929, U.S. Army Research Office, Durham

R. A. Scholtz, W. Cascell

We are studying the problem of estimating the process $\omega(t)$ from the observation

$$x(t) = N_c(t) \cos\left(\int^t \omega(\alpha)\, d\alpha\right) + N_s(t) \sin\left(\int^t \omega(\alpha)\, d\alpha\right) + n(t)$$

where $N_c(t)$, $N_s(t)$, $n(t)$ and $\omega(t)$ are Gaussian processes. Emphasis is being placed on designing a causal system to perform the estimation procedure. One such system, with an analytic signal input $z(t)$ having real part $x(t)$, is shown in Figure 1. Double lines indicate complex signals. This system has been analyzed in detail, and results will soon be published.

A second tracking method is now being explored (see Figure 2). This method involves the passing of an i.f. signal through two filters with adjacent passbands. The difference in energy of the two filter outputs is used to construct a tracking error signal. Our present research objective is to analyze this second system and ultimately to compare the performance of these two approaches.

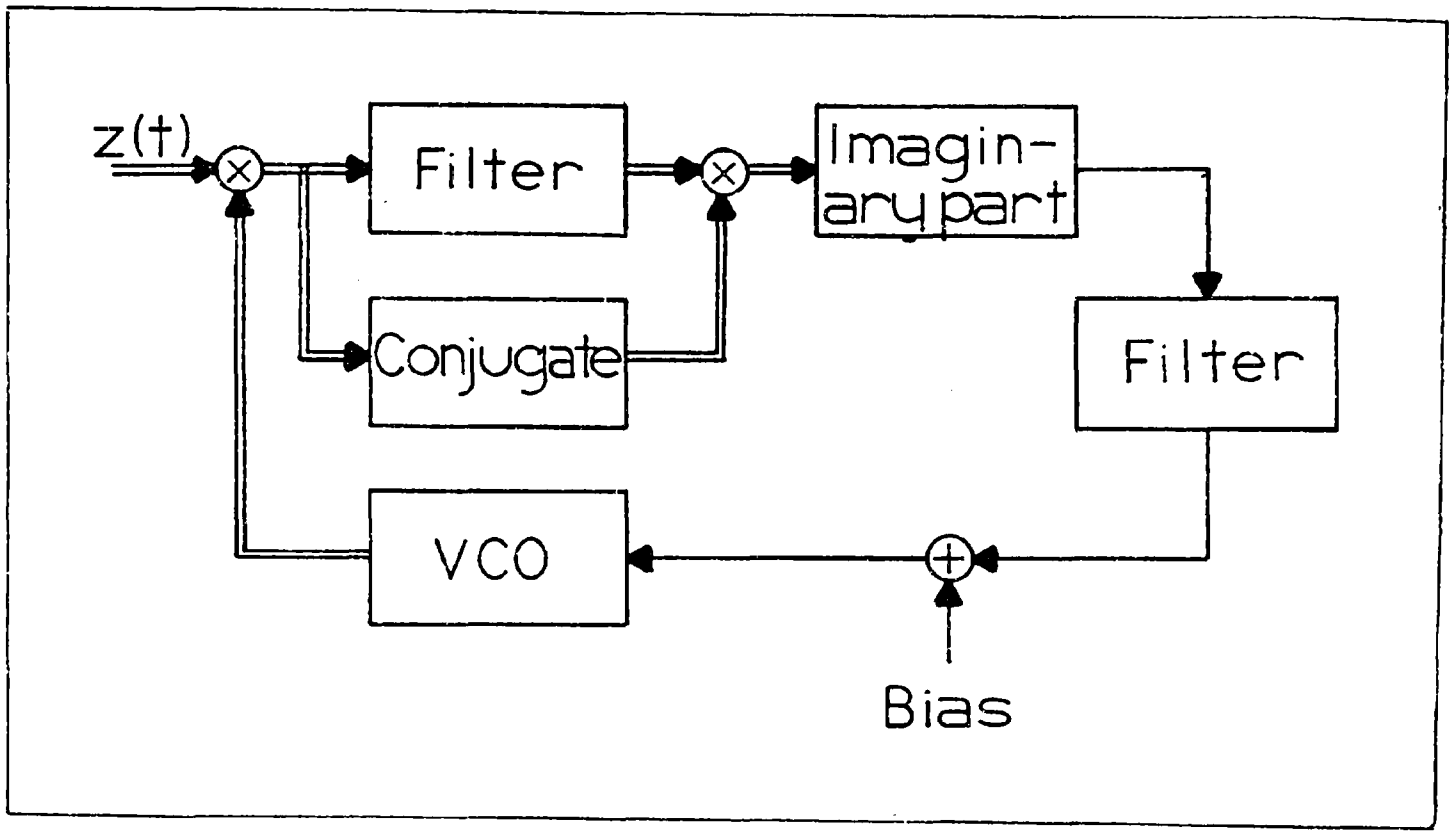

Fig. 1. A system for estimating the center frequency of z(t), copied after the maximum a-posteriori estimator.

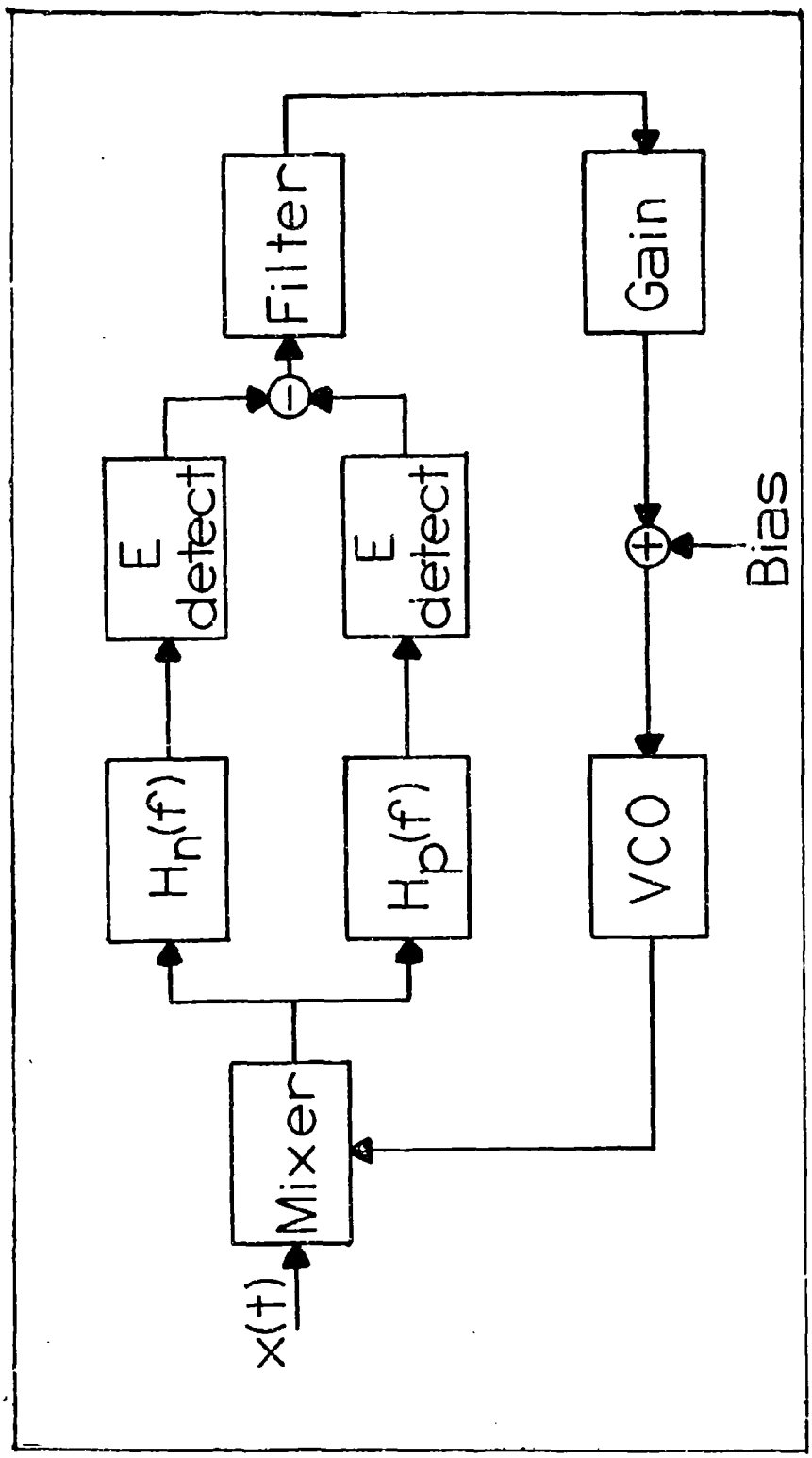

Fig. 2 A double frequency gate tracking loop

3.2.7 Pioneer VI Solar Faraday Rotation Experiment

Partially sponsored by Grant GU 1559, National Science Foundation

J. E. Ohlson, W. V. T. Rusch, C. T. Stelzried

A. Introduction

In November 1968, the Pioneer VI Spacecraft underwent solar occultation as it passed approximately one astronomical unit behind the sun. Before and after occultation by the visible disk, the spacecraft signals passed through the solar corona on their way to earth and experienced Faraday Rotation. This effect is a spatial rotation of the plane of polarization of a linearly polarized wave when it passes through a plasma in the presence of a longitudinal magnetic field. A sensitive receiving system was developed to measure this effect, and a large amount of data was obtained during the occultation. Three startling transient phenomena were observed, and measurements of the steady-state coronal contribution were made. This experiment was performed jointly with personnel of the Communications Elements Research Section of the Jet Propulsion Laboratory, G. S. Levy, B. Seidel and T. Sato.

B. Experiment Description

During the occultation, the spacecraft was tracked with the 210 feet in diameter NASA/JPL parabolic antenna at Goldstone, California. The r.f. hardware and receivers were extensively modified to effectively provide a cross-linearly-polarized feed system which can be automatically rotated to any position. This is the heart of the system. One feed produces an error signal which is continuously driven to zero by servo-positioning the feed system. The second feed is thus automatically aligned with the signal vector and provides a reference for the detection of the error signal. A pair of mechanically rotatable waveguide-section quarter-wave plates is used to synthesize the effectively rotating feed system. The position of one plate is accurately fixed and the position of the other tracks the received signal. Its position was digitally recorded and processed

through a celestial coordinate conversion program to obtain the Faraday Rotation undergone by the signal.

Several factors made this a difficult experiment:

(1) The signal was very weak from traversing a distance of two astronomical units.

(2) Intense radio noise of the sun entering the antenna sidelobes reduced the signal-to-noise ratio and prevented following the spacecraft to and from the photospheric limbs.

(3) Coronal turbulence produced severe spectral broadening of the signal which made tracking difficult.

(4) The earth's ionosphere contributes a rotation of 1-7^{o} to the signal. This ionospheric rotation was measured separately with a geostationary satellite and is being removed from the data.

C. Experimental Results

For several months prior to November 1968, data were taken with a manual version of the experimental system. This gave a data baseline and data on the ionosphere. Starting approximately November 1, the system was in its final form. On November 4, the first indication of solar effects was obtained. Over a period of about two hours a rotation of some 40^{o} was observed. This correlated exactly with enhanced spectral broadening of the signal measured by a second experiment. On November 8 and 12 similar events occurred, again correlated with enhanced spectral broadening. These three events appear to be correlated with decametric solar radio bursts and intense decimetric regions on the sun. A possible explanation is that a dense plasma cloud was expelled from the sun and passed between the spacecraft and the earth. As the spacecraft neared the sun an increasing steady-state rotation was measured. These data are just now being analyzed.

D. Future Plans

(1) Completion of data reduction.

(2) Examination and fitting of coronal models to the data.

3.2.8 Image Processing by Digital Computer

JPL 952312, Jet Propulsion Laboratory
NGR-05-018-044, National Aeronautics and Space Administration

H. C. Andrews, W. K. Pratt

The Video Systems Laboratory in the Electrical Engineering Department is extensively involved in the application of digital computers to image processing. The purchase of a third generation digital computer (HP 2116B), with associated periferal equipment, has allowed the staff to digitally implement various two dimensional transformations on images in the search for a bandwidth reduction and noise coding immunity in a digital communication system environment. In addition, the fields of optical data processing by digital computer, image enhancement by computer techniques, two dimensional pattern recognition, antenna diffraction pattern analysis, image evaluation, graphic display techniques, digital holography and many other applications are under investigation.

The specific mathematical transformations under current investigation for application in the area of image coding are the two dimensional Fourier transform and Hadamard/Walsh transform. Both of these transformations have the property of compacting a large percentage of the total energy in a picture into a very few number of coefficients. This is a result of the fact that pictures of interest tend to have some degree of two dimensional correlation which the transformations take advantage of. If an image is grid sampled at N^2 different points, it can be expressed as a sampled function $f(x,y)$. Then the discrete two dimensional transformations described above become:

Fourier:

$$F(u,v) = \frac{1}{N} \sum_{x=0}^{N-1} \sum_{y=0}^{N-1} f(x,y) \exp\left\{ -\frac{j2\pi}{N} (ux+vy) \right\}$$

Hadamard/Walsh:

$$F(u,v) = \frac{1}{N} \sum_{x=0}^{N-1} \sum_{y=0}^{N-1} f(x,y) (-1)^{\sum_{i=0}^{n-1} u_i x_i + v_i y_i}$$

where $N = 2^n$, and u_i, x_i, v_i, y_i refer to the binary variables in the binary representation of the parameters u, x, v, y respectively. Considerable success has been achieved in using these transformations for bandwidth reduction and noise immunity coding[1-8].

References

1. Pratt, W. K., Kane, J., and Andrews, H. C., "Hadamard Transform Image Coding", IEEE Proceedings, Vol. 57, No. 1, pp. 58-68 (January 1969).

2. Pratt, W. K., and Andrews, H. C., "Application of Fourier-Hadamard Transformation to Bandwidth Compression", M.I.T. Symposium on Picture Bandwidth Compression, April 1969.

3. Andrews, H. C., and Pratt, W. K., "Transform Data Coding", P.I.B. Symposium on Computer Processing in Communications, April 1969.

4. Pratt, W. K., and Andrews, H. C., "Transform Processing and Coding of Images", Final Report for California Institute of Technology, Jet Propulsion Laboratory, Contract No. 952312.

5. Andrews, H. C., and Pratt, W. K., "Transformation Coding for Noise Immunity and Bandwidth Reduction", Hawaii International Conference on System Sciences (January 1969), pp. 545-548.

6. Andrews, H. C., and Pratt, W. K., "Digital Computer Simulation of Coherent Optical Processing Operations", IEEE Computer Group News, pp. 12-19, Vol. 2, No. 6, November 1968.

7. Pratt, W. K., and Andrews, H. C., "Two Dimensional Transform Coding of Images", 1969 IEEE International Symposium on Information Theory, Ellenville, New York.

8. Andrews, H. C., and Pratt, W. K., "Television Bandwidth Reduction Encoding Spatial Frequencies", JSMPTE, Vol. 77, No. 2, pp. 1279-1281, December 1968.

3.2.9 Orthogonal Transformations by Digital Computer

NGR-05-018-044, National Aeronautics and Space Administration

H. C. Andrews

The use of orthogonal transformations in data processing by digital computer has many and varied applications. Probably the most familiar use of orthogonal transformations is the technique of breaking a function up into its Fourier spectral components. On a digital computer, multiplying an orthogonal matrix by a data vector is equivalent to decomposing the data into a set of coefficients of the orthogonal waveforms making up the matrix. If the entires of the matrix are complex trigonometric waveforms, then the vector-matrix product is equivalent to a Fourier transform. If the orthogonal entires of the matrix are other waveforms, then the decomposition results in a generalized spectral analysis. Implementation of such decompositions in a digital computer normally require N^2 operations for a vector-matrix product. However, if there is some built-in redundancy in the definition of the matrix, then often this redundancy can be used to implement the vector-matrix product in less than N^2 operations. A class of orthogonal transformations are being investigated[1] which are implementable in $pN \log_p N$ operations where $N = p^n$. This class of transformations has led to the fast Fourier transform, the fast Hadamard transform and many other types of generalized orthogonal transformations.

Application of the above class of fast orthogonal transformations to the area of pattern recognition is expected, especially in the search for maximum energy dimensions in the feature selection, classification process. In addition, orthogonal transforms are useful in the search for a dimensionality reduction in a variety of data processing activities where dimensionality constraints exist and where redundancy is inherent in the data gathering process. Two vivid examples of this are the audio and visual processes of sound and sight. It is hoped that with a more

general class of rapidly implementable orthogonal transformations, greater inroads can be made into the bandwidth and data processing problems.

Reference

1. Andrews, H. C., and Kane, J., "Kronecker Matrices, Computer Implementation, and Generalized Spectra", submitted to the ACM.

3.2.10 Hybrid Processing of Complex Radar Signals

GK-3303, National Science Foundation

J. E. Ohlson

Work is continuing on the problem of utilizing digital techniques to assit in the generation and processing of radar signals of the "chirp" class. Effort during this reporting period has been in two areas:

(1) It is desirable that zero-crossing frequency measurements be analyzable so that this simple analog-to-digital conversion technique can be used with confidence in radar processing. The zero-crossing problem for gaussian noise is being investigated with a new approach. So far, several results have been produced which have appeared before only as special cases of other approaches. Extension of present results seems probable at this time.

(2) A large class of low-ambiguity radar signals exists. These signals however are very difficult to generate, requring complicated envelope and phase variations. A desirable form for efficient generation is the constant amplitude, phase-modulated pulse. A special case, which is a variation of the classical "chirp", has been investigated that seems to be well suited for practical use. Unambiguous measurement of range and doppler simultaneously from a single pulse is possible with relatively simple processing.

3.2.11 On the Enumeration of Finite State Synchronous Sequential Machines

DA-AROD-31-124-G-929, U.S. Army Research Office, Durham

I. P. Bottlik and I. S. Reed

Two finite state sequential machines can be termed equivalent in more than one way. If the behavior of two sequential machines is the same, the machines are said to be functionally equivalent. Of secondary importance is permutational equivalence wherein two machines can be made to have the identical representation by a permutation of the input and output symbols, and a relabeling of the internal states. Functional and permutational equivalence are similar notions under a suitable permutation of the input and output symbols.

A computer program has been written which determines a canonical set of permutationally and functionally inequivalent machines and hence the number of such machines. Results have been obtained for small values of the parameters. Specifically if k is the number of states, n the number of input symbols, and m the number of output symbols, then results have been obtained for $m = 1$, $n = 1$, $1 \leq k \leq 5$; $m = 1$, $n = 2$, $1 \leq k \leq 4$; $m = 2$, $n = 1$, $1 \leq k \leq 5$; $m = 2$, $n = 2$, $1 \leq k \leq 3$. For $k = 5$, $n = 1$, $m = 2$ there are 100,000 representations out of which only 70 are functionally and permutationally distinct. Obtaining results for larger values of the parameters would require modification of the computer program due to storage restrictions, i.e., secondary storage on a disc would be required for an efficient program, and would involve excessive run times. Such an extension of the program is not presently contemplated since the computer results were primarily obtained to gain an insight and to serve as a check on some theoretical formulations which were obtained.

In searching the literature it was found that Haraly had developed a formula for the number of permutationally inequivalent machines.

A computer program has been written and results obtained for small values of the parameters which determines a canonical set of such machines. The number of such machines for the above values of the parameters has been checked against the Haraly formula. The proof of his formula, which was presented only sketchily in Haraly's publication, has been proven in a more rigorous manner.

The problem of enumerating functionally inequivalent machines is unsolved. To treat this problem an examination of computer results lead the authors to restrict attention to a subset of all finite state synchronous sequential machines. This subset composes the "group machines". These are machines for which the next state function is restricted to be a permutation of the states rather than a mapping of the states into the states. The Haraly's formulation for the permutationally inequivalent machines was found to be no longer applicable to these machines. This formulation depended for its proof on theorems which relate the cyclic structure of the elements of a composite group to the cyclic structure of the elements of the groups of which it is composed. One such composition, termed the Power Group of two groups, was found to be totally inapplicable to the group machines. A theorem has been proven which makes it possible to calculate the number of permutationally inequivalent group machines.

3.2.12 USC Speech Processing Program

AFOSR-68-155-A, Air Force Office of Scientific Research

DA-ARO-D 31-124-C930, Supp #1, Army Research Office, Durham

S. W. Golomb, C. S. Fuzak

Current research is directed toward the determination of a probability density to serve as a model for voicing duration in connected speech. A six parameter model has been proposed, and a $3^2 \times 5$ factorial experiment on text, pace, and speaker has been conducted to test the model. It has been observed that under certain conditions the model may

be reduced to a two parameter log-normal probability density. The fidelity of the six parameter model is now under investigation.

The factorial experiment has shown that the voicing duty factor (percentage of time spent in the voiced mode over a fixed interval of about fifteen seconds duration) may serve as a measure of speech pace, since this statistic is independent of text.

3.2.13 Cross-correlation of Linear Recurring Sequences

DA-ARO-D 31-124-C930, Supp #1, Army Research Office, Durham

S. W. Golomb and Herbert M. Trachtenberg

Let $A = \{a_i\}$ be a maximum length linear recurring sequence of degree n over GF(p), p an odd prime. It is well known that the length of such a sequence is $p^n - 1$ and that there exist p-1 "natural orientations" of the sequence A such that $a_{pi} = a_i$ for all i. It is known also that if A is in a natural orientation, then the sequence $B = \{b_i\} = \{a_{ri}\}$ is also a maximum-length linear recurring sequence in natural orientation whenever $(r, p^n-1) = 1$. When r is not a power of p, the sequences A and B are distinct.

We define the (unnormalized) cross-correlation of the sequences A and B to be the function

$$C_{AB}(\tau) = \sum_{i=0}^{p^n-2} \chi(a_i)\, \chi(b_{i+\tau})$$

where $\chi(a) = \rho^a$, and ρ is a primitive p^{th} root of unity. We have proved that with this definition of cross-correlation, $C_{AB}(\tau)$ is always real valued even though it is a sum of complex numbers.

It was observed experimentally that for many values of r, $C_{AB}(\tau)$ is three-leveled as τ ranges from 0 to $p^n - 2$. Theorems have been found which predict many values of r resulting in three-valued cross-

correlation:

1. For odd n, any $r = \frac{p^{2k}+1}{p^k+1}$ leads to three-valued cross-correlation. The values which occur are -1 and $-1 \pm p^{\frac{n+2}{2}}$ where e = GCD (k,n).

2. For odd n, any $r = p^{2k} - p^k + 1 = \frac{p^{3k}+1}{p^k+1}$ leads to three valued cross-correlation, where the values which occur are again -1 and $-1 \pm p^{\frac{n+e}{2}}$. This result has also been established for the case p = 2 by L. Welch.

3. The specific value $r = p^{n-1} + p - 1$ leads, for all odd n, to three-level cross-correlation. The correlation values are -1, and $-1 \pm p^{\frac{n+1}{2}}$.

4. It has been conjectured that for odd n, any $r = \frac{p^{(2m+1)k}}{p^k+1}$ also results in three-level cross-correlation. A partial proof of this result has been found. Note that for m = 1 we have the result given in 2.

3.2.14 Three Level Cross Correlation

DA-ARO-D 31-124-C930, Supp #1, Army Research Office, Durham

S. W. Golomb, L. R. Welch

During the report period, we developed another approach to the analysis of observed occurrences of three level cross correlation. In addition, a student has extended tables of three level cross correlation up through degree fifteen (length 32,767).

It was observed that in each case of three level cross correlation the values were -1, $-1+2^k$, $-1-2^k$, for appropriate choice of k. In the trace formulation, the binary sequences become functions on the Galois field $GF(2^N)$. One of the sequences plays a role similar to

$\exp(2\pi i \frac{t}{N})$ the complex number field and the cross correlation values, when properly arranged and incremented by one, play the role of fourier coefficients. With this interpretation, sequences with three level cross correlation correspond to functions whose double convolution is equivalent to scalar multiplication. That is:

$$f*f*f(x) = 2^{2k} f(x), \qquad x \in GF(2^n)$$

At present there are two theorems and one conjecture accounting for various occurrences of three level correlation. These were known to cover all such occurrences through degree 12 with two exceptions. The conjecture was known to be valid also for degree 13. This work has been extended through degree fifteen. The theorems and conjecture cover all but six cases and the conjecture is valid through degree fifteen. The exceptional cases seem to fall in some pattern which has not been correctly formulated yet.

The difficulty of extending this work can be estimated by noting that for degree n, roughly $\frac{2^n-1}{n}$ sequences must be examined and for each of these, $\frac{2^n-1}{n}$ correlation coefficients must be computed, each requiring 2^n-1 additions or subtractions. This is a total computation of roughtly $\frac{2^{3n}}{n^2}$ additions or subtractions. This is shortened by rejecting a sequence as soon as four different values of correlation have occurred. The amount of work on this basis seems to be a moderate (~ 10) multiple of $\frac{2^{2n}}{n^2}$.

3.2.15 Study of Synchronization Techniques for Optical Communications Systems

NGR-05-018-104, National Aeronautics and Space Administration

R. M. Gagliardi

During this reporting period some investigation of the relationship of Poisson shot noise processes to its inherent intensity was made. The objective was to examine the mathematical feasibility of representing stochastic processes by Poisson shot noise processes. The results of the study are reported in USCEE Report 334, "On the Representation of a Continuous Stochastic Intensity by Poisson Shot Noise", the abstract of which is given below.

"In many applications a poisson shot noise (PSN) process is said to statistically "represent" its intensity process. In this paper an investigation is made of the relationship between a PSN process and its intensity, when the latter is a sample function of a continuous stochastic process. The difference of the moments and the mean square difference between the two processes is examined. The continuity assumption on the intensity permits the development of a sequence of moment relationships in which the effect of the PSN parameters can be seen. The results simplify and afford some degree of physical interpretation, when the component functions of the PSN are "rectangular", or when the intensity process does not vary appreciably over their time width. An integral equation is derived which defines the component function that minimizes the mean square difference between the two processes. It is shown that a "degenerate" form of component function induces complete statistical equality of the two processes. The problem has application to optical communication systems using photodetectors."

3.3 SWITCHING, AUTOMATA THEORY, COMPUTERS

3.3.1 Circuit Partitioning via Simulation, Activity Directed Circuit Simulation and Backward Simulatio

AF-AFOSR 69-1622, Joint Services Electronics Program

M. A. Breuer

I. Introduction

A system capable of simulating a digital logic circuit is useful for verifying the correctness of the design, for race analysis, and for generating fault tests. Since simulation is a slow process, the design of ultra-efficient simulators is of great importance. We have developed a number of new techniques for increasing the efficiency of a logic simulator, among these is a new circuit partitioning algorithm.

II. Logic Partitioning via Simulation

Given a digital computer, it is often necessary to simulate the logic for a given instruction and numerous different sets of operands. To efficiently carry out this simulation, one should simulate only that logic which is "active" for this instruction. We have developed a technique for automatically partitioning the logic to obtain this "active" logic.

The algorithm is based upon the following result. Let F_0, F_1, F_x be a partition of the input lines and flip flops to a circuit, where $i \in F_d$ if line i is at value d, $d \in \{0, 1, x\}$. The value x refers to an unspecified line value. Using F_0, F_1, F_x as an initial condition, the logic can be simulated. Let G_0 and G_1 be the set of lines at value 0 and 1 in the circuit. Then we have the following result.

Theorem: Given two partitions F_0, F_1, F_x and F'_0, F'_1, F'_x, where $F'_0 \supseteq F_0$ and $F'_1 \supseteq F_1$. Then $G'_0 \supseteq G_0$ and $G'_1 \supseteq G_1$.

In our case F_0 and F_1 are specified by the instruction. All those signal lines not specified by the instruction are assigned the value x. Given G_0 and G_1, an algorithm has been constructed which will determine

all gates which need be simulated in order to specify the next state of the machine. Hence, no matter what data is being simulated, we have that $F'_0 \supseteq F_0$ and $F'_1 \supseteq F_1$ and hence only the logic which effects the next state is considered. This leads to a great increase in system efficiency.

III. Activity Directed Logic Simulation

The concept behind activity directed logic simulation is the following: the output of a gate will not change state unless at least one of its inputs changes states. We have designed a logic simulator based upon this concept; i.e., whenever a gate g changes state, we place the name of all gates having an input from g on a push down stack. The gates on this stack will then be simulated at the proper time. This work is similar to that of Ulrich's[1]. The advantages of this technique are:

a) Since only a small percentage of the logic of a computer is active at any one instant of time, this technique is very efficient.

b) Race conditions can be analyzed.

c) Cyclic logic can be easily simulated.

IV. Backward Simulation

It is often useful to be able to simulate the logic of a system in the reverse direction, i.e., given the output, what is the input. We have developed a backtrack algorithm which solves this problem. Unlike forward simulation, backward simulation need not produce a unique result. The algorithm is capable of generating all solutions. The two main applications for this technique are:

1) Generation of fault detection tests, a la the consistency algorithm of Roth[2].

2) In the logic partitioning algorithm, where one is given the state of certain control lines and desires to know the state of the flip flops which produce these control states.

References

1. E. G. Ulrich, "Time-Sequenced Logical Simulation Based on Circuit Delay and Selective Tracing of Active Network Paths," Proc. ACM 20th Natl. Conf., 1965, pp. 437-448.

2. J. P. Roth, "Diagnosis of Automata Failures: A Calculus and a Method", IBM J. of Research and Development, pp. 278-291, July 1966.

3.3.2 Generalization of the Classical Switching Synthesis Problem

AF-AFOSR 69-1622, Joint Services Electronics Program

M. A. Breuer

I. Introduction

A classical problem in switching theory is the synthesis of a Boolean function. Most of the work on this problem deals with the synthesis of minimal cost circuits, as exemplified by the work of Karnaugh, Veitch, Quine, McCluskey, Roth, etc. The first generalization of this problem was to consider the synthesis of multi-output function. Later, the use of universal circuits was studied. We propose to study the following generalization, namely given a set of multi-output functions, determine a single minimal circuit which, by proper labeling of inputs and outputs, can be used to synthesize each multi-output function individually. This problem has both significant theoretical as well as practical importance.

Its practical importance comes about in the area of LSI and MI S circuits. Here, there is a great cost in the initial design of a circuit card. This cost is related to the problem of layout, mask-making, and checkout procedures. Hence there is a great motivation to reduce the number of different circuit chips which need be designed. This is exactly the problem which we are considering, but for the case of combinational logic circuits only.

II. The Generalized Synthesis Problem (GSP)

Given switching functions

$$f_1^i, f_2^i, \ldots, f_{n(i)}^i$$

for i=1,2,...,N. The GSP is to find a single circuit, of "minimal cost", such that for each i there exists a proper labeling of inputs and outputs such that the circuit realizes $f_1^i, \ldots, f_{n(i)}^i$. Note that this problem includes the problem of universal circuit design, the multi-output problem (N=1), and the single output problem (N=1, n(1) = 1). The "minimal cost" criteria is usually some function of the number of I/O pins, the number of inputs to gates, and the number of gates.

III. Initial Results

The synthesis of the desired circuit in two level AND-OR form has been considered. This problem has been formulated as an integer linear program given an assignment of output functions to output gates. The synthesis criterion in this case is the minimization of the number of first level AND gates.

The second problem considered is that of minimizing the number of input pins, given a gate realization of the sets of functions. A heuristic algorithm for solving this problem has been developed.

Finally, a heuristic algorithm for reducing the number of input pins has been developed, where n(i) = 1 for i=1,2,...,N, and where the assignment of product terms to AND gates is not known, a priori.

IV. Future Work

1. Develop more efficient synthesis techniques;
2. Obtain an exact solution to the minimal pin-count problem;
3. Identify when the minimal solution is a universal circuit;
4. Counting problems.

3.3.3 Automata and Formal Language Theory

AF-AFOSR 69-1622, Joint Services Electronics Program

R. Card, W. Chandler, S. Ginsburg

Background

During the past five years, a multitude of different types of acceptors and the languages they recognize have been introduced. Recently, it was observed[1] that most of these devices and languages would be subsumed and unified within the notions of an "abstract family of acceptors", abbreviated AFA, and an "abstract family of languages", abbreviated AFL. This has resulted in a flood of new questions and results, hitherto unsuspected. Whereas before the advent of AFA, there was a surfeit of devices, after AFA there was a sudden scarcity. This situation arose because there were not enough different types of extant devices to answer the new questions.

Progress

Roger Card is still studying the properties of "associative memory acceptor languages". He is in the process of writing up his results and a report should be available within six months.

William Chandler is writing up his results on languages accepted by one-way deterministic acceptors. In addition to the characterization of these languages by closure operations, he has shown that these operations are mutually independent. He also has some relations between languages accepted by deterministic acceptors and those accepted by nondeterministic acceptors.

A paper, "Multitape AFA", was written and submitted for publication. In it the notation of acceptors with multi-storage tapes, each of a possibly different type was studied. The basic theorem of the paper is a characterization of the languages accepted by multitape AFA in terms of the AFL associated with each storage tape type.

References

1. S. Ginsburg and S. Greibach, "Multitape AFA", submitted to the Journal of the Association for Computing Machinery.

2. S. Ginsburg and G. F. Rose, "A Note on Preservation of Languages by Transducers", Information and Control, Vol. 12, 1968, pp. 549-552.

3. S. Ginsburg and E. H. Spanier, "Derivation-bounded Languages", Journal of Computer and System Sciences", Vol. 2, 1968, pp. 228-250.

4. S. Ginsburg and J. Hopcroft, "Two-way Balloon Automata and AFL", accepted for publication in the Journal of the Association for Computing Machinery.

3.3.4 Mathematical Pattern Recognition

NGR-05-018-044, National Aeronautics and Space Administration

W. S. Meisel and W. W. Yuan

In their widest sense, patterns are the means by which we interpret the world. A child learns to distinguish the visual patterns of mother and father, the aural patterns of speech and music, the tactile patterns of cold and warmth, patterns of the senses. As he grows older, he refines the detail of this pattern recognition; he may be able to distinguish a symphony by Beethoven from a symphony by Bach, or a painting by Renoir from a painting by Rembrandt. He abstracts his sensory discrimination to indirect patterns; a mathematician detects patterns in mathematics (an "elegant" proof), a social scientist finds patterns in the data he analyzes.

Mathematical pattern recognition is the study of techniques which allow a machine to duplicate or aid a human in some of the above tasks. The lion's share of such work has been oriented toward sensory pattern recognition. Since the human in such problems is the ideal against which the machine's performance is judged, the machine is wrong by

definition in cases of disagreement. It is thus likely that only specialized success can be expected in sensory pattern recognition. Humans, after all, can do the job. On the other hand, the computer can feasibly excel in indirect pattern recognition, such as the recognition of patterns in data. Humans often attempt to translate numerical data into sensory patterns--as evidenced by extensive use of graphs and charts--while a computer is in its natural medium. It is in areas where a great deal of numerical data must be analyzed that mathematical pattern recognition techniques can extend human capabilities. This abstract pattern recognition problem is a major target of our work.

We have done a great deal of work on practical potential function methods in pattern recognition[2]. A basic problem of abstract pattern recognition is the assignment of points of a finite-dimensional vector space to one of a family of classes on the basis of samples of those classes. Most methods of doing so reduce to the construction of discriminant functions $\rho_i(x)$, one for each class, such that if

$$\rho_j(x) > \rho_i(x) \quad \text{for all } i \neq j \ ,$$

the point x is classified as a member of class j. This paper is concerned with methods where the discriminant function is constructed as a superposition of potential functions $\gamma(x,y)$, i.e.,

$$\rho_i(x) = \frac{1}{M} \sum_{j=1}^{M} \gamma(x, y_j) \ ,$$

where the sum is over the sample points of class i. (The function γ may be different for each class, or even each sample).

Since only the points of a single class are used in constructing the discriminant function for that class, these algorithms provide an approach to the more general problems of reconstructing a probability density from samples of the process or of constructing a characteristic function for a fuzzy set. This is in contrast to error-correction methods

which emphasize differences between classes and do not yield characteristic discriminant functions.

The characteristics and generality of potential functions were examined. We developed algorithms for implementation of the concepts, including a reexamination and extension of Specht's work.

We are continuing a major comparison of pattern recognition techniques applied to artificially generated 10-dimensional data[3]. We are obtaining revealing results, and in the process are discovering new techniques and original combinations of older techniques.

References

1. Meisel, W. S., "Mean-Square Methods in Abstract Pattern Recognition", Information Sciences, Vol. 1, No. 1 (December 1968).

2. W. S. Meisel, "Potential Functions in Abstract Pattern Recognition", IEEE Trans. Computers, to be published.

3. W. S. Meisel and W. W. Yuan, "Tables of Artificial Data for Pattern Recognition", USCEE Report No. 302, June 1968.

4. BIOMEDICAL ENGINEERING AND MATHEMATICS

4.1 CARDIOVASCULAR AND RESPIRATORY SYSTEMS

4.1.1 Mathematical Model of Respiratory Chemostat

PO1 GM 16437-02, Department of Health, Education and Welfare (USPHS)
TO1 GMO 172403, Department of Health, Education and Welfare (USPHS)
G. A. Bekey, J. C. Maloney, and F. S. Grodins

We have begun a restudy of the mathematical model of respiratory control published by Grodins, Buell and Bart[1] with the following long range objectives:

1. Transformation of the digital program into a hybrid one, in order to reduce the running time and make on-line simulation possible in real time.

2. Addition of an active lung to the model, so that studies of both pulmonary mechanics and of more refined control hypotheses which explicitly couple "neural" and "chemical" control can be carried out.

3. The present model represents the transport of blood gases by flow terms, including Q (cardiac output) and Q_B (cerebral blood flow). However, the cardiovascular system is not included as such, and hence, it is not possible to use the model to study the interaction of the respiratory and cardiovascular control systems. One of our long-term objectives is to obtain such a combined model.

4. To study the effect of acute metabolic disturbances, it will be necessary to augment the model by including provisions for intravenous infusion, a more detailed description of bicarbonate exchange between blood, brain and tissue, and an initial empirical description of kidney function.

We have made some limited progress on the first of the above objectives and made a start on the second.

Transformation of the digital computer program to a hybrid program has required a careful study of the computational difficulties associated with the present program. The first of these is that associated with the calculation of time delays involved in the transport of blood gases to and from the lungs, the sensors and the tissues. For example, the arterial concentration of CO_2 at the entrance to the brain compartment, $C_{aB(CO_2)}$ can be expressed in terms of its concentration at the exit of the lung compartment τ_{aB} seconds earlier (where τ_{aB} is the lung to brain arterial transport time), as

$$C_{aB(CO_2)}(t) = C_{a(CO_2)}(t-\tau_{aB}) \tag{1}$$

The delay time τ_{aB} was computed in the model of Ref. (1) from the iterative expression

$$\tau_{aB} = \frac{V}{\frac{1}{\tau_{aB}-\tau_{aB(1)}} \int_{t-\tau_{aB}}^{t-\tau_{aB(1)}} Q\,dt} + \frac{V_B}{\frac{1}{\tau_{aB(1)}} \int_{t-\tau_{aB(1)}}^{t} Q_B\,dt} \tag{2}$$

In this equation V and V_B represent the volumes of the vascular segments involved in the transport of the total cardiac output Q and the cerebral blood flow Q_B while $\tau_{aB(1)}$ represents that fraction of the total delay τ_{aB} concerned with the flow Q_B only. This equation was solved by an iterative

procedure, based on integration of the blood flow-time functions backwards at each instant of time, and stopping the integration when the value of the integral became equal to the appropriate vascular volume, V or V_B. The end of this integration interval then became the appropriate value of τ_{aB} for substitution into equation (1). This was a time-consuming procedure.

In order to alleviate the difficulties associated with the above process, the time delays will now be computed by application of the Leibnitz formula for differentiation under an integral sign (2) as follows: Let the relation between flow and volume be expressed singly as

$$V = \int_{t-\tau}^{t} Q(y)\, dy \tag{3}$$

where τ is unknown and V is known. Now, if we differentiate eq. (3) with respect to running time, t, we obtain

$$\dot{V} = Q(t) - (1-\dot{\tau})(Q(t-\tau)) \tag{4}$$

which can be solved for $\dot{\tau}$

$$\dot{\tau} = \frac{\dot{V} - Q(t)}{Q(t-\tau)} + 1 \tag{5}$$

This is a differential equation for the unknown time delay which requires only Q(t) and $Q(t-\tau)$ as inputs. The vascular volume can be constant (in which case $\dot{V} = 0$) or variable. The hybrid implementation of this time delay program is shown in Figure 1. The variable time delay for the digital portion of the system, operating under analog control, already exists in our laboratory, as developed by Nilsen[3].

To date we have implemented the digital version of equation (5) for every time delay in the system. The full hybrid implementation will be done within the next few months. This will be of general utility in all of our studies involving transport lags.

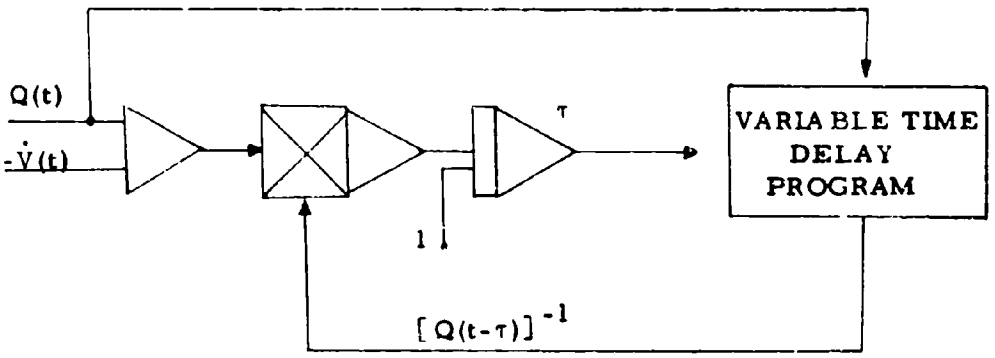

Figure 1

References

1. Grodins, F. S., J. Buell, and A. J. Bart, Mathematical analysis and digital simulation of the respiratory control system, J. Applied Physiol. 22: 260, 1967.

2. Wylie, C. R., Advanced Engineering Mathematics, McGraw-Hill Book Co., (3rd edition), 1966, p. 274.

3. Nilsen, R. N., Hybrid simulation of a variable transport lag, Simulation 12: 65-70, February 1969.

4.1.2 Theoretical Studies on Optimization of Respiratory Cycle

PO1 GM 16437-02, Department of Health, Education and Welfare (USPHS)

S. Yamashiro, F. S. Grodins, M. B. Wolf

Although more than 40 years have elapsed since Rohrer[1] first suggested that minimization of the work of breathing might play a role in the control of respiratory frequency, a thorough study of this possibility has yet to be made. Recent interest in this question has been stimulated by attempts to treat the respiratory system as an optimal control system[1,2].

Using a theoretical treatment similar to Rohrer's, Otis, Fenn,

and Rahn[4] confirmed the prediction that there was an optimal frequency of breathing which minimized total inspiratory work per minute. Their treatment assumed that the air flow pattern was sinusoidal, that expiration was passive, and that the mechanical properties of the system comprised a linear compliance and both viscous and turbulent resistance to flow. Comparison with experimental data in man[4] as well as in dogs, cats and guinea pigs[5] showed that the observed frequencies could be closely predicted. In 1960, Mead[6] claimed that frequencies predicted on the basis of "minimum average force of the respiratory muscles" matched observed values in guinea pigs and man better than those predicted on the basis of minimum work. Closer examination reveals that Mead's actual criterion was one of minimum peak to peak pressure amplitude, and that this is equivalent to minimal pressure variance in the sinusoidal airflow pattern which he assumed. In fact, "average pressure" falls monotonically as frequency increases and does not go through a finite minimum. Both the Otis and Mead criteria predict optimal frequencies which are close in value, and both are characterized by broad rather than sharp optima. This makes an experimental decision between them very difficult if not impossible on the basis of frequency measurements alone. Accordingly, we have begun a theoretical exploration of this problem which brings other control variables into consideration. We have so far examined two such features: (1) The variation of dead space with tidal volume, and (2) Airflow pattern for minimum rate of inspiratory work or minimum pressure variance.

(1) Dead Space-Tidal Volume Behavior (Widdicombe and Nadel)

Widdicombe and Nadel[7] have proposed that the tone of airway smooth muscle is regulated in such a way as to minimize either the criterion function of Mead or of Otis. Figure 1 schematically shows their formulation:

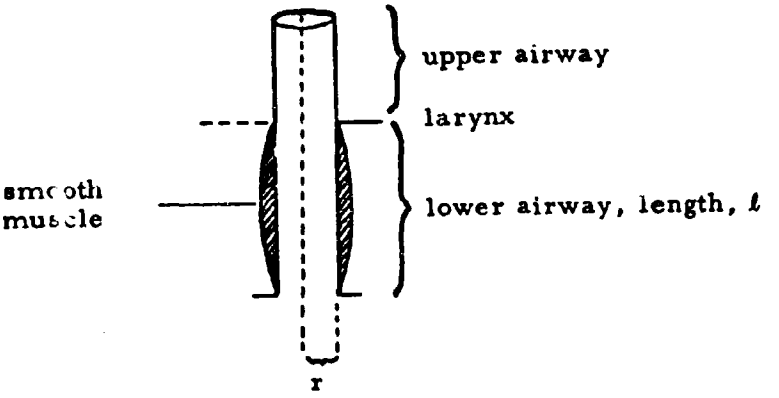

Figure 1

The following equations summarize their approach:

$$DS = DS_{UA} + DS_{LA} \tag{1}$$

where DS = total dead space

DS_{LA} = lower airway dead space

DS_{UA} = upper airway dead space

By Poiseuille's Law, the resistance of the lower airway is:

$$R_{LA} = \frac{8}{\pi} \eta \frac{\ell}{r^4} \tag{2}$$

where η = viscosity factor

The volume of the lower airway is

$$DS_{LA} = \pi r^2 \ell \tag{3}$$

If ℓ and r are adjusted by smooth muscle tone in a proportional way, then:

$$\ell = k_1 r \tag{4}$$

where k_1 = constant of proportionality.

Then:

$$R_{LA} = \frac{8\eta k_1^2}{DS_{LA}} \tag{5}$$

By letting

$$a = 8\eta k_1^2 \ , \tag{6}$$

(1) becomes

$$DS = DS_{UA} + \frac{a}{R_{LA}} \tag{7}$$

Since regulation of R_{LA} for optimal conditions will change DS, the comparison of predicted DS for different levels of ventilation with the experimental results of Gray, Grodins, and Carter[8] seems appropriate. Gray, et al., experimentally found that dead space varies linearly with tidal volume. The question we are asking is whether both the Otis and Mead criteria can successfully predict these experimental results. Assuming sinusoidal airflow pattern, the object is to determine both frequency, f, and R_{LA} which will minimize both criteria functions. Minimization was performed on the digital computer (G.E. 265) using the Fletcher-Powell (1963) minimization algorithm. This algorithm is probably the most powerful general procedure for finding a local minimum. Most of the parameters were obtained from Widdicombe and Nadel except for the values for DS_{UA} and a. DS_{UA} was set equal to the dead space given by Gray, et al., for zero tidal volume. The parameter, a, was chosen for best fit to the experimental data plotted as dead space versus tidal volume.

Figures 2 and 3 show how the theoretical predictions using the Otis and the Mead criteria compare with the experimental data of Gray, et al. Both criteria fit the data equally well with closely similar values of a. All other parameters were equal. Thus, both criteria are adequate for inclusion of R_{LA} as a controlled variable.

Otis Criterion - Trial #4

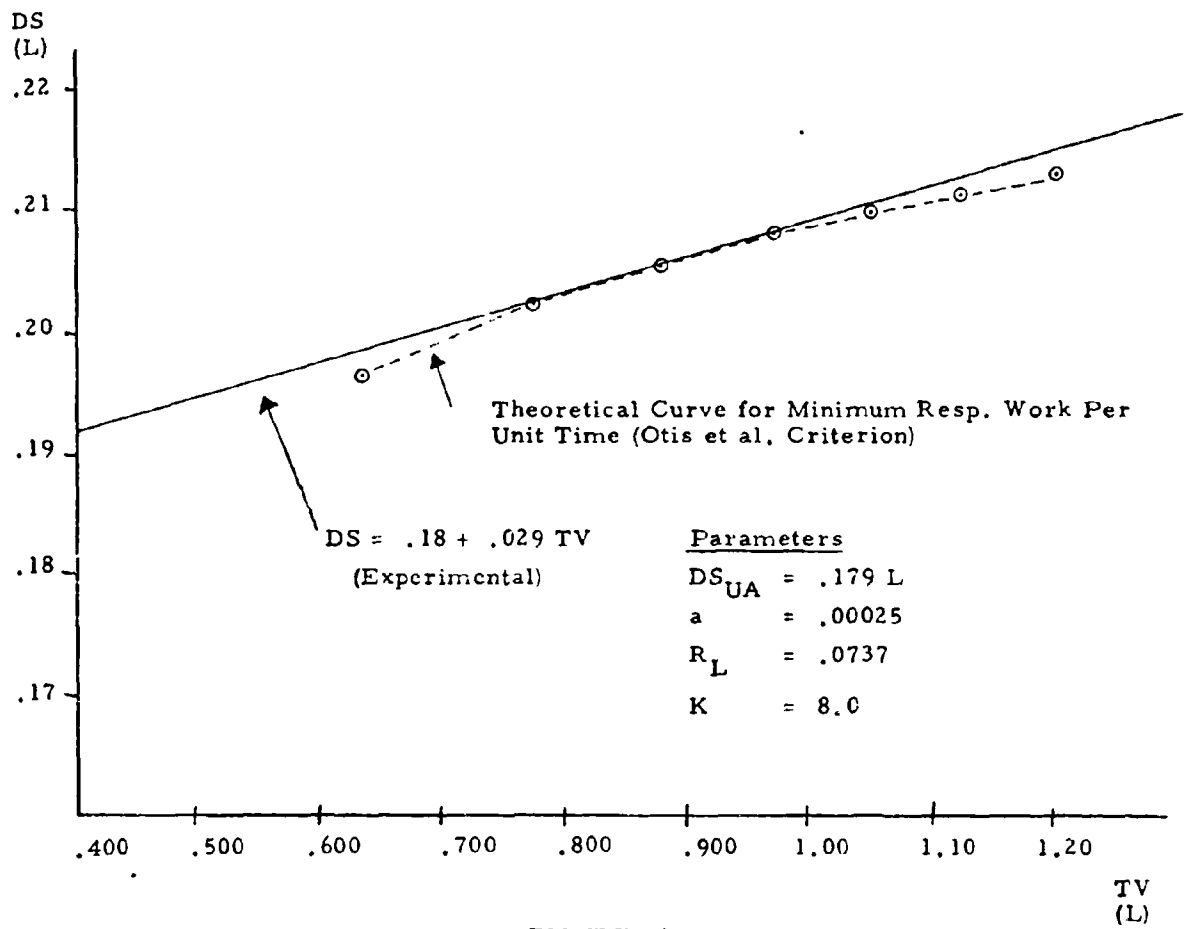

FIGURE 2

FIGURE 4

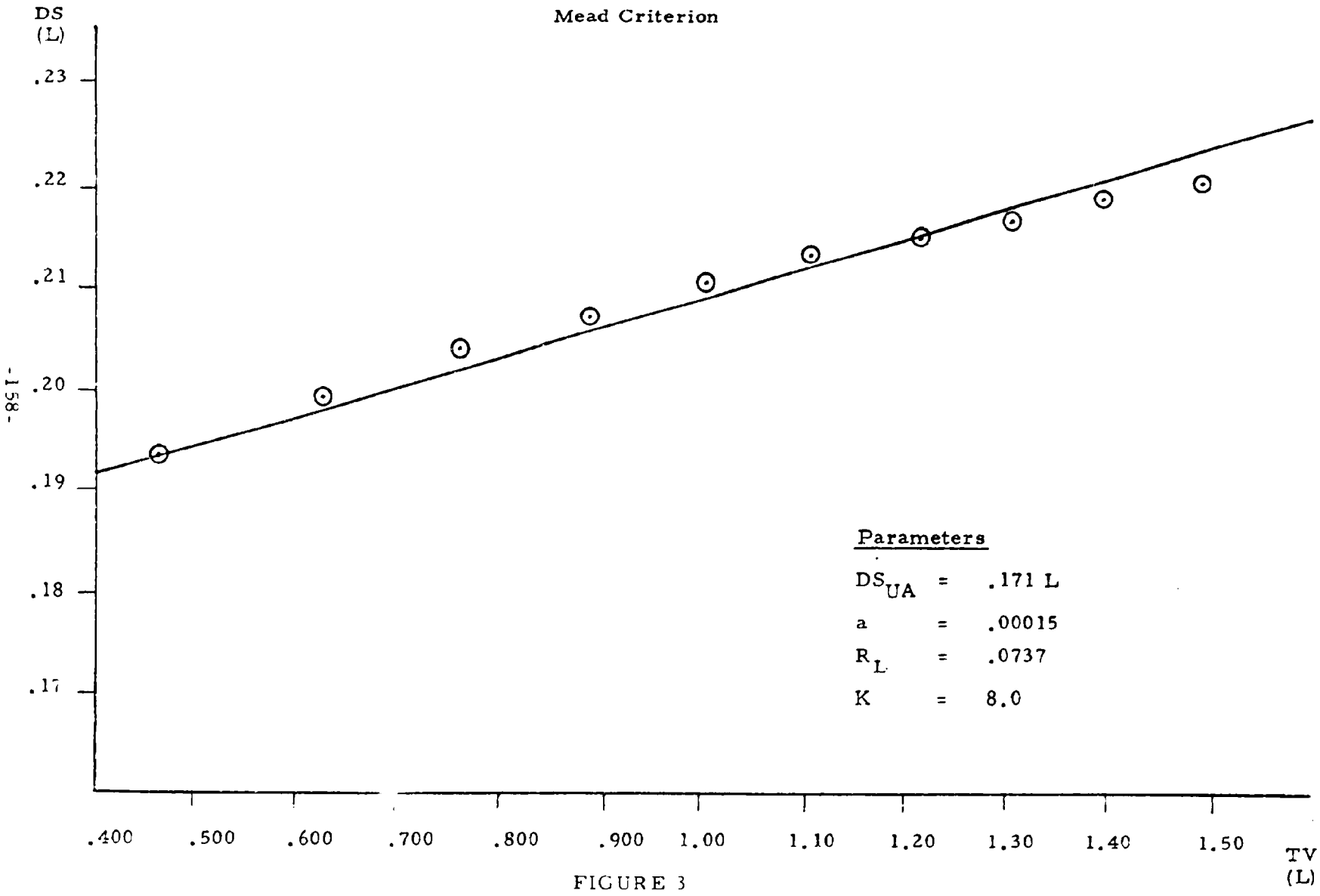

FIGURE 3

(2) Optimal Airflow Pattern

All formulations considered thus far have assumed sinusoidal airflow, primarily for mathematical convenience. However, Otis, et al.[4], recognized the desirability of determining the exact airflow pattern for minimum work. We have begun a theoretical study of this problem, using both the Otis and the Mead Criteria.

(a) Minimum Rate of Inspiratory Work. As a first approximation, inspiration will be assumed to take up exactly half of the total respiratory cycle. If expiration is passive the shape of the expiratory airflow is unimportant for work calculations. Thus, the pattern will be assumed to be symmetrical for mathematical convenience. Within these limitations, the respiratory airflow pattern can be described by a Fourier series containing only sine terms. That is:

$$\dot{V} = \sum_{m=1}^{\infty} a_m \sin(m\omega t) \tag{8}$$

where

$\omega = 2\Pi f$

f = respiration frequency

The tidal volume V_T is given by

$$V_T = \int_0^{\Pi/\omega} \dot{V}\, dt$$

$$= \sum_{n=1}^{\infty} \frac{2a_{2n-1}}{(2n-1)\omega} \tag{9}$$

The work for a single inspiration is:

$$W = \int_0^{V_T} P\, dv \tag{10}$$

Figure 4 shows the electrical analog of the assumed mechanical model.

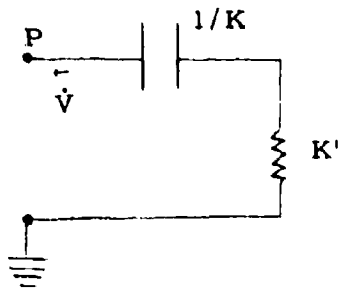

Figure 4

The node equation is:

$$P = KV + K'\dot{V} \tag{11}$$

Thus (10) becomes

$$W = \int_0^{V_T} KV dv + K' \int_0^{\Pi/\omega} \left(\sum_{m=1}^{\infty} a_m \sin (m\omega t) \right)^2 dt \tag{12}$$

$$= \frac{1}{2} KV_T^2 + \frac{K'\Pi}{2\omega} \sum_i a_i^2$$

The rate of inspiratory work is:

$$\dot{W} = Wf$$

$$= \frac{1}{2} KfV_T^2 + \frac{K'}{4} \sum_i a_i^2 \tag{13}$$

The constant alveolar ventilation and dead space constraint can be included as:

$$V_T = V_D + \frac{\dot{V}_A}{f} \tag{14}$$

The problem is to minimize (13) subject to the constraint of (14). We will apply the standard Lagrange multiplier method to solve this problem. In more conventional terminology we wish to minimize the function:

$$\dot{W}(f, a_1, a_2, a_3, \ldots) = \frac{1}{2} Kf \left(V_D + \frac{\dot{V}_A}{f} \right)^2 + \frac{K'}{4} \sum_i a_i^2 \qquad (15)$$

Subject to the constraint:

$$V_D f + V_A - \frac{1}{\Pi} \sum_i \frac{a_{2i-1}}{(2i-1)} = 0 \qquad (16)$$

Following the Lagrange multiplier method, let:

$$F = \frac{K}{2f} \left(V_D f + \dot{V}_A \right)^2 + \frac{K'}{4} \sum_i a_i^2 + \lambda \left[V_D f + V_A - \frac{1}{\Pi} \sum_i \frac{a_{2i-1}}{2i-1} \right] \qquad (17)$$

Then the extremum may be found by solving:

$$\frac{\partial F}{\partial f} = \frac{K}{f} \left(V_D f + \dot{V}_A \right) V_D - \left(V_D f + \dot{V}_A \right)^2 \frac{K}{2f^2} + \lambda V_D = 0 \qquad (18)$$

$$\frac{\partial F}{\partial a_i} = \left\{ \begin{array}{ll} \frac{K' a_i}{2} & i \neq 2j-1 \\ \frac{K' a_i}{2} - \frac{\lambda}{\Pi i} & i = 2j-1 \end{array} \right\} = 0 \qquad (19)$$

for all i.

From (19)

$$\lambda = \frac{\Pi(2i-1)}{2} K' a_{2i-1} \qquad (20)$$

Substituting (20) into (16)

$$\lambda = \frac{\left(V_D f + \dot{V}_A \right) \Pi^2 K'}{2 \sum \frac{1}{(2i-1)^2}} \qquad (21)$$

Since

$$\sum_i \frac{1}{(2i-1)^2} = \frac{\pi^2}{8} \tag{22}$$

(21) becomes

$$\lambda = 4K' V_D f + \dot{V}_A \tag{23}$$

Substituting (23) into (18)

$$f_{opt} = \frac{\sqrt{1 + 32RCV_A/V_D} - 1}{16\,RC} \tag{24}$$

where $R = K'$, $C = 1/K$

Substituting (22) into (20)

$$a_{2i-1} = \frac{4}{\pi(2i-1)}\ 2\left(V_D f + \dot{V}_A\right) \tag{25}$$

Equation (25) corresponds to a square wave of amplitude $2(V_D f + \dot{V}_A)$. Thus the optimal wave form for minimum rate of inspiratory work subject to the constraints of onstant alveolar ventilation and dead space is a square wave. This optimal airflow pattern actually minimize average power dissipation. Otis[9] points out that there is no theoretical optimal frequency when expiration is active. However, the square wave airflow pattern minimizes the power requirement for breathing in both active and passive expiration.

(b) Minimum Pressure Variance. The criterion actually minimized by Mead was pressure variance. Average pressure does not have a finite minimum, and mean squared pressure leads to a different equation for optimal frequency than that given by Mead. We define variance as:

$$\sigma_p^2 = \overline{(p-\bar{p})^2} = \overline{p^2} - (\bar{p})^2 \qquad (26)$$

where $\overline{(\quad)}$ denotes

$$\frac{1}{T}\int_0^T (\quad)\, dt$$

Using the same model as described by (11), and representing airflow by (8):

$$\sigma_p^2 = \frac{K^2 T^2}{8\Pi^2} \sum_i \frac{a_i^2}{i^2} + \frac{K'^2}{2} \sum_i a_i^2 \qquad (27)$$

We wish to minimize (27) subject to the constraint (14). Following the Lagrange multiplier method:

$$F = \left[\frac{K^2}{8\Pi f^2} \sum_i \frac{a_i^2}{i^2} + \frac{K'^2}{2} \sum_i a_i^2 \right] + \lambda \left[V_D f + V_A - \frac{1}{\Pi} \sum_i \frac{a_{2i-1}}{2i-1} \right] \qquad (28)$$

The extrema are found by solving:

$$\frac{\partial F}{\partial f} = -\frac{K^2}{4\Pi f^3} \sum_i \frac{a_i^2}{i^2} + \lambda V_D = 0 \qquad (29)$$

$$\frac{\partial F}{\partial a_i} = \left\{ \begin{array}{ll} \dfrac{a_i K^2}{4\Pi f^2 i^2} + a_i K'^2 , & i \neq 2j-1 \qquad (30a) \\ \dfrac{a_i K^2}{4\Pi f^2 i^2} + a_i K'^2 - \dfrac{\lambda}{\Pi i} , & i = 2j-1 \qquad (30b) \end{array} \right\} = 0$$

From (30a)

$$a_i = 0 \quad \text{for} \quad i \neq 2j-1 \qquad (31)$$

Equations (30b), (29) and (14) must be solved simultaneously to determine the optimal breathing pattern. These equations are nonlinear and thus difficult to solve. We plan to solve them by numerical techniques in the near future. However, if the resistive "cost" dominates (i.e., K = 0), an analytical solution is possible. From (30b)

$$a_{2j-1} = \frac{\lambda}{\Pi(2j-1)K'^2} \tag{32}$$

Substituting (32) into (14)

$$\lambda = 8K'^2 \left(V_D f + \dot{V}_A \right) \tag{33}$$

Thus (32) becomes:

$$a_{2j=1} = \frac{8}{\Pi} \frac{\left(V_D f + \dot{V}_A \right)}{(2j-1)} \tag{34}$$

Equation (34) corresponds to a square wave of amplitude $2(V_D f + \dot{V}_A)$. Thus the square wave airflow pattern optimizes the Mead criterion when the resistive "cost" dominates. Note that here too what is actually minimized is average power.

Figures 5 and 6 compare sinusoidal and square wave airflow patterns for the Otis and Mead criteria. All parameters except dead space were obtained from Agostoni, Thimm, and Fenn[5] for the dog. Dead space variation with tidal volume was obtained by fitting a straight line to the data of Williams and Rayford[10].

As shown in the figures, there is no significant difference between the optimal frequencies predicted by the sinusoidal or rectangular pattern. The Mead criterion predicts a higher optimal frequency than the Otis criterion, but this difference is in general a function of the level of alveolar ventilation, so that no simple conclusions can be drawn. The major differences revealed by these figures are those associated with

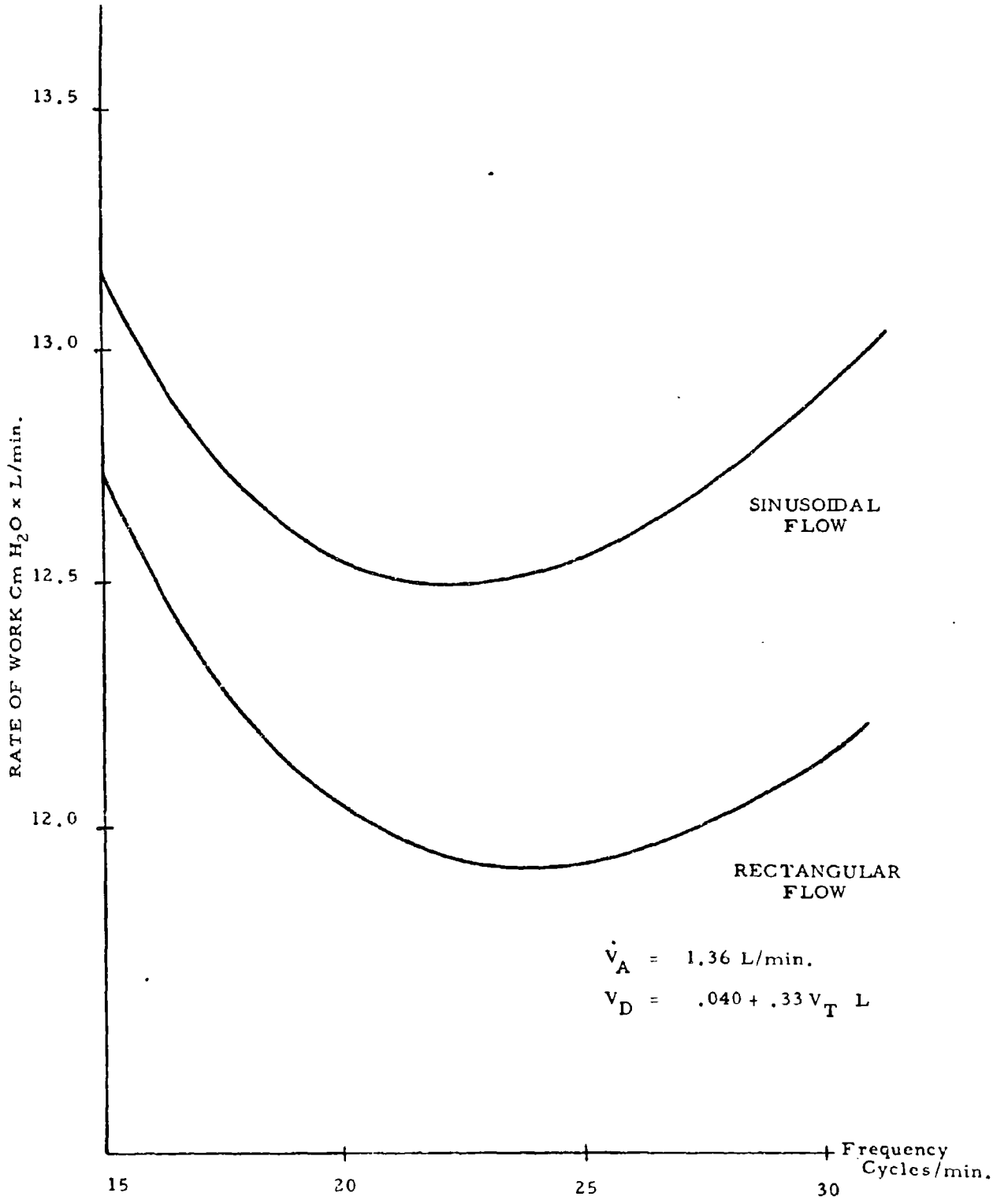

FIGURE 5. Rate of work of Breathing vs. Breathing Frequency for Given Rate of Alveolar Ventilation

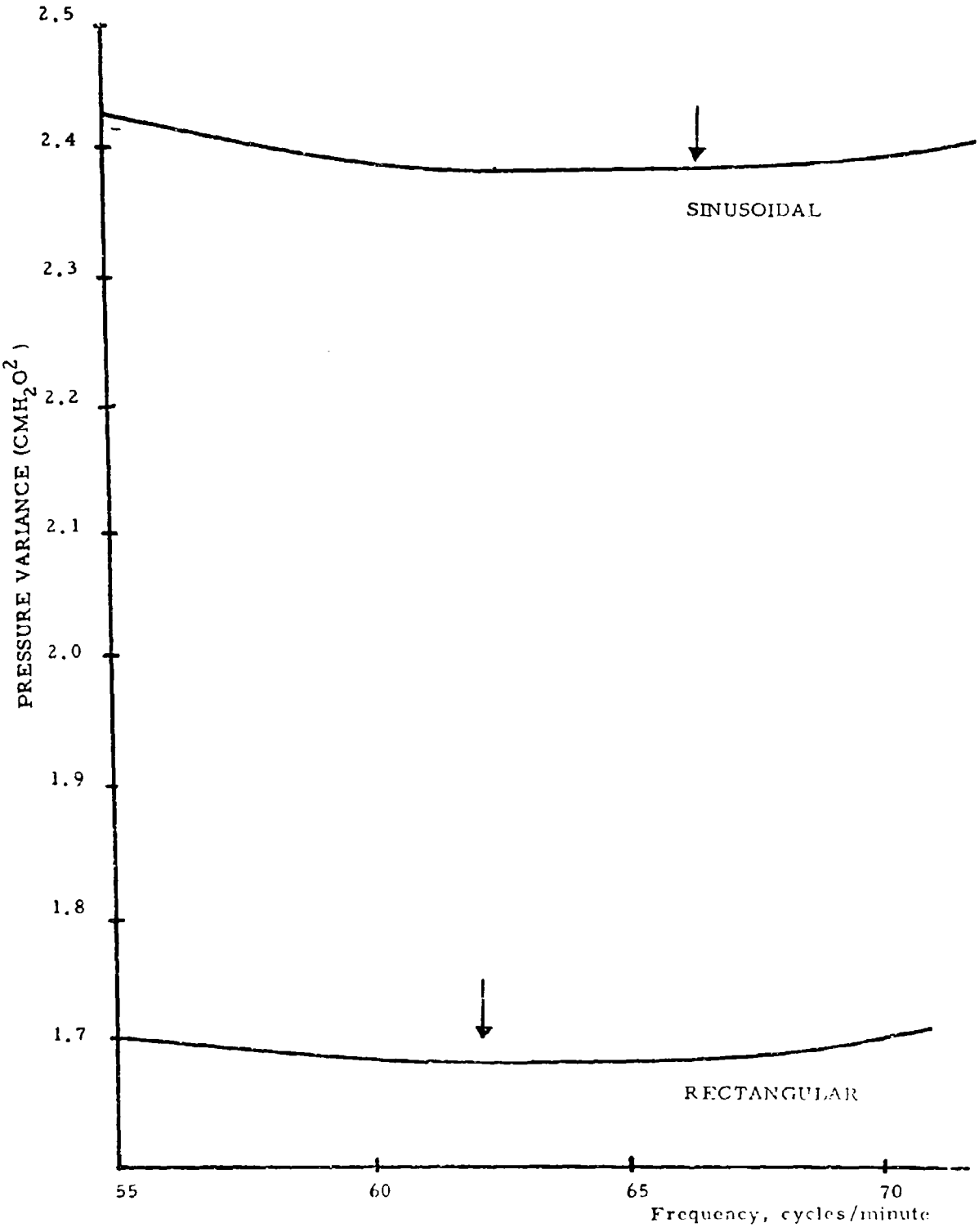
2.5
2.4
2.3
2.2
2.1
2.0
1.9
1.8
1.7
PRESSURE VARIANCE (CMH_2O^2)
SINUSOIDAL
RECTANGULAR
55
60
65
70
Frequency, cycles/minute

FIGURE 6

airflow pattern. Thus, significant differences in the magnitude of the criteria functions are revealed for the two patterns. In fact for the Mead criterion, the difference due to pattern far exceeds that due to frequency over the range considered.

Morrow and Vosteen[11], on the basis of pneumotachographic studies, have reported that the resting unmedicated dog has a square wave airflow pattern. Thus the criterion of Otis successfully predicts the airflow pattern in the resting dog. Mead's criterion also predicts this under conditions of dominant resistive "cost". The criterion of minimum average power requirement for breathing also predicts the same pattern and actually appears to combine both the Otis and Mead criteria as far as airflow pattern is concerned.

References

1. Rohrer, F., In: Handbuch der Normalen und Path. Physiolgie, Eds. A. Bethe, et al., Springer, Berlin, 1925, Vol. 2, pp. 70-127.

2. Priban, I. P. and W. F. Fincham, Nature 208, 339-343, 1965.

3. Grodins, F. S., Some Simple Principles and Complex Realities of Cardiopulmonary Control in Exercise, Circulation Res. 20 and 21 (Supp. II): 171, 1967.

4. Otis, A. B., W. O. Fenn, and H. Rahn, J. Appl. Physiol. 2: 592-607, 1950.

5. Agostoni, E., F. F. Thimm and W. O. Fenn, J. Appl. Physiol. 14: 679-683, 1959.

6. Mead, J., J. Appl. Physiol. 15: 325-336, 1960.

7. Widdicombe, J. G. and J. A. Nadel, J. Appl. Physiol. 18: 863-868, 1963.

8. Gray, J. S., F. S. Grodins and E. T. Carter, J. Appl. Physiol. 9: 307-320, 1956.

9. Otis, A. B., in: Handbook of Physiology, Section 3, Respiration (I), Eds. W. O. Fenn and H. Rahn, American Physiological Society, Washington, D. C., 1964, pp. 463-476.

10 Williams, M. H., Jr., and C. M. Rayford, J. Appl. Physiol. 9: 30-32, 1956.

11. Morrow, P. E. and R. E. Vosteen, J. Appl. Physiol. 5: 348-360, 1953.

4.1.3 Separation of Control and Peripheral Roles in Control of Respiration

PO1 GM 16437-02, Department of Health, Education and Welfare (USPHS)

S. Yamashiro, F. S. Grodins, M. B. Wolf

1. Background

Controversy over the relative roles of the central and peripheral chemoreceptors in controlling ventilatory responses to metabolic acid-base disturbances continues. The importance of the peripheral chemoreceptors as proposed by Mitchell[1] is directly challenged by Fencl, et al.[2] The conclusions of these investigators were largely based on simultaneous measurements of ventilation, blood pH, and CSF pH before and after acid-base disturbances. From these, an empirical relationship between ventilation and the pH level of spinal fluid and/or arterial blood was derived. Fencl, et al., found no need to include the arterial blood pH in such a description, while Mitchell includes both variables. One complication in interpreting these results is the inherent coupling of pH and P_{CO_2} in acid-base disturbance. Both variables are potential independent stimuli to ventilation. No attempt was made by these investigators to experimentally isolate the effects of each stimulus. Also lacking is the comparison of responses to a single stimulus before and after peripheral denervation. Katsaros[3] compared ventilatory responses to acid-base disturbances before and after peripheral denervation, but did not experimentally isolate the effects of pH and P_{CO_2}. We agree with Comroe[4] that there are no valid comparisons of the ventilatory response to changes in pH before and after peripheral denervation.

Another problem concerns the techniques used to measure CSF pH. Spinal fluid is poorly buffered, and traces of buffer or rinsing solution in the sampling system or loss of CO_2 into minute air bubbles trapped in the sampling syringe may cause erroneous pH readings. As pointed out by Fencl, et al.[2], these errors may be large compared to physiologically significant variations. They associate a change of only 0.01 pH unit with a 20% change in alveolar ventilation. Apparently, Fencl, et al., believe that loss of CO_2 into minute air bubbles is the dominant source of error as they use a technique which calls for a pH reading within 15 seconds of sample withdrawal. In this way, pH is determined before air bubbles have a chance to equilibrate with the sample. On the basis of theoretical calculations, we found that a 0.01 ml air bubble in a 1.0 ml spinal fluid sample will cause a pH error of 0.008 if complete equilibration is allowed. Thus we conclude that air bubbles are a significant problem to consider. Mitchell on the other hand appears to believe that traces of buffer and rinsing solution are the dominant source of error. We assume that he uses the sampling technique described by Severinghaus, et al.[5] This technique uses repeated fillings of the sample chamber until duplicate or triplicate readings agree to within 0.003 pH unit. This would insure that all residual buffer or rinsing solution is removed from the sample chamber. Fencl, et al., point out that successive pH readings on samples taken from the same syringe often increased by .01-.02 units. Whether this is due to air bubble equilibration or rinsing out of residual fluid or both is the presently unanswered question. We feel that part of the disagreement over the chemical regulation of breathing may be explained by the answer to thi question. We now present preliminary results of an in-vitro experiment designed to answer it.

2. Experimental Validations of Techniques for CSF pH Measurement

The following two sampling methods were compared in an in-vitro experiment: (1) the sample is inserted into the measuring chamber of the pH meter and read as soon as a stable reading is obtained; (2) the

sample is inserted into the measuring chamber and allowed to equilibrate for 30 seconds before noting the pH reading. More of the same sample is then flushed in and again allowed to equilibrate. This process is repeated until two identical consecutive pH readings are obtained. Mock spinal fluid of the composition used by Alexander, et al.[6], was employed, i.e., 0.025 M $NaHCO_3$ with 0.135M NaCl solution. This solution was equilibrated at 38°C with gas of precisely measured composition (4.83% and 9.88% CO_2). Total CO_2 content of 1 ml samples was determined after equilibration by the Van Slyke manometric apparatus. A minimum equilibration time of half an hour was allowed. Duplicate pH determinations were then made using both techniques in randomized order. All pH measurements were made with a Corning glass-electrode unit with sample chamber temperature set at 38°C. Buffer solutions obtained from Corning were used for calibration. pH values computed from the P_{CO_2} of the equilibration gas and CO_2 content measurements were considered to be the true values. Acid-base constants for spinal fluid given by Mitchell[15] were used in the computations. Changes in pK with pH were included. Figure 1 shows how measured pH values compare with computed values for the two techniques. No definite conclusion is possible at this time because the number of data points is insufficient to make a significant statistical comparison. However, it appears that Method 1 tends to underestimate pH and Method 2 tends to overestimate pH in the vicinity of pH = 7.3. Thus far conventional 1 ml syringes have been used for sampling. Although these syringes have matched barrels and plungers, air leakages is still possible and this would tend to cause an overestimate of pH. Results using Method 2 should be improved if this leakage could be eliminated. We have recently obtained special gas tight syringes (Hamilton Company) for this purpose. The experiment will be repeated using these syringes. Sufficient data points will be taken to allow a statistical comparison.

3. Denervation Experiments

We have already mentioned the controversy over the relative

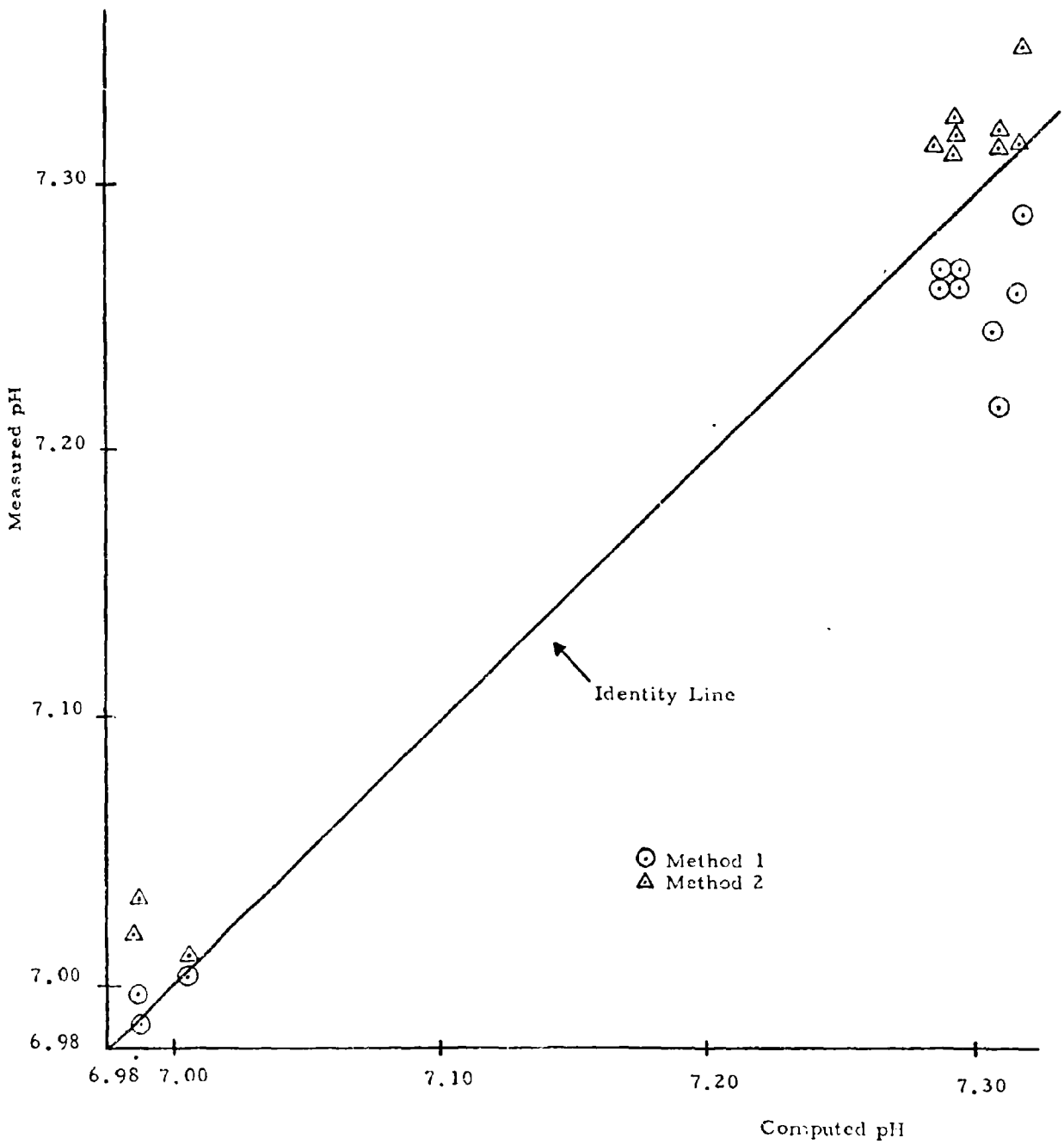
7.30
7.20
7.10
7.00
6.98
Measured pH
Identity Line
Method 1
Method 2
6.98
7.00
7.10
7.20
7.30
Computed pH

FIGURE 1

roles of the central and peripheral chemo-receptors. We hope to resolve this by a series of experiments on anesthetized dogs in which ventilatory responses to acute metabolic acidosis and alkalosis will be measured before and after peripheral denervation. Alveolar P_{CO_2} will be maintained at a constant level by varying the composition of inspired gas. In this way the CO_2 stimulus to ventilation will be kept constant and the isolated effect of pH studied. Progress to date on these experiments has been hampered by the late delivery of key instruments, but necessary techniques have been developed.

Thus the carotid body denervation technique on dogs has been perfected. Denervation is accomplished by cutting all nerves in the area of the carotid bifurcation, and completeness is verified by the lack of ventilatory stimulation following injection of 0.5 cc of 0.003 M KCN into both carotid arteries.

An alveolar P_{CO_2} control system has also been constructed. It is similar to that described by Lambertsen and Wendel[7], and a block diagram is shown in Figure 2. A Beckman LB-1 medical gas analyzer is used to monitor end-tidal CO_2 levels. The micro-catheter sampling technique is used with a flow rate of 500 cc/min. The sample is returned via the respiratory J-valve. This system has been tested on anesthetized dogs subjected to intravenous $NaHCO_3$ administration. Alveolar P_{CO_2} can be controlled within $\pm$ 0.5 mm Hg. In the series of experiments which we plan, airflow pattern changes will also be studied. A pneumotachograph and associated pressure transducer has been order but has not yet been delivered.

References

1. Mitchell, R. A., In: Cerebrospinal Fluid and the Regulation of Ventilation, Eds. Brooks, Kao and Lloyd, Blackwell Scientific Publications, 1965.

2. Fencl, U., T. B. Miller and J. R. Pappenheimer, Am. J. Physiol. 210, 459-472, 1966.

3. Katsaros, B., Plügers Archiv. 282: 157-178, 1965.

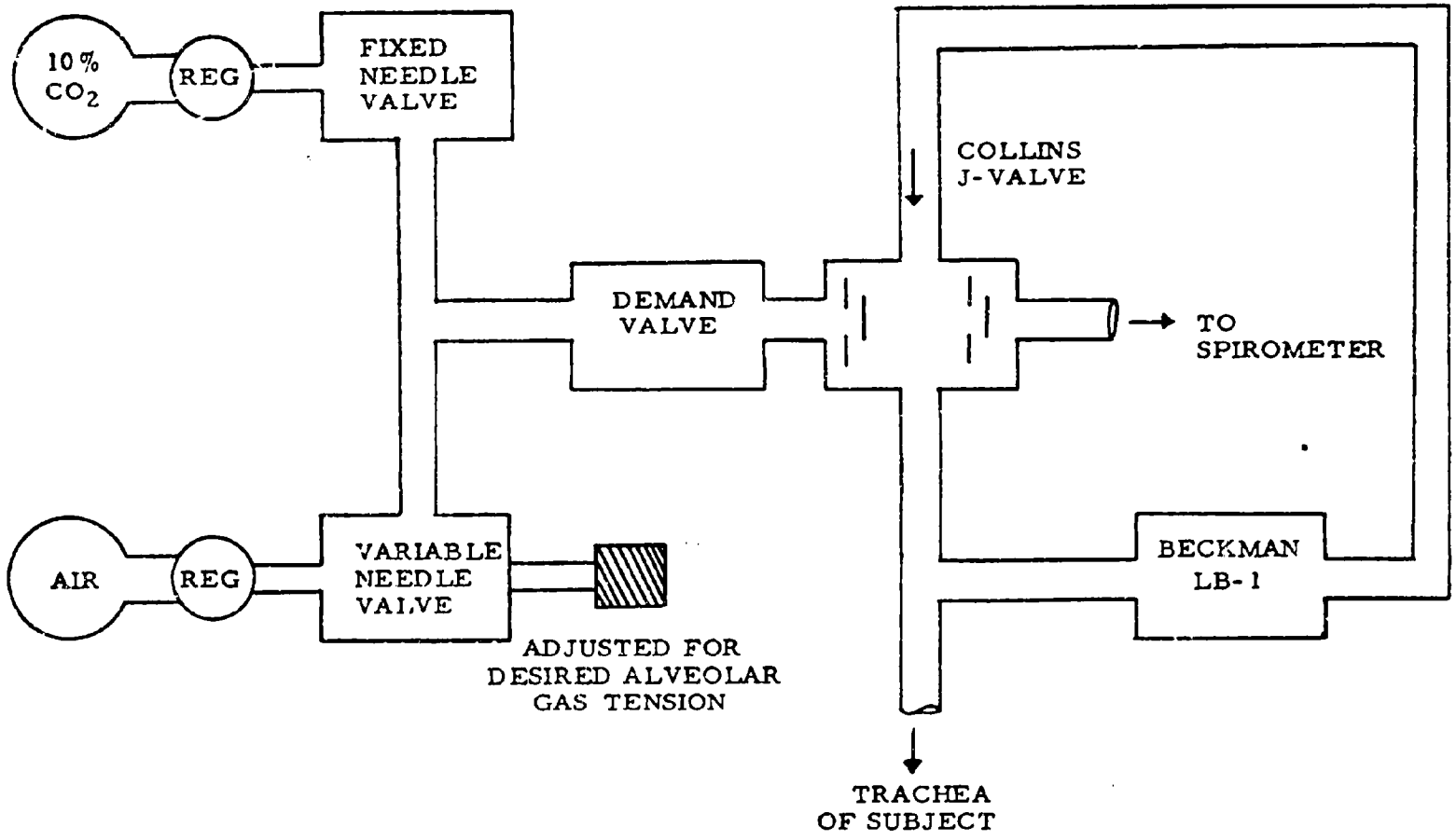
10 %
CO_2
REG
FIXED
NEEDLE
VALVE
COLLINS
J-VALVE
DEMAND
VALVE
TO
SPIROMETER
AIR
REG
VARIABLE
NEEDLE
VALVE
BECKMAN
LB-1
ADJUSTED FOR
DESIRED ALVEOLAR
GAS TENSION
TRACHEA
OF SUBJECT

FIGURE 2

4. Comroe, J. H., Jr., In: Handbook of Physiology, Section 3, Respiration (I), Eds. W. O. Fenn and H. Rahn, American Physiological Society, Washington, D.C., 1964, pp. 557-583.

5. Severinghaus, J. W., R. A. Mitchell, B. W. Richardson and M. M. Singer, J. Appl. Physiol. 18: 1155-1166, 1963.

6. Alexander, S. C., R. Gelfand and C. J. Lambertsen, J. Biol. Chem. 236: 592-596, 1961.

7. Lambertsen, C. J. and H Wendel, J. Appl. Physiol. 15, 43-48, 1960.

4.1.4 Baroceptor Reflexes in the Near Term Fetus

POI GM 16437-02, Department of Health, Education and Welfare (USPHS)

TOI GMO 172403, Department of Health, Education and Welfare (USPHS)

L. W. Morrison, G. A. Bekey, N. S. Assali

This study represents a combined experimental and theoretical attempt to assess the activity of the carotid baroceptor reflex in the near term fetus. The starting point for the theoretical part was a previously published mathematical model of the fetal circulation in the hemodynamic steady state[1]. This model had lumped parameter representations of (a) the left and right hearts, with the foramen ovale included as a unidirectional shunt between the atria, (b) the great vessels, with the ductus arteriosus represented as a bi-directional shunt between the aorta and the pulmonary artery, (c) the pulmonary vascular bed, represented as an elastic reservoir, (d) the systematic vascular bed as another elastic reservoir, (e) the placental circulation, represented as a network parallel to the systemic circuit. The pumping action of the ventricles was represented by sinusoidal volume changes and no attempts were made to include either neural or humoral control mechanisms. Parameter values were determined from previously available data for the fetal lamb. Thus, this model represented the isolated, uncontrolled "cardiovascular plant".

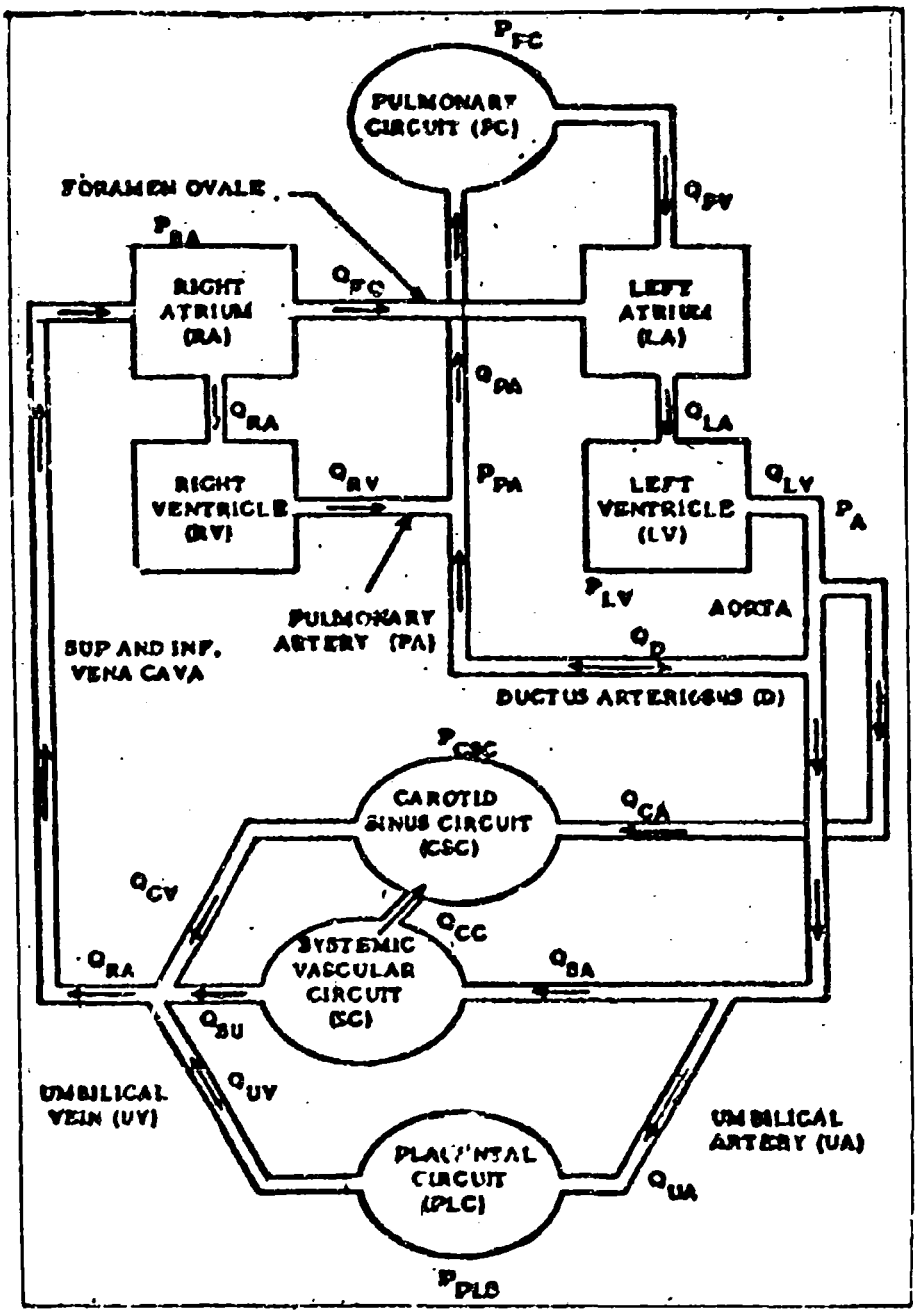

Figure 1. A Schematic Diagram of the Fetal Cardiovascular System

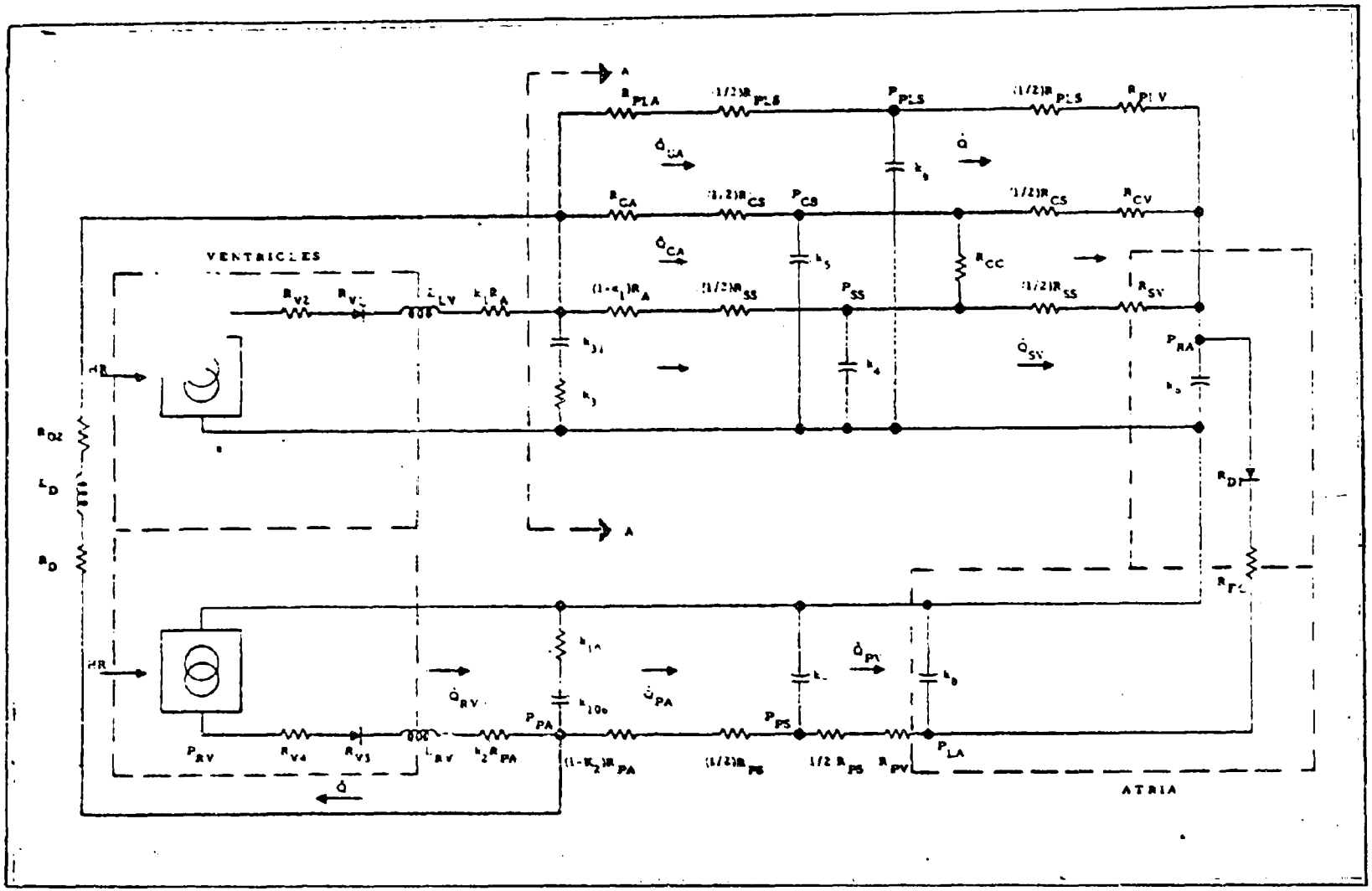

Figure 2. A Circuit Diagram Analogous to the Fetal Cardiosvascular System

In the present study, this model was extended by adding a carotid baroceptor control loop, and this required separate representation of the carotid circuit in the equations of the plant. A diagram of this modified fetal cardiovascular plant is shown in Figure 1, and its electrical analog in Figure 2. The latter employs conventional circuit elements (resistors, capacitors, inductors) to represent lumped hemodynamic parameters (viscance, compliance, inertance). Instead of representing the pumping action of the ventricles by sinusoidal volume changes as in the previous model, the simulation was now driven by previously recorded intraventricular pressure wave forms from the left and right hearts of experimental animals which had been digitized and stored in computer memory. The control loop was represented by the following equations:

$$\dot{R}_p + a_1 R_p = a_2 \dot{e}_p + a_3 e_p + a_4 \dot{e}_{co} + a_5 e_{co} \tag{1}$$

$$\dot{T}_{ds} = b_1 T_{ds} + b_2 e_p + b_3 e_{co} \tag{2}$$

$$HR = \left(T_{ds} + T_s \right)^{-1} \tag{3}$$

where R_p is the peripheral resistance, e_p is the difference between mean carotid sinus pressure and the reference pressure (a pressure error term), e_{co} is an assumed cardiac output error term, HR is the heart rate, T_{ds} is the diastolic period, T_s is the systolic period, and a_i and b_i are arbitrary gain constants.

Experimental data for comparison with the model were obtained at UCLA by Assali and Brinkman using near term fetal lambs, as described in previous publications[2,3]. Basically, the fetus is delivered by Cesarean section, and marsupialized to the uterine wall. The fetal chest is entered to make monitoring of flows and pressures possible. Access to the carotid sinus in the fetal lamb is extremely difficult, since the bifurcation of the carotid artery is located above and behind the jaw bone. Consequently, one common carotid artery was

ligated proximally and a catheter inserted distally to measure pressure in the region of the carotid sinus. An electromagnetic flow meter and clamp were placed on the opposite common carotid to make possible both the control a d monitoring of blood flow. Following occlusion of this carotid artery, changes were observed in the fetal arterial pressure (abdominal aorta via femoral catheter) as well as in the pressure recorded from the opposite carotid sinus area, as indicated by the tracings from two experiments in Figure 3. Table 1 gives the average % changes in systemic arterial pressure, ductus flow, effective cardiac output, and systemic peripheral resistance produced by carotid occlusion in 8 fetal lambs. This is compared with the "best fit" model performance which could be obtained by adjusting the control parameters, a_j and b_i.

Table 1

Percentage Changes Following Carotid Artery Occlusion

	Animal	Computer
Systemic pressure	+10% (mean)	+10% (systolic) +20% (diastolic)
Ductus arteriosus flow	-15%	-25%
Effective cardiac output	-10%	-25%
Systemic vascular resistance	+30%	+25%

The two major physiological questions which arise in this study are: (1) Does the baroceptor reflex exist in the fetal lamb?, and (2) If it does, what plant parameters does it operate on? Even if there were no baroceptor reflex, one would expect that carotid occlusion might produce a rise in peripheral resistance and arterial pressure through purely hemodynamic effects. However, simulated carotid occlusion in the open-loop model (i.e., the isolated plant) increased systemic resistance only 9% compared to the 30% change observed in the animal

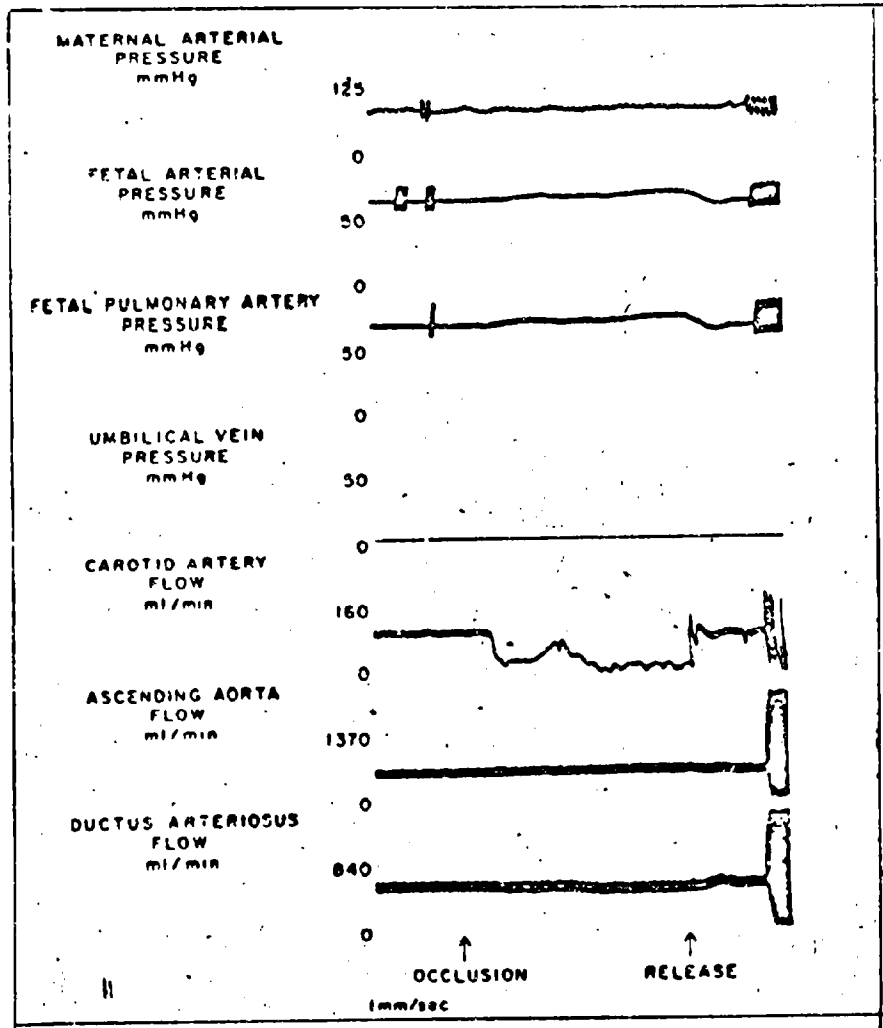

8 January 1968
Experiment #2
Fetus 5.3 Kg

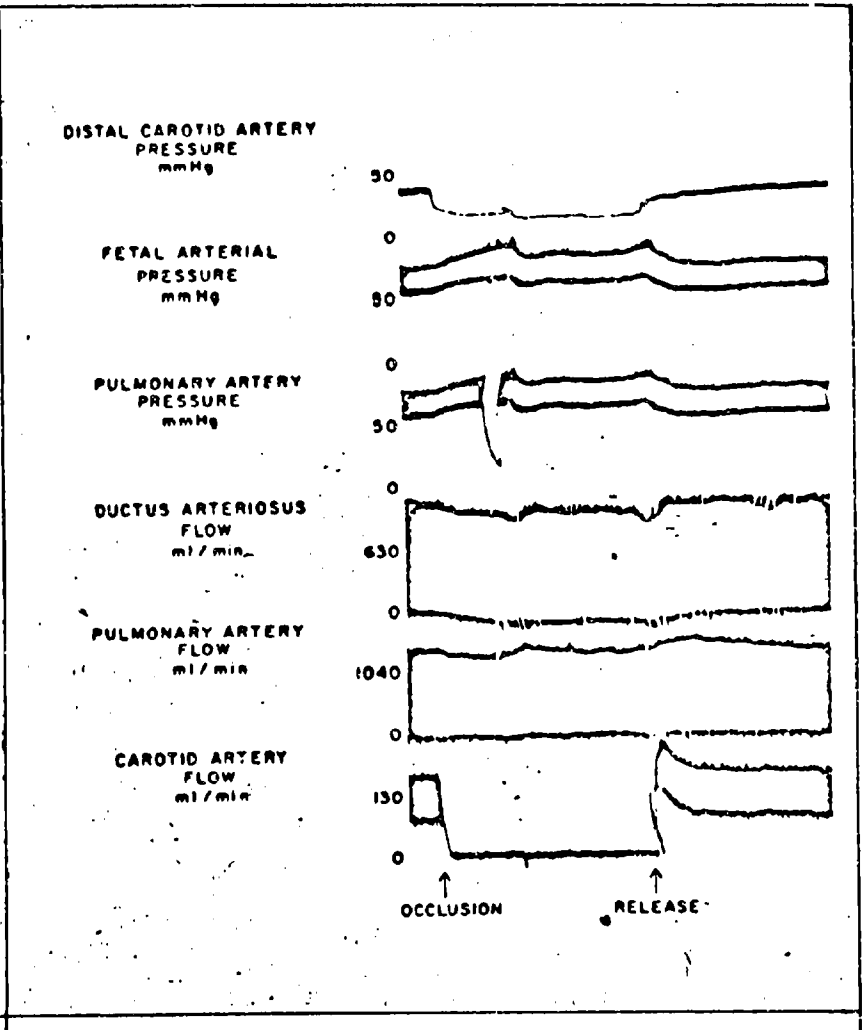

19 April 1968
Experiment #7
Fetus 4.0 Kg

FIG. 3

experiments. This type of indirect evidence is particularly important here because technical difficulties made it impractical to compare animal responses before and after carotid sinus denervation. Although the animal data showed to significant changes in umbilical vein flow and pressure during carotid occlusion, simulation in the model showed that when the placental circuit conductance was kept constant, the remaining systemic conductance had to fall to zero to achieve the observed rise in arterial pressure. This indicates that small % changes within the range of measurement error must have occurred in the large conductance of the placental shunt during carotid occlusion. Finally, since the model controller did not manipulate ductus parameters, it is probable that the decrease in ductus flow observed in the animals was a passive hemodynamic effect.

It is important to note that the conclusions (1) that a baroceptor reflex exists, and (2) that it must operate in part on the conductance of the placental circuit both depend on the results of isolated plant simulations which do not involve the control loops at all. Despite the encouraging agreement of experimental and closed-loop model simulation behavior in Table 1, further studies will be required to establish the validity of the control equations (1-3). In particular, we have no present knowledge of a physiological mechanism which can directly monitor cardiac output.

References

1. Morris, J. A., G. A. Bekey, N. S. Assali and R. Beck, Dynamics of Blood Flow in the Ductus Arteriosus, Am. J. Physiol. 208: 471, 1965.

2. Assali, N. S. J. A. Morris, R. W. Smith and W. A. Manson, Studies on Ductus Arteriosus Circulation, Circulation Res. 13: 478, 1963.

3. Assali, N. S., N. Sehgal and S. Marable, Pulmonary and Ductus Arteriosus Circulation in the Fetal Lamb Before and After Birth, Am. J. Physiol. 202: 536, 1962.

4.2 FLUID-ELECTROLYTE AND RENAL SYSTEM

4.2.1 Simulation of the Combined Artificial Kidney-Patient System

GM 16437-02, Department of Health, Education and Welfare (USPHS)

M. B. Wolf, R. Kalaba, J. Buell and S. Karuza

This research involves the prediction of the changes of body fluid chemical distribution in uremic (no kidney function) patients who are undergoing artificial kidney treatment (hemodialysis) and the specification of an optimum treatment procedure.

The first two phases of this research have been completed: (1) Mathematical description and simulation of the steady state characteristics of an artificial kidney[1] and (2) Simulation of a combined artificial kidney-patient system for single chemical species[2]. Figure 1 shows some of the results of these phases. The clinician may now use data of this sort to predict the time necessary for a given patient to undergo hemodialysis treatment to achieve a desired end result.

Current Phase of Research

1. Predicting an Optimal Treatment Procedure. Various optimal control techniques including dynamic programming, linear programming, are being explored in order to predict the maximum rate of removal of chemical substances from the body without producing prohibitively large inter-compartmental chemical gradients.

2. Identification of Parameters for Potassium Exchange Model. The quasilinearization method will be used to identify the mass transfer parameter for potassium exchange between the body compartments and across the dialyzer membrane. Clinical data will be used of plasma potassium concentration and rate of potassium removal from the body versus time.

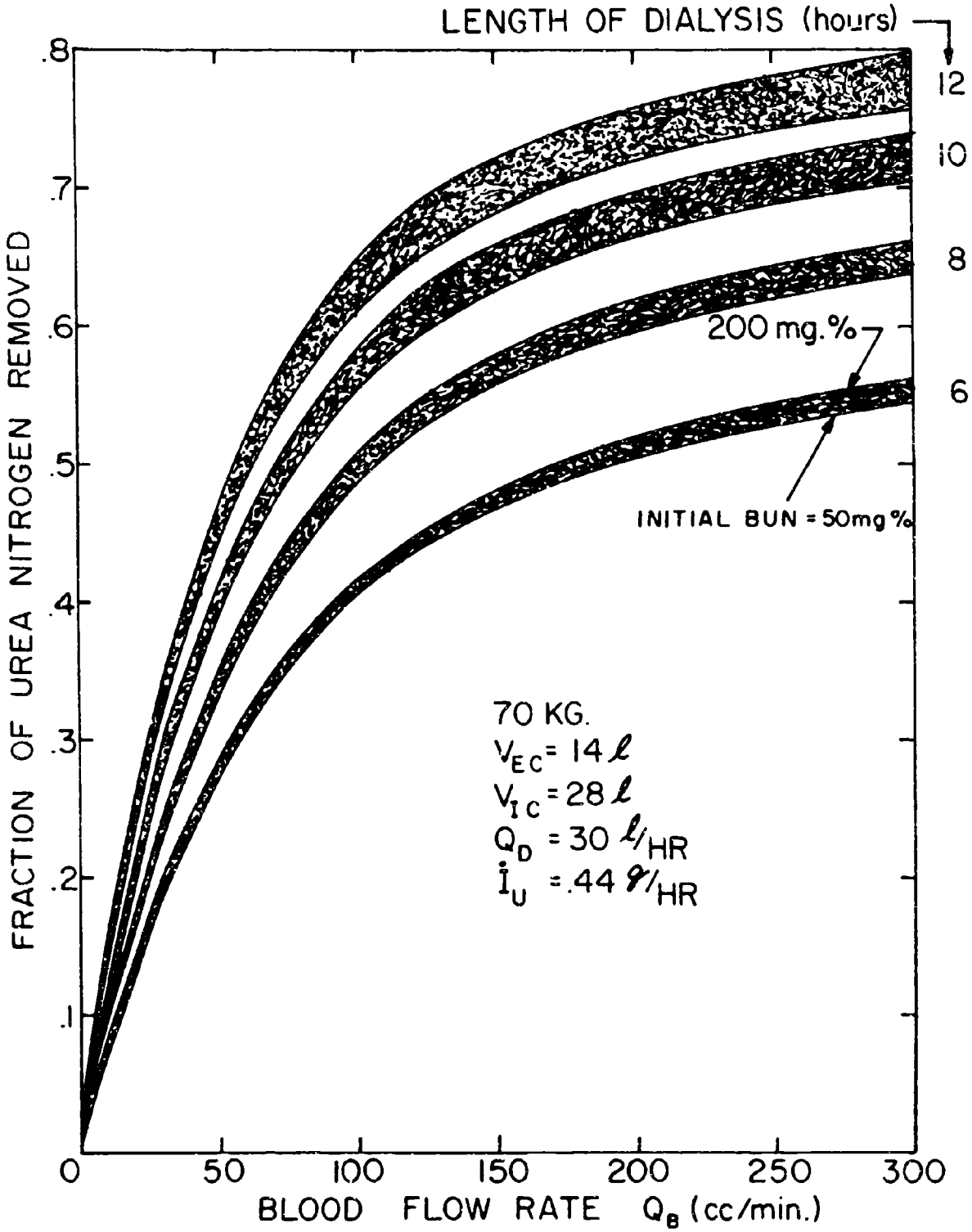
LENGTH OF DIALYSIS (hours)
12
10
8
6
200 mg.%
INITIAL BUN = 50mg%
70 KG.
V_{EC} = 14 ℓ
V_{IC} = 28 ℓ
Q_D = 30 ℓ/HR
$\dot{I}_U$ = .44 g/HR
FRACTION OF UREA NITROGEN REMOVED
.8
.7
.6
.5
.4
.3
.2
.1
0
50
100
150
200
250
300
BLOOD FLOW RATE Q_B (cc/min.)

Figure 1

3. Simulation of Steady State Chemistry in Uremics During Hemodialysis Treatment. This effort is still groing on but is hampered by lack of adequate computer facilities. Computing is done at the RAND Corporation on their 360/65 one a one day a week basis. The object is to use a quasi-dynamic model to predict changes in the hundreds of chemical species in the body during the course of treatment.

References

1. Kaplan, S., A. McNabb and M. B. Wolf, "Input-Output Relation for a Counter-Current Dialyzer by the Method of Invarient Imbedding," USCEE Report 255, Feb. 1968.

2. Wolf, M. B., P. D. Watson and B. H. Barbour, "Theoretical Evaluation of a Patient-Artificial Kidney System Using a Kul Dialyzer," USCEE Report 332, Feb. 1969.

4.2.2 Measurement of Body Fluid Chemistry in Uremics

GM 16437-02, Department of Health, Education and Welfare (USPHS)

M. B. Wolf and B. H. Barbour

This study is aimed at the measurement of the chemical distribution in uremic patients and animals before, during, and after the hemodialysis treatment.

The work in progress consists of measuring the plasma volume (PV) and red cell volume (RCV) during the course of dialysis. I^{131} albumen was initially used on two patients to measure the plasma volume. The PV results expressed in liters of volume are shown below.

Patient	Date	Time After Beginning of Dialysis (Hours)									
		0	1	2	3	4	5	6	7	8	9
D.E.	1-2-68	2.86		2.95					2.88		
D.E.	3-18-68	3.06		3.42	3.71						
	3-25-68	3.28		3.46	3.58						
	4-1-68	3.41		3.09	3.30						
Estr.	3-15-68	3.84		3.99		3.99					
	3-22-68	3.40		3.79		3.65					
	3-28-68	3.70		3.51	4.20						

These numbers, although far from conclusive, show a general increase in PV during the course of dialysis.

It was decided to next use Cr^{51} dilution to obtain a more continuous measurement of this quantity. Some of these results follow.

Patient	Date	Time After Beginning of Dialysis (Hours)										
		0	1	2	3	4	5	6	7	8	9	10
A.M.	11-4-68	6.6	6.7			7.1				7.0		6.9
C.H.	10-21-68	4.2	4.6			4.5				3.8		4.6
P.E.	10-18-68	3.2	3.4			3.5				3.6		3.8
L.C.	11-8-68	4.3	4.5			4.4				4.7		5.1

Again these results show a general increase in PV. Efforts are currently underway to take more data on individual patients although progress has been slowed by lack of personnel.

4.2.3 Interrelations of Respiratory and Renal Systems in the Control of Acid Base Balance

GM 16437-01 and FR 07012-02, Department of Health, Education and Welfare (USPHS)

S. Yamashiro, S. Karuza, M. B. Wolf and F. S. Grodins

The project is concerned with both theoretical and experimental approaches to the study of the control of acid-base balance by the various concerned systems of the body.

Experimental Work

1. Respiratory System. Experiments are currently underway to measure the changes in blood and cerebrospinal fluid acid-base chemistry following acute metabolic disturbances of acid base-balance. These experiments will hopefully elucidate the mechanism of how pulmonary ventilation is controlled as a result of these disturbances.

2. Renal Systen . Experiments have been initiated to measure dynamic changes in blood and urine chemistry during acute metabolic disturbances of acid-base balance. The aim is to be able to predict the time course of acid-base excretion of the kidney as a function of body chemistry.

Theoretical Work

1. Respiratory System. The model of respiratory control developed by Grodins[1] will be extended in the areas of blood, other body fluid and cerebrospinal fluid chemistry with the addition of the more detailed chemistry of the bicarbonate buffering system and intercompartmental chemical exchange.

2. Renal System. A model of the renal system will be added to the respiratory system. Initially the model will be an empirical input-output description of the kidney with respect to acid base balance. Later this model will be extended to include the actual physico-chemical details of kidney function.

Reference

1. Grodins, F. S., J. Buell and A. J. Bart, "Mathematical Analysis and Digital Simulation of the Respiratory Control System", J.A.P. Vol. 22, No. 2, Feb. 1967, pg. 260.

4.3 NEURAL SYSTEMS

4.3.1 Studies of Neuronal Interaction

NB 08207-0151, Department of Health, Education and Welfare (USPHS)

G. P. Moore, R. J. Sclabassi

This study is being undertaken to develop techniques for investigating the structure and function of neuronal networks. Of prime importance in such a study is the development of mathematical and computer techniques which enable an experimental record (consisting of multiple neuron signals) to be analyzed to determine if the observed neurons are connected to each other.

In the period under review experiments have continued to provide numerous examples of multiple neuron data which have been processed with our laboratory computing facilities. The principal technique used to determine whether neurons are interacting by means of connections between them is the processing of the data using cross-correlation methods. A report of the technique and the methods for interpreting results were presented at the IFAC Congress in September 1968[1] and will appear presently in the journal Automatica.

When experimental records have been suitably processed, inferences concerning possible network structures can be made, and hypotheses about the network can be simulated using a variety of computer programs which we have developed[2,3]. Using these programs the behavior of various networks can be tested against the experimental observations (e.g., 4).

References

1. "Application of the Theory of Stochastic Point Processes in the Detection and Analysis of Neuronal Interaction", with D. H. Perkel and J. P. Segundo, Proc. IFAC Symposium on Technical and Biological Problems of Control, Yerevan, Armenia, 1968 (in press).

2. "Continuous-Time Simulation of Ganglion Nerve Cells in Aplysia", with D. H. Perkel and J. P. Segundo, Biomedical Sciences Instrumentation, V. 1, Proc. of 1st National Biomedical Sciences Instrumentation Symposium, F. Alt, ed. ISA - Plenum Press, New York, 1963, pp. 347-357.

3. R. J. Scalabassi, "A Generalized Nerve Net Model", USCEE Report 356, June 1969.

4. "Input-Output Relations in Computer-Simulated Nerve Cells", with J. P. Segundo and others, Kybernetik, 4, 1968, 157-171.

4.3.2 Models of Neuronal Activity

GM 16437, Department of Health, Education and Welfare (USPHS)

G. P. Moore, J. Penaloza, R. J. Sclabassi, J. L. Gehrich

This study begins with experimental observations of pulse sequences of individual neurons of the brain and attempts to develop hypotheses of the neuronal network which is generating the observed signals. The hypothetical network is simulated on a digital computer, or developed as a mathematical model, and its behavior is compared with the experimental data. Each comparison and each new experiment results in further development of the model or results in the rejection of one of the models under consideration.

At the present time, three areas of the brain are under active study.

(1) The visual system of the brain where distinctive patterns of pulse activity have received widespread attention from network theorists. We are doing experiments to obtain high quality data from these areas and are considering several network models to account for these observations (see 1 for general techniques of neuron modeling and a specific discussion of this network).

(2) Sensory pathways for touch and propriception in the brainstem where a unique discharge pattern has been observed. We presently believe that the observed pulse pattern does not arise from network structure but from a special property of the individual neurons involved, and predictions based on this theory have had reasonable success[2,3].

(3) Special chemoreceptor neurons which send information to the brain concerning the levels of carbon dioxide and oxygen in the blood have been observed, again with a characteristic quantifiable discharge pattern. Seven models of this receptor are currently under investigation.

References

1. "Engineering Approaches to the Study of Neuron Networks", In: Biomedical Engineering, J. H. Brown (edt.), McGraw-Hill, 1969 (in press).

2. R. Sclabassi and G. P. Moore, "Parameter Estimation Methods for Sensory Neuron Models", 8th ICMBE, Chiago, Ill., July, 1969.

3. R. J. Sclabassi and G. P. Moore, "Influence of Accommodation on Neuron Firing Statistics", Feb., 1969, Biophysical Society Meeting, Los Angeles.

4.4 BIOMATHEMATICS

GM-16197-01, Department of Health, Education and Welfare (USPHS)

R. Bellman and others cited in subsections

The research activities in the areas of Mathematics in Biology and Medicine are described briefly in the following subsections.

4.4.1 Chemotherapy and Drug Administration

One of our major areas of research continues to be chemotherapy, with particular emphasis upon pharmacokinetics and the clinical administration of drugs. June Buell and Robert Kalaba are pursuing their close collaboration with Dr. Roger Jelliffe of the Los Angeles County-University of Southern California Medical Center in connection with the administration of digitalis and other drugs.

The mathematical investigations center about three aspects: descriptive, control, and identification. By descriptive we mean a numerical prediction of the consequences of certain biochemical assumptions; by control we mean a determination of the drug regimen that will produce desirable results, by identification we mean a determination of biochemical and patient parameters so that effective dosage can be administered.

For treatment of certain descriptive and control aspects, see References 1 through 4. These investigations concern the optimal administration of drugs such that body levels are kept within prescribed bounds. R. Kalaba is currently working on control problems where some of the patients' "rate constants" are subject to stochastic variations during the dosage regimen[5]. For a treatment of identification processes see reference 6 and 7. The recent work of Brocker and Jelliffe[8], will permit an enlargement of the kinetic models of digitoxin and digoxin dynamics.

A. Yakush is using the general quasilinearization program of Buell, QUASI, to identify rate constants in a model of potassium dynamics. G. Bloom and C. Shoemaker are also writing computer programs in this general area.

S. Schloss is continuing his study of the estimation of drug parameters. The determination of individual drug distribution parameters in nonlinear models may be performed by using a dynamic programming algorithm which requires preliminary estimates and measurement error variances. The method provides sequentially smoothed estimates of parameters and converges in general despite the presence of appreciable measurement noise and relatively large errors in preliminary estimates. Initially the chemical rate parameter estimation problem of Bellman-Jacquez-Kalaba-Schwimmer was studied since (1) it was sufficiently complex due to the nonlinearity of the state differential equation to be challenging, (2) it can be solved using another method, namely quasilinearization, (3) it was a problem of low dimension, and (4) it is related to drug models.

Initial numerical results are encouraging. The quasilinearization method results in a value of $.46 \times 10^{-5}$ for one parameter after two iterations and sequential smoothing also provides $.46 \times 10^{-5}$ but after one pass through the raw data. The same initial estimate of 1×10^{-6} was used in both approaches. Probably due to the use of a crude numerical integration technique in the sequential smoothing program the second parameter was not estimated as accurately to provide a very good fit to the data. Numerical integration is employed in two places in the computer program. Schloss is now putting in a standard IBM integration routine to see if this improves the performance. The theoretical development and application to the above problem has been written up in preliminary form.

The sequential smoothing technique was applied to the myocardial parameter estimation problem in the manner indicated in H. S. Schloss, "Sequential Stochastic Identification of Myocardial Parameters,"

Mathematical Biosciences, Vol. 2, 1968, pp. 139-144. The resulting computer program has been partially successful. In the initial portion of the ventricular depolarization phase, the wave spreads downward and to the right. When the initial portion of the wave is analyzed, or somewhat equivalently a simulated heart just consisting of several septal segments, the estimation process works well, that is converges to the true values for both simulated hypertrophy and infarction conditions. However, if applied to later portions of the wave as it spreads to the right and left ventricles, the estimation process diverges. This is probably due to the following: if there is a deviation in value of the potential from what is expected, the estimator may increase the potential in one direction or decrease the potential in the opposite direction. Half of the time the result will be the wrong one.

The following two changes will be made which should improve the performance: (1) the cost function will have an added term to cause parameters to remain in "realistic" ranges of values, and (2) since often one knows from other data, for example x-rays, that hypertrophy is or is not a possibility, there will be a "switch" in the program to modify appropriately the values of these ranges of the parameters.

References

1. J. Buell, R. Jelliffe, R. Kalaba, and R. Sridhar, "Modern Control Theory and Optimal Drug Regimens--I: The Plateau Effect," USCEE-323, December 1968. To appear in Mathematical Biosciences.

2. -----, Modern Control Theory and Optimal Drug Regimens--II: Combination Theory", USCEE-324, December 1968. To appear in Mathematical Biosciences.

3. R. Bellman, "Use of Digital Computers in Defining Pharmacokinetic Parameters, USCEE-355, May 1969. Presented at the Workshop in Pharmacokinetics, Berlin, 1969.

4. R. Jelliffe, J. Buell, R. Kalaba, R. Sridhar, and R. Rockwell, "A Mathematical Study of the Metabolic Conversion of Digitoxin to Digoxin in Man," USCEE-347, May 1969. To appear in Mathematical Biosciences.

5. R. Jelliffe, P. Kalaba, and R. Sridhar, "Modern Control Theory and Optimal Drug Regimens--III: Stochastic Effects", in preparation.

6. S. Kaplan and M. B. Miloud, "On Eigenvalue and Identification Problems in the Theory of Drug Distribution", USCEE-310, October 1968.

7. J. Buell and R. Kalaba, "Quasilinearization and the Fitting of Nonlinear Models of Drug Metabolism to Experimental Kinetic Data", USCEE-312, November 1968. To appear in Mathematical Biosciences.

8. G. Brooker and R. W. Jelliffe, "Determination of Serum Digoxin by Enzymatic Isotope Displacement of H_3 Digoxin from Na-K ATPase", Proc. Fed. Amer. Soc. Exper. Biology, Vol. 23, 1969, p. 600.

4.4.2 Identification of Systems

The determination of the internal structure of systems on the basis of convenient, inexpensive, and painless observations continues to be another of our major directions of research.

In the previous section we mentioned work of J. Buell, R. Kalaba, and S. Kaplan connected with pharmacokinetics. Following is some work of a more general nature. R. Bellman and R. Roth have continued their collaborative efforts in the areas of dynamic programming and segmental differential approximation (See Reference 1 and 2). One of the drawbacks of the application of quasilinearization lies in the necessity of solving complex functional equations. Another is the requirement of obtaining a sufficiently close initial estimate of the parameters to be identified. A new method recently developed promises to avoid both of these obstacles. (See Reference 3).

A general computer program by Buell and Kalaba that will treat Fredholm integral equations with composite kernels of particular form will permit the study of isotropic scattering in a cylindrical and spherical medium. This will be important in radiation therapy and diagnosis and in the identification of micro-organisms by their reflective

and absorptive properties in solution. This connects with work done by Denman and Kaplan on tumor location and with that by Friedland[4, 5] concerning the use of radio-isotopes and scanning.

R. Bellman and Professor L. Zadeh of the Department of Electrical Engineering, University of California, Berkeley, are investigating the use of the theory of "fuzzy systems" to handle certain identification problems that escape classical formulation.

References

1. R. Bellman and R. Roth, "Curve Fitting by Segmented Straight Lines," USCEE-313, November 1968. To appear in J. Amer. Stat. Assoc.

2. R. S. Roth and M. M. Roth, "Data Unscrambling and the Analysis of Inductible Enzyme Synthesis," Mathematical Biosciences, to appear.

3. R. Bellman, "A New Method for the Identification of Systems", USCEE 337, March 1969. To appear in Mathematical Biosciences.

4. S. S. Friedland, "Activation Analysis in Nuclear Medicine", USCEE 212, June 1967.

5. H. S. Katzenstein, L. Kleinrock, A. Stubberud, and S. S. Friedland, "Application of the Mathematical Theory of Sequential Sampling to Gamma Scanning in Nuclear Medicine", USCEE-230, October 1967. To appear in Mathematical Biosciences, Vol. 4, 1969.

4.4.3 Physiological Models

R. Bellman and R. Tomović, the noted expert in control theory and prosthetics from the University of Belgrade, will spend three months, October, November, and December, 1969, working on a detailed and sophisticated model of the human muscular system. Since there are only about 360 different muscles in the human body, there appears to be an excellent chance to construct a realistic mathematical model which would have fundamental applications to prosthetics and orthotics as well as to the general theory of the control of complex systems. Preliminary discussions of this model were held in Dubrovnik in August 1968 and in Paris in

February 1969.

R. Kalaba and M. Wolf are preparing a paper on the optimization of the removal of urea in hemodialysis using invariant imbedding and dynamic programming. A. Yakush has carried out the required programming. R. Sridhar, a distinguished expert in modern control theory will leave California Institute of Technology to join our USC group working in the area of physiological control. G. Cohen of the University of Rochester will spend the sabbatical year 1969-70 on the application of computers to biomathematical problems.

S. Kaplan, R. Bellman, and S. Ulam of the University of Colorado have carried out some preliminary investigations of evolutionary processes. S. Kaplan and A. Yakush have completed computational studies of the evolution of aging begun in 1968. A paper on the results of this work is almost complete.

S. Schloss has been studying the simulation of emphysematous conditions in conjunction with a Los Angeles physician specializing in respiratory ailments, using a Grodins-Buell-Bart computer program.

. Shoemaker is preparing a paper on the control of ecosystems (ecological systems) using dynamic programming.

4.4.4 Neurophysiology

We have two principal activities in the field of neurophysiology; the research of S. Kaplan and D. Trujillo in occasional collaboration with H. M. Lieberstein, and that of H. Sugiyama in collaboration with G. Moore and D. Perkel.

The Kaplan-Trujillo work is concerned with the simulation of neuronal phenomena. A computer program has been written to solve the partial differential equations governing the conduction of a nerve impulse down an axon. The initial use of this program has been to explore a

controversy surrounding Lieberstein's inclusion of an inductance term in the basic equations and his insistence that this term determines the propagation velocity of the nerve impulse.

The question of the role played by the inductance has been carefully investigated in these equations. The investigation examined: (i) the role of inductance in the case of a passive membrane; i.e., how do solutions of the telegrapher's equation grade between those of the wave equation and those of the diffusion equation? (ii) the role in the case of the active membrane; what is the effect of inductance on the (nonlinear) action potential?

It was found that there are two regimes present in one of which Lieberstein's view is substantially (though not exactly) correct and in the other in which it seems to be clearly wrong. These results are described in Reference 1. Having dealt with this conceptual matter, they are now turning to physiological questions. They intend to explore and simulate: (1) the situation at a presynaptic knob--the effect of size and type of membrane, (2) "floating wire" experiments in which a piece of wire is put into the axon, (3) the situation occurring at bifurcations in the axon, (4) buildup and inhibitions in dendrites, and (5) propagation in myelinated axons.

Ultimately, this model can be extended to include synapses and networks of neurons. A great deal of work is required to help clarify the field and stimulate meaningful laboratory experimentation. It is intended that this line of work will develop into one of the main themes of the mathematical biosciences group.

The H. Sugiyama work is to appear in Reference 2. In this paper, some general models for neuronal spike production are presented and the corresponding spike interval distributions (i.e., the first-passage distributions) are derived in closed form in terms of the Laplace transform. In certain cases, the spike interval distribution is obtained directly, in its

closed form. This is a very useful and important result. The models are classified into two cases: (1) the "continuous Markov model" which corresponds to the neuronal fluctuations of neuronal membrane potential in the absence of synaptic input from other neurons, and (2) the "mixed Markov model" in which discrete changes in membrane potential, resulting from input from other neurons, are included. In the case of mixed Markov models, some typical spike interval distributions are given, obtained by solving the generalized diffusion equations numerically, with initial and boundary conditions.

In a second paper, some approaches to the inverse problem of estimating parameters in the models are given. Maximum likelihood estimates are obtained in some cases. Then, in the general cases, the gamma-type distribution is assumed for spike interval statistics, since this type of distribution is rather broadly applicable to fit real spike interval statistics. Then, its Laplace transform is compared with the Laplace transform of the first passage distribution obtained in the previous paper. The sum of squares of their differences over a sufficiently large number of parameter values of the Laplace transform is minimized.

Using the same minimization procedures, the prediction of the spike interval distribution based upon gamma type statistics, in the continuous Markov case is possible, given a set of model parameter values.

The second paper deals with the inverse problem (identification of parameters) using the hill-climbing method and stochastic approximation. H. Kato has written a computer program for this, starting with the single neuron system. He is currently preparing the multineuron case.

Since the parabolic cylinder function plays a very important role in the prediction and the inverse problem of the spike interval distributions in the models described above, some kind of tabulation of this function will be very helpful for neurophysiology. A paper is being written entitled "Tabulation of the Parabolic Cylinder Function." It is

interesting to note that the functional values of the parabolic cylinder function can be obtained, inversely, by solving the diffusion equation numerically with initial and boundary-value conditions.

In the paper, "Some Stochastic Models and Analysis Concerning Neuronal Spike Production--III," two neuron cells A and B governed by the mixed type Markov systems discussed in the previous papers are considered. Assuming the existence of a common neuron C sending discrete jump signals governed by the same Poisson process, the cross-correlation function between the two series of spike trains generated by cells A and B is investigated.

References

1. S. Kaplan and D. Trujillo, "Numerical Studies of the Hodgkin-Huxley Partial Differential Equations--I: The Significance of Lieberstein's Inductance Term", USCEE 351, April 1969.

2. G. Moore, D. Perkel, and H. Sugiyama, "Some Stochastic Models and Analysis Concerning the Neuronal Spike Production--I, in preparation.

4.4.5 Psychodynamics

We are actively continuing our efforts in another major direction, psychodynamics. One of our objectives is to rewrite the computer program described in

R. Bellman, M. B. Friend, and L. Kurland, "A Simulation of the Initial Psychiatric Interview", The RAND Corporation, R-449-RC, 1966,

-----, "On the Construction of a Simulation of the Initial Psychiatric Interview," Behavioral Sciences, Vol. 11, 1966, pp. 389-399,

-----, "A Simulation of the Initial Psychiatric Interview: Revised and Expanded Version", USCEE 240, December 1967,

so as to make it available for CRT (cathode ray tube) display, rather than the original typewriter format which possesses a number of disadvantages. This work, carried out by R. Luthardt, R. Reynolds, and J. Rosenberg,

will be finished by the end of the summer. It involes a number of major revisions and additions to the original problem.

P. Kell and R. Bellman are preparing a library of short computerized simulations (vignettes) covering a wide range of situations encountered in initial interviews. W. Hopgood and K. Colby, Stanford University, both consultants, are assisting in this effort. A detailed discussion of what is involved in this is contained in: R. Bellman, W. Hopgood, and P. Kell, "On the Construction of Simulations of Parts of the Initial Psychiatric Interview--I," in preparation. This covers Case I of a list of eight cases for which detailed writeups of the others will follow. This material will form part of a book by Bellman and Kell entitled Computers, Simulation and Psychotherapy, to be published by Basic Books in a series edited by Dr. Werner Mendel of the USC Medical School.

Contact has been made with R. Littman, Director of the Suicide Prevention Center, Los Angeles, with plans to use analogous simulation processes in the training of telephone answerers at the SPC. Similarly, we are exploring the possibility of using computerized simulation processes in role-playing training in a number of areas. P. Kell is participating in a seminar on simulation techniques and discussions have been inaugurated with L. Adler and M. Wexler of the USC Medical School Department of Psychiatry and with A. Marston, Director of Clinical Training, USC Department of Psychology, concerning various applications of simulation processes for training purposes.

4.4.6 Operations Research in Hospitals and Community Clinics

Many of the major problems in hospitals, both from the standpoint of patient care and administration, center about the scheduling of activities. Continuing previous work in this area by R. Bellman, A. Esogbue, T. Odanaka, and J. Saksena, we are examining various types of scheduling problems. We are particularly interested in processes

where the cost of inspection and observation becomes an appreciable part of the overall cost. Results of this nature are presented in

T. Odanaka, "Analytic and Computational Studies of Optimal Inventory Processes--I: Approximation of Quantity", USCEE 352, April 1969.

-----, "Analytic and Computational Studies of Optimal Inventory Processes--II: Approximation in Time", USCEE 353, April 1969.

I. Nabeshima of the University of Electrocommunications, Tokyo, is spending one year at USC working in the area of mathematical scheduling, and he may be able to stay another year. He and R. Bellman are completing a joint book entitled, Mathematical Aspects of Scheduling Theory, to be published by American Elsevier Publishing Company.

S. Osaki, University of Kyoto, an expert in mathematical scheduling theory, will spend a year here, 1970-71, working in this general area. M. Sedlar, University of Belgrade, an expert in graph theory and scheduling theory, will join the group in October to head this effort. These activities will be closely coordinated with the program of the Department of Industrial Engineering. Some of the major new directions of the Department of Industrial Engineering will be scheduling theory, Markovian decision processes, analysis of complex systems, etc., all connected with operational aspects of the administration of hospitals and community clinics.

A detailed discussion of the computerization of the patient information at LAC-USC Medical Center is given in

F. Mitchell, PAINS, USCEE-311, October 1968.

PAINS is an acronym of Patient Information System. This report brings to a close our four-year colloaborative effort with R. Maronde of the Department of Pharmacology, USC Medical School, in the computerization of hospitals. The county has now instituted a formal program under the leadership of G. Thompson and our direct efforts are no longer needed.

We have inaugurated a joint effort with the USC School of Dentistry, in collaboration with W. Finke, Director, Patient Assignment

Office, for the computerization of dental clinics. J. Goldstein will serve as mathematician-programmer and his father, C. Goldstein, a Santa Monica dentist, will serve as unpaid consultant. I. Nabeshima and M. Sedlar will assist in this program.

4.4.7 Auxiliary Mathematical Research

A major part of our program is the development of analytic and computational techniques for the solution of complex functional equations of the type that arise with frequency in biomedical research. In addition to the research that is sponsored by the NIH, we have support from the Atomic Energy Commission and the National Science Foundation for mathematical research of closely connected nature. For example, one of the major problems that ties mathematical physics and invariant imbedding to our mathematical biosciences program is the study of the effect of radiation upon human tissue and conversely the use of various radiation patterns for the location of tumors, etc. This is part of the general identification problem. The work that E. Angel has been doing in the solution of potential equations is aimed at a number of diagnostic problems in the field of cardiology. See, for example, References 1, 2, 3 and 4.

A principal difficulty, particularly in control processes that arise in prosthetics and orthotics and drug administration, is that of "dimensionality." Even with the best of modern computers, high-dimensional systems of ordinary differential equations, differential-difference equations, and partial differential equations, present severe difficulties as far as numerical solution is concerned. Over the past year, considerable progress has been made in this area. See References 5, 6 and 7.

The use of the digital computer is greatly enhanced by formulation of problems in initial-value form such as in References 8, 9 and 10.

References

1. E. Angel, "Discrete Invariant Imbedding and Elliptic Boundary-value Problems Over Irregular Regions", USCEE-279, 1968.

2. E. Angel, "A Building Block Technique for Elliptic Boundary-value Problems Over Irregular Regions", USCEE-285, June 1968.

3. E. Angel, "Inverse Boundary-value Problems: Elliptic Equations", USCEE-343, April 1969.

4. R. Kalaba and E. Ruspini, "Invariant Imbedding and Potential Theory", USCEE-335, March 1969.

5. D. Collins, "Terminal Dynamic Programming", USCEE 338, March 1969.

6. R. Bellman, "A New Type of Approximation Leading to Reduction of Dimensionality in Control Processes", USCEE 329, February 1969.

7. A. Lew, "Some Results in Differential Approximation", USCEE 314, November 1968.

8. A. McNabb and A. Schumitzky, "Factorization of Integral Operators--II: A Nonlinear Volterra Method for Numerical Solution of Linear Fredholm Equations", USCEE 330, March 1969.

9. J. Buell, H. Kagiwada, A. McNabb, and A. Schumitzky, "Computation of Resolvents for the Auxiliary Equations of Radiative Transfer", J. Quant. Spectros. Radiative Transfer, Vol. 8, 1968.

10. J. Buell, R. Kalba, and E. Ruspini, "Numerical Results for a Mixed Boundary-Value Problem of Potential Theory Using Invariant Imbedding", USCEE 346, April 1969.

APPENDIX A

Publications

Andrews, H. C.

"Two Dimensional Transform Coding of Images", with W. K. Pratt, 1969 IEEE International Symposium on Information Theory, Ellenville, New York.

"Digital Computer Simulation of Coherent Optical Processing Operations", with W. K. Pratt, IEEE Computer Group News, November 1968.

"Hadamard Transform Image Coding", with W. K. Pratt and J. Kane, Proceedings of IEEE, Vol. 7, No. 1, pp. 58-68, January 1969.

"Television Bandwidth Reduction by Encoding Spatial Frequencies", with W. K. Pratt, JSMPTE, V. 77, N. 2, pp. 1279-1281, December 1968.

"Transform Coding for Noise Immunity and Bandwidth Reduction", with W. K. Pratt, Hawaii International Conference on System Sciences, pp. 545-548, January 1969.

Bekey, G. A.

"Mathematical Approach to the Study of Fetal Circulation Dynamics", with W. Morrison, Vol. II, pp. 117-142, ed. by N. S. Assali, M.D., to be published by Academic Press.

"Identification of Sampling Intervals in Sampled-Data Models of Human Operators", with C. B. Neal, IEEE Trans. on Man-Machine Systems, Vol. MMS-9, pp. 138-142, December 1968.

"Synthesizing Optimal Controls for Modulated Discrete-Time Systems", with L. R. Nardizzi, Intern. Journal of Control, Vol. 8, pp. 571-590, 1968.

Bellman, R.

"Mathematics and Society", USCEE 327, February 1969.

"A New Method for the Identification of Systems", USCEE 337, March 1969, to appear in Mathematical Biosciences.

"Use of Digital Computers in Defining Pharmcokinetic Parameters", in preparation, to appear in Proc. Workshop in Pharmacokinetics, Berlin, 1969.

"On the Construction of Simulations of Parts of the Initial Psychiatric Interview--I", with W. Hopgood and P. Kell, in preparation.

"Curve Fitting by Segmented Straight Lines", USCEE 313, November 1968, with R. Roth, to appear in Journal of the American Statistical Association.

Breuer, M. A.

"Fault Detection in Linear Cascades of Identical Sequential Machines", Proc. IEEE Conference on Switching and Automata Theory, pp. 235-244, October 1968.

"Hardware Fault Detection", Proc. FJCC, vol. 33, pp. 1502-1503, December 1968

"Combinatorial Equivalence of (0,1) Circulant Matrices", J. Computer and System Sciences (accepted for publication).

"Generation of Optimal Code for Expressions Via Factorization", Comm. ACM (accepted for publication).

"Circuit Partitioning Via Simulation, Activity Directed Circuit Simulation, and Backward Simulation", IEEE Trans. on Electronic Computers (submitted for publication).

"Fault Detection in Linear Cascades of Identical Sequential Machines", IEEE Trans. on Electronic Computers (submitted for publication).

"Simplification of the Covering Problem withe Applications to Boolean Expressions", Journal ACM (submitted for publication).

Brook, R. J.

"Pore-Grain Boundary Interactions and Grain Growth," to be published, J. Am. Cer. Soc. 52 (1), 1969).

"Pores and Grain Growth Kinetics", to be published, J. Am. Cer. Soc. 52 (5), 1969.

Crowell, C. R.

"Normalized Thermionic-Field (T-F), Emission in Metal-Semiconductor (Schottky) Barriers", with V. L. Rideout, Solid-St. Electron., V. 12, pp. 89-105, 1969.

"General Normalized Current-Voltage Characteristic of Quasi Ohmic Contacts", presented at the Electrochemical Society Symposium on Ohmic Contacts, Oct. 1968, Montreal, in press.

"Thermionic-Field Resistance Maxima in Metal-Semiconductor (Schottky) Barriers", with V. L. Rideout, Appl. Phys. Letters, V. 14, 85 (1969)

"Surface State and Interface Effects on the Capacitance-Voltage Relationship in Schottky Barriers", with G. I. Roberts, to be published.

"Richardson Constant and Tunneling Effective Mass for Thermionic and Thermionic-Field Emission in Schottky Barrier Diodes", Solid St. Electron., V. 12, pp. 55-59, 1969.

"Metal-Semiconductor Interfaces", Surface Sciences, V. 13, No. 1, pp. 13-16, 1969.

Daybell, M. D.

"Temperature Control", with W. A. Steyert, Mossbauer Effect Methodology, Vol. 4, p. 1. Plenum Press (New York 1968).

"Sub-Kondo Temperature Properties of Localized Moments in Metals", with W. A. Steyert, Journal of Applied Physics, March 1969.

"Kondo Transition in Cu(Cr): Susceptibility and Specific Heat", with W. P. Pratt, Jr., and W. A. Steyert, Phys. Rev. Letters 22, 401 (1969).

DeShazer, L. G.

"Spectral Control of Laser Oscillators by Secondary Light Sources", with E. A. Maunders, IEEE J. Quan. Elect. QE-4, 642 (1968).

"Observation of Optical Pulse Shaping by the Self-Focusing Effect", with G. L. McAllister and J. H. Marburger, Phys. Rev. Letters 21, 1648 (1968).

"Spectroscopic Determination of Local Field Parameters", with M. M. Mann, Phys. Rev. Letters 22, 404 (1969).

"Low-Temperature Suppression of Absorption from Excited Levels", with M. M. Mann, J. Opt. Soc. Am. 59, no. 4 (1969).

"Atomic Multipole Radiation in Anisotropic Media", with M. M. Mann, paper presented at the Meeting of the Optical Society of America, San Diego, Calif., March 11-14, 1969.

"Saturated Absorption and Transmission of Laser Radiation by Organic Compounds", with L. Huff, paper presented at the Meeting of the Optical Society of America, San Diego, Calif., March 11-14, 1969.

"Laser Saturation of Optical Transitions in a Starch Components: The Amylose-Iodine-Iodide Complex", with L. Huff and F. W. Schneider, Science 163, (1969).

"Near Fields of Truncated Gaussian Apertures", with J. P. Campbell, J. Opt. Soc. Am., to be published.

"Atomic Multipole Radiation in Anisotropic Media", with M.M. Mann, Phys. Rev., to be published.

"Energy Levels and Spectral Broadening of Neodymium Ions in Laser Glass", with M. M. Mann, Phys. Rev., to be published.

"Optical Pulse Shaping by the Self-Focusing Effect", with G. L. McAllister, to be presented at 1969 IEEE Conference on Laser Engineering and Applications, Washington, D.C., May 26-28, 1969.

Ginsburg, S.

"Multitape AFA", with S. Greibach, submitted to the Journal of the Association for Computing Machinery.

"A Note of Preservation of Languages by Transducers", with G. F. Rose, Information and Control, Vol. 12, 1968, pp. 549-552.

"Derivation-bounded Languages", with E. H. Spanier, Journal of Computer and System Sciences", Vol. 2, 1968, pp. 228-250.

"Two-way Balloon Automata and AFL", with J. Hopcroft, accepted for publication in the Journal of the Association for Computing Machinery.

Gagliardi, R. M.

"Radiation Models Using Discrete Radiator Ensembles", with S. Karp and I. S. Reed, Proceedings of the IEEE, Vol. 56, No. 10, October 1968, pp. 1704-1711.

"The Design of a PPM Optical Communication System", with S. Karp, NASA Technical Document, TN D-4814, Electronic Research Center, Cambridge, Mass., October 1968.

"M-ary Poisson Detection and Optical Communications", IEEE Transactions on Communication Technology, April 1969.

Golomb, S. W.

"Theory of Transformation Groups of Polynomials Over GF(2) with Application to Linear Shift Register Sequences, J. Information Sciences, V1, pp. 87-109, 1968.

Halloran, M. H.

"Apparatus for Adiabatic Rotation of a Sample in a Magnetic Field of Liquid Helium Temperatures", with J. E. Kunzler, Rev. Sci. Inst. 39, 1501 (1968).

Kim, Y. B.

"Flux-Flow and Instabilities in Superconductors", Proceedings of International Cryogenic Engineering Conference, Kyoto, Japan, (Heywood-Temple Industrial Publication, London, 1968), p. 168.

"Some Rate Dependent Aspects of the Superconducting to Normal Transitions of Type II Materials", F. Tothwarf, D. Ford, G. Articola, G. P. Segal, Proceedings of the 1967 Applied Superconductivity Conference, Austin, Texas, to appear in Journal of Applied Physics, 1968.

"Low Temperature Physics", with W. A. Little, Science 159, 1495 (1968).

Kleinman, D. A.

"Parametric Interaction of Focused Gaussian Light Beams", with G. D. Boyd, J. Appl. Phys., 39, 3597 (1968).

"Theory of Optical Parametric Noise", Phys. Rev., 174, 1027 (1968).

"Infrared Detection by Optical Mixing", with G. D. Boyd, J. Appl. Phys., to be published.

Kroger, F. A.

"The System Al-O," J. Am. Ceram. Soc. 51 (1968, pp. 700-705, with H. Yanagida.

"Point Defects and Phase Stability in Transition Metal Compounds", J. Phys. Chem. Solids 29 (2968).

"Long Wavelength Absorption in Brominated AgBr," with P. B. P. Phipps, J. Phys. Chem. Solids (in press).

"Stabilized Zirconia as an Oxygen Pump", with D. Yuan, J. Electrochem. Soc., March 1969.

"The Sodium Activity of Liquid Na-Sn Alloys", with D. Yuan, accepted for publication by J. Phys. Chem.

"NH_4Cl, a Mixed Conductor", submitted for publication to J. Chem. Phys.

Kuehl, H. H.

"Excitation of Longitudinal Wave Resonances in an Inhomogeneous Magnetized Plasma Slab", with B. B. O'Brien and G. E. Stewart, Bull. Amer. Phys. Society, Series II, Vol. 13, No. II, p. 1533.

Lindsey, W. C.

"Nonlinear Analysis and Synthesis of Generalized Tracking Systems", University of Southern California, USCEE 317, December, 1968, Los Angeles, California; also accepted for publication in Proceedings of IEEE.

"Statistical Dynamics of Second-Order Phase-Locked Loops", to be presented at the International Communications Conference, June 8-11, 1969, Boulder, Colorado; also submitted to IEEE Transactions on Communication Technology, January, 1969.

"The Performance of Phase-Locked Loops in Cascade", submitted for publication to IEEE Transactions on Communication Technology, February, 1969.

Marburger, J. H.

"Computer Studies of Self Focusing", with E. L. Dawes, Physical Review, March 1969.

"Stationary Self Trapping of Optical Beams", with L. Huff, J. Reichert, W. G. Wagner, Physical Review.

"Observation of Optical Pulse Shaping by Self Focusing", with G. L. McAllister, Phys. Rev. Letters 21, 1648 (1968, December).

"Large Scale Self Focusing of Optical Beams in the Paraxial Ray Approximation", Phys. Rev. 175, 256 (1968, November), with W. G. Wagner, H. A. Haus.

Meisel, W. S.

"Potential Functions in Abstract Pattern Recognition", IEEE Trans. Computers, to be published.

Moore, G. P.

"A Neuromuscular Actuation System Model", with D. T. McRuer and R. E. Magdaleno, IEEE Trans. on Man-Machine Systems 9, 1968, 61-71.

"Input-Output Relations in Computer-Simulated Nerve Cells", with J. P. Segundo and others, Kybernetik, 4, 1968, 157-171.

"Statistical Analysis of Membrane Potential Fluctuations", with H. Levitan and others, Biophys. J. 8, 1968, 1256-1274.

"Applications of the Theory of Stochastic Point Processes in the Detection and Analysis of Neuronal Interaction", with D. H. Perkel and J. P. Segundo, Proc. IFAC Symposium on Technical and Biological Problems of Control. Yerevan, Armenia, 1968 (in press).

"A Neuromuscular Actuation System Model", with D. T. McRuer and R. E. Magdaleno, Proc. IFAC Symposium on Technical and Biological Problems of Control, Yerevan, Armenia, 1968 (in press).

"New Approaches to Human-Pilot/Vehicle Dynamic Analyses", with D. T. McRuer and others, Technical Report AFFDL-TR-67-150, Air Force Flight Dynamics Laboratory, Air Force Systems Command, Wright-Patterson Air Force Base, Ohio, 1968, pp. 188.

"Small Perturbation Dynamics of the Neuromuscular System in Tracking Tasks", with R. E. Magdaleno and D. T. McRuer, NASA Report CR-1212, December, 1968, pp. 119.

Murr, L. E.

"Energetics of Grain-Boundary Triple Junctions and Corner-Twinned Junctions: Transmission Electron Microscope Studies", J. Appl. Phys. 39, 557 (1968).

"Shock-induced Deformation Faults in 70/30 Copper-Zinc Alloy", with F. I. Grace and M.C. Inman, British J. Appl. Phys., 1, 1437 (1968).

'Reply to Comments on: "Investigation of Relative Interfacial Free Energies in 304 Stainless Steel by Electron Transmission and Diffraction Microscopy"', Scripta Met., 3, 5 (1969).

"Addendum to: Grain Growth Kinetics in Erbium Oxide Films", Scripta Met., March (1969).

"Optical Properties of Thin Films of Ni, Cu, and Ni + 60% Cu in the Wavelength Range 3000-6000 Å", Thin Solid Films, to be published.

"Shock Deformation of Inconel 600 Alloy: Effect of Coherent Precipitates to Explosive-Shock Hardening", with J. V. Foltz, J. Appl. Phys., to be published.

Nahi, N.

"On the Absolute Stability of a Dynamic System with a Nonlinear Element Function of Two State Variables", with S. Partovi, IEEE Transactions on Automatic Control, Vol. AC-13, No. 5, pp. 573-576 (October 1968).

"On the Absolute Stability of a Dynamic System Containing Non-linearities Function of Several State Variables", with S. Partovi, IFAC Symposium on Multivariable Control Systems, Duesseldorf, Germany, October 1968.

"Optimal Recursive Estimation with Uncertain Observation", IEEE Transactions on Information Theory, July 1969.

"Estimation Theory and Applications", Book, John Wiley, 1969.

O'Brien, B. B.

"Excitation of Longitudinal Wave Resonances in an Inhomogeneous Magnetized Plasma Slab", with H. H. Kuehl and G. E. Stewart, Bull. Amer. Phys. Society, Series II, Vol. 13, No. II, p. 1533.

"A Simple Technique for High Resolution Time Delay and Group Velocity Measurements at Radio Frequencies", submitted for publication in IEEE Trans. Inst. and Meas.

Ogawa, S.

"Nuclear Magnetic Resonance and Relaxation of the Heusler Alloy", with J. Smit, J. Phys. Chem. Solid 29, 2787 (1968).

Ohlson, J. E.

"A Polarimeter for Measuring Faraday Rotation of Space Probe Signals in the Solar Corona", USNC/URSI Spring Meeting, Washington, D.C., April 21, 1969, with G. S. Levy, T. Sato, B. Seidel and C. T. Stelzried.

"S-Band Faraday Rotation Measurements of the Solar Corona Using Signals from Pioneer VI Solar Occultation", COSPAR (International Space Science Committee) Conference, Prague, Czechoslovakia, May 1969, with G. S. Levy, W.V.T. Rusch, T. Sato, B. Seidel and C. T. Stelzried.

"Measurement of Transient Microwave Faraday Rotation Phenomena Observed During the Solar Occultation of Pioneer VI", submitted to Science, with G. S. Levy, W.V.T. Rusch, T. Sato, B. Seidel and C. T. Stelzried.

Porto, S.P.S.

"One Phonon Spectrum of $BaTiO_3$", with M. DiDomenico, S. Wemple, and R. P. Bauman, Phys. Rev. 174, 522, 1968.

"Optical Phonons of Yttrium Aluminum Garnet", with J. P. Hurrell, I. F. Chang, S. S. Mitra and R. P. Bauman, Phys. Rev. 173, 851, 1968.

"The Raman Effects of $CeCl_3$ and $PrCl_3$", with T. C. Damen, A. Kiel, S. S. Singh, Sol. State Com. 8, 671, 1968.

"The Electronic Raman Effect of $CeCl_3$", with A. Kiel, T. C. Damen, S. Sing, and S. F. Varsanyi, Phys. Rev.

"Multiple-Phonon-Resonance Raman Effect in CdS", with M. V. Klein, Physical Review Letters, Vol. 22, No. 15, April, 1969.

Pratt, W. K.

"Digital Computer Simulation of Coherent Optical Processing Operations", IEEE Computer Group News (November, 1968), pp. 12-19, with H. C. Andrews.

"Television Bandwidth Reduction by Encoding Spatial Frequencies", Journal Society of Motion Picture and Television Engineers (December, 1968), pp. 1279-1281, with H. C. Andrews.

"Two Dimensional Transform Coding of Images", 1969 IEEE International Symposium on Information Theory, (January, 1969), with H. C. Andrews.

"Transformation Coding for Noise Immunity and Bandwidth Reduction", Proceedings Second Hawaii International Conference on System Sciences, (January, 1969), with H. C. Andrews.

"Hadamard Transform Image Coding", Proceedings IEEE, Vol. 57, with H. C. Andrews and J. Kane, to appear.

Rusch, W.V.T.

"Application of a Comprehensive Computer Program to the Analysis of Axisymmetric Microwave Reflector-Antenna Systems", with H. L. Strachman, Symposium Record, IEEE Northeast Electronics Research and Engineering Meeting, pp. 20-21, Boston, Mass., November 1968.

"Observations of the Total Lunar Eclipse of October 18, 1967, at a Wavelength of 3.3 MM", with S. D. Slobin, C. T. Stelzried, and T. Sato, Astrophysical Journal, March, 1969.

"'Loss-Budget' Versus 'Comprehensive' Analysis of Gain Loss for Microwave Reflector Antennas", with H. L. Strachman, IEEE Trans. on Antennas and Propagation, 1969.

"S-Band Faraday Rotation Measurements of the Solar Corona Using Signals from Pioneer VI Solar Occultation", COSPAR (International Space Science Committee) Conference, Prague, Czechoslovakia, May 1969, with J. E. Ohlson, G. S. Levy, T. Sato, B. Seidel and C. T. Stelzried.

"Measurement of Transient Microwave Faraday Rotation Phenomena Observed During the Solar Occultation of Pioneer VI", submitted to Science, with G. S. Levy, J. E. Ohlson, T. Sato, B. Seidel and C. T. Stelzried.

Sholtz, R. A.

"Statistical Synchronization Techniques", presented at the Second Hawaii International Conference on Systems Sciences, with R. M. Storwick, January 1969.

Silverman, L.M.

"Inversion of Multivariable Linear Systems", to appear in IEEE Transactions on Automatic Control.

"Generalizations of a Theorem of Dolezal", with R. S. Bucy, presented at The Second Hawaii Conference on System Sciences, January 1969.

"Reciprocal Realization of A-matrices," presented at the 1968 IEEE International Symposium on Circuit Theory, December, 1968 (to be published in IEEE Trans. on Circuit Theory.

Smit, J.

"Onsager Relations and the Pauli Equation", Physics Letters 28A, 56 (1968).

"Ion Configuration in Spinels", Solid State Communications 6, October (1968).

"Nuclear Resonance and Relaxation in the Heusler Alloy", J. Phys. Chem. Solids 30, (1969).

Spitzer, W. G.

"Local Modes Spectra of Li Complexes in GaAs", with M. Levy and O. Lorimor, J. Applied Physics, 39, 1914 (1968).

"Site Transfer of Si in GaAs", with W. Allred, Appl. Phys. Letters 12, 5 (1968).

"Local Mode Absorption and Defects in Compensated Silicon-Doped Gallium Arsenide", with W. Allred, J. Applied Physics, 39, 4999 (1968).

"Vibrational Modes of Defects in Gallium Phosphide", with W. Allred, S. E. Blum, and R. J. Chicotka, J. Applied Physics, to be published.

"Site Distribution of Silicon in Silicon-Doped GaAs", with G. Cumming, J. Kuhg and W. Allred, Proc. of the 2nd International Conference on Gallium Arsenide, to be published.

"Optical Reflectivity of Irradiated Semiconducting Compounds", with A. Kahan, L. Bouthillette, J. Applied Physics, to be published.

Steier, W. H.

"Pulse Shuttling in a Half-Mile Optical Lens Guide", with D. Gloge, BSTJ, Vol. 47, May-June, 1968, pp. 767-782.

"Optical Shuttle Pulse Measurements on Gas Lenses", Applied Optics, Vol. 7, Nov. 1968, pp. 2295-2300.

"Experimental Simulation of a Multiple Beam Optical Waveguide", with D. Gloge, BSTJ, to be published.

Sworder, D. D.

"On the Stochastic Maximum Principle", J. of Math. Analysis and Applications, Vol. 24, No. 3, pp. 627-640, December 1968.

"On the Design of Random Circuits", Symposium Digest, 1968 IEEE International Symposium on Circuit Theory, pg. 16, 1968, with D. Elliott.

"Feedback Control of a Class of Linear Systems with Jumps Parameters", IEEE Trans. on Automatic Control, Vol. AC-14, No. 1, February 1969.

"Applications of a Simplified Multidimensional Stochastic Approximation Algorithm", 1969 Joint Automatic Control Conference, (to appear).

Wang, R.

"The Crystal Structure of In_5Bi_3", with B. C. Giessen and N. J. Grant, Z. Krist, in press (1969).

"New A_3B_5 Phases of the Ti-Group Metals with Rhodium", with B. C. Giessen and N. J. Grant, Trans. AIME, in press (1969).

Weber, C. L.

"Cascaded Phase Locked Loops", with J. J. Stein, presented at the National Electronics Conference, Chicago, Illinois, December, 1968.

"A New Simulation Technique for White Noise", with J. J. Stein, presented at the Polytechnic Institute of Brooklyn-Microwave Research Institute Symposium on Computer Processing in Communications, April 1969.

"On the Globally Optimum M-ary Noncoherent Digital Communication System", with M. S. Stone, Proceedings of the IEEE (in press).

"Noncoherent Transmitter Optimization", with M. S. Stone, IEEE Transactions on Information Theory (to be submitted).

"Doppler Jitter Versus Error Rate in Digital Coherent Systems", submitted to the International Telemetry Conference, Washington, D.C.

Welch, L. R.

"Solution of the Heawood Map-Coloring Problem - Case 4", jointly with C. M. Terry and J. W. T. Youngs, submitted to Journal of Combinatorial Theory.

"Algebraic Coding and the Lee Metric", jointly with S. W. Golomb, appears in Error Correcting Codes, edited by H. B. Mann (John Wiley 1968).

Wilcox, W. R.

"Validity of the Stagnant Film Approximation for Mass Transfer in Crystal Growth and Dissolution", Mat. Res. Bull. (in press), presented at A.I.Ch.E. meeting in Los Angeles, December 1968.

"Directional Solidification of Comphor-Anthracene Mixtures", Trans. A.I.M.E. (in press), presented at WESTEC meeting in Los Angeles, March 1969.

"Fractional Solidification Phenomena", Separation Science (in press).

"Anomalous Movement of Gas-Liquid Inclusions in a Temperature Gradient", Ind. Eng. Chem. (in press), presented at A.P.S. meeting in San Diego, December 1968.

Wittry, D. B.

"Electron Beam Modulated Reflectance of Semiconductors, with J. H. McCoy, Appl. Phys. Letters, 13, 272-274 (1968).

"Microanalysis in the Transmission Electron Microscope by Selected Area Electron Spectrometry", with R. D. Ferrier and V. C. Cosslett, Vth International Congress on X-Ray Optics and Microanalysis, Tubingen, 1968 (proceedings to be published).

"Recent Advances in Instrumentation for Electron Probe Microanalysis", Vth International Congress on X-Ray Optics and Microanalysis, Tubingen, 1968 (proceedings to be published).

Wolf, M. B.

"Some Examples of Systems Identification in Biology", with G. A. Bekey, Simulation, Vol. 11, No. 2, p. 57, August 1968.

"The Anomalous Distribution of Body Water Under an Alkaline Osmotic Stress in Hypothyroid Dogs", with P. Dorr, J. V. Maloney, Jr., and E. C. DeLand, RAND Corporation Memorandum P-3969, December 1968 (accepted for publication in Jour. Surg. Res.)

"Theoretical Evaluation of a Patient-Artificial Kidney System Using a Kiil Dialyzer", with P. D. Watson and B. H. Barbour, USCEE 338, February 1969 (accepted for publication in J. Math. Biosci.)

Security Classification

DOCUMENT CONTROL DATA - R & D

(Security classification of title, body of abstract and indexing annotation must be entered when the overall report is classified)

1. ORIGINATING ACTIVITY (Corporate author) Electronic Sciences Laboratory University of Southern California	2a. REPORT SECURITY CLASSIFICATION UNCLASSIFIED 2b. GROUP

3. REPORT TITLE

Consolidated Semiannual Progress Report No. 9

4. DESCRIPTIVE NOTES (Type of report and inclusive dates)

5. AUTHOR(S) (First name, middle initial, last name)

6. REPORT DATE April 1969	7a. TOTAL NO. OF PAGES 227	7b. NO. OF REFS
8a. CONTRACT OR GRANT NO. AF-AFOSR-69-1622A; Also see acknowledgement page at front of report b. PROJECT NO. c. d.	9a. ORIGINATOR'S REPORT NUMBER(S) 9b. OTHER REPORT NO(S) (Any other numbers that may be assigned this report)	

10. DISTRIBUTION STATEMENT

This document has been approved for public release and sale; its distribution is unlimited.

11. SUPPLEMENTARY NOTES	12. SPONSORING MILITARY ACTIVITY Joint Services Electronics Program, through the Air Force Office of Scientific Research, Arlington, Virginia

13. ABSTRACT

This document is Semiannual Progress Report No. 9 issued by the Electronic Sciences Laboratory, University of Southern California, Los Angeles, California. It summarizes the research activity during the period 1 October 1968 through 31 March 1968.

DD FORM 1 NOV 65 1473

Security Classification

14 KEY WORDS	LINK A		LINK B		LINK C	
	ROLE	WT	ROLE	WT	ROLE	WT
Semiconductors						
Quantum Electronics and Lasers						
Magnetism						
Defects in Crystals						
Metals						
Plasmas						
Millimeter Wave Radiometry						
Control Systems						
Communication and Radar Systems						
Switching, Automata Theory, and Computers						
Biomedical Engineering						
Biomedical Mathematics						